Role of sensory input in structural plasticity of dendrites in adult neuronal networks

Dissertation
zur Erlangung des Grades eines Doktors
der Naturwissenschaften

der Fakultät für Biologie der
Ludwig-Maximilians-Universität München

vorgelegt von

Arnab Chakrabarty, M. Sc.

aus Asansol, Indien

17. Januar, 2013

Betreuer:	Prof. em. Dr. Bert Sakmann
Erstgutachter:	Prof. Dr. Tobias Bonhoeffer
Zweitgutachter:	Prof. Dr. Barbara Conradt
Promotionsgesuch eingereicht am:	17.01.2013
Datum der mündlichen Prüfung:	12.03.2013

Eidesstattliche Versicherung:

Ich versichere hiermit an Eides statt, dass ich die Dissertation mit dem Titel „Role of sensory input in structural plasticity of dendrites in adult neuronal networks“ selbständig und ohne unerlaubte Beihilfe angefertigt habe. Ich habe mich dabei keiner anderen als der von mir ausdrücklich bezeichneten Hilfen und Quellen bedient.

Erklärung:

Hiermit erkläre ich, dass ich mich nicht anderweitig einer Doktorprüfung ohne Erfolg unterzogen habe. Die Dissertation wurde in ihrer jetzigen oder ähnlichen Form bei keiner anderen Hochschule eingereicht und hat noch keinen sonstigen Prüfungszwecken gedient.

München, den 17. Januar, 2013

Arnab Chakrabarty

To Life…

(*Memento mori, infinitum nihil*)

Table of Contents

List of figures

Summary

Although structural plasticity at all compartments of a neuron has been widely shown during development, the documentation of the same in adult animals remains confined mostly to dendritic spines and axons. Recent studies using modern imaging techniques have indicated that gross dendritic structures remain relatively unchanged in adult networks, although older studies using conventional cell labelling techniques have reported the contrary. All the recent imaging studies, however, have investigated plasticity of short dendritic stretches of genetically unidentified cells in superficial cortical layers due to technical limitations. This has served studies on spine dynamics well so far. However, cortical plasticity is widely believed to be cell-type and layer specific and hence, these results cannot be extended to all cell types and complete dendritic arborisations. Therefore, the most effective way to study this contentious issue is to investigate the complete dendritic trees of genetically identified cell types using conventional cell-filling techniques. With the availability of cell-type specific EGFP labelling in transgenic mice lines, it is now technically possible to study arborisation patterns in genetically identified neurons with defined input and output pathways.

Using one of these recently made-available mouse lines, in my thesis, I have investigated the influence of sensory inputs on the restructuring of dendritic arborisations in thick-tufted layer Vb pyramidal cells in adult cortex. Using a mouse line with EGFP labelling of a defined subpopulation of cells in layer Vb, I found that sensory deprivation, in the form of whisker trimming, leads to shrinkage of apical and oblique dendrites. Layer Vb thick-tufted GLT cells in primary somatosensory cortex (S1) showed the maximum differences in between experimental groups in comparison to cells in vibrissa motor cortex (vM1). Considering that the shrinkage of dendrites also simultaneously leads to the loss of spines, both stable and transient, one can gauge the amount of loss of spines for an affected cell. The profound implications of such dendritic shrinkage and accompanying spine loss and/or turnover on experience-dependent plasticity and learning in an animal become even more evident, when these numbers are extended to a whole cortical column or the complete barrel field.

1 Introduction

High fidelity transfer of sensory cues from the environment is crucial for the existential guarantee of an organism. Through evolutionary need for the 'survival of the fittest', it is indispensable that an organism is able to form a physical representation of its environment, which subserves the potential for the animal to make judgements and decisions, tailor-made for a given scenario. Through the years of evolutionary history, such mechanisms of information transfer from the external environment to the sensorium of an organism have been perfected to the present level. A fundamental challenge of neuroscience, then, is to map the neuronal circuitry in the higher processing centre of the brain, the cortex, in order to obtain a better idea about how it processes the multi-dimensional sensory information that it receives (Mountcastle, 1988, Freeman, 1998, Mountcastle, 2003, Aronoff et al., 2010, Freeman, 2011). One such higher order cognitive ability is the capacity to incorporate experiences into behaviour, a process commonly known as learning (Buonomano and Merzenich, 1998). Obviously for the survival of an organism, it is not only necessary to have a physical representation of the world around it, but to also use the acquired information to base their future decisions, including goal-directed behaviour, on (Aronoff et al., 2010).

Since quite some time now, scientists have been involved in the exploration of the brain vis-à-vis how an interconnected mass of tissue achieves the representation of the physical world outside into an internal representation in the animal (Mountcastle, 1988). Such exploratory initiatives were primarily based on anatomical and morphological techniques available at the time, to describe the structural details of this mass of tissue, the brain. With the availability of physiological techniques, especially electrophysiology, scientists have been able to probe the functioning of single nerve cells as well as clusters of functionally similar cells under varying conditions (Mountcastle, 1998). Although the minutes of sensory information transfer at the level of a single cell have been detailed out to a large extent, the mechanism behind co-operative functioning of networks of many cells, realising cognitive functions, still remains unclear (Parker, 2010).

A lot has been elucidated on what the cellular underpinnings of learning might be, albeit the lack of a coherent theory as to what cellular and network mechanistic interplay constitutes learning (Malenka and Nicoll, 1999). Ever since the discovery of the phenomenon of long term potentiation, LTP, by Andersen and Lomo (Andersen and Lomo, 1967), about 40 years back, extensive

inquisitions have resulted in a detailed explanation of the cellular mechanisms that lead to the increased output of a cell to the same given stimulus over a period of time, a phenomenon described as synaptic plasticity (Mountcastle, 1998, Malenka and Nicoll, 1999, Malenka, 2003, Malenka and Bear, 2004, Kullmann, 2012). Through the decades of research that followed, it has been established that the nerve cells employ various mechanisms to achieve such scaling of its responses in the face of the given sensory environment, namely, physiological, structural, genetic and/or biochemical (Buonomano and Merzenich, 1998, Fox and Wong, 2005, Sur and Rubenstein, 2005).

The scope of this thesis is limited to the investigation of the extent of structural reorganisation in response to deprivation of sensory input in the adult neocortex. Intuitively, if through the process of learning, an organism can alter its behaviour to a given sensory stimulus, it follows that a lack of the same might also be instrumental in inducing changes at the level of neuronal geometry. In this doctoral project, I have looked at possible structural remodelling of dendrites induced by a lack of sensory input, as such structural alterations form an important mechanism of activity/experience-dependent plasticity in the brain (Maletic-Savatic et al., 1999, Cline, 2001).

1.1 Levels of sensory processing

Sensory information from the external world is received by the first level of processors which are usually the peripheral sensory receptors (for example the mechanoreceptors for touch, pressure, etc.), and are then sequentially and multi-synaptically sent to various levels of higher order information processing hubs, ultimately culminating at the cortex (Mountcastle, 1998). This passage of sensory information through the afferent sensory pathways of the nervous system renders it susceptible to modifications due to various natural synaptic constraints, as well as influences of the higher centres of the cortex and local circuits along the pathway, mainly at the level of the thalamus (Alitto and Usrey, 2003, Lavallee et al., 2005, Cudeiro and Sillito, 2006, Furuta et al., 2010). An interesting feature worth mentioning here is that the somatosensory, visual and the auditory systems are connected in a topographically representative manner (Tunturi, 1950, Hubel and Wiesel, 1962, Woolsey and Van der Loos, 1970, Kaas, 1997, Weisz et al., 2004, Thivierge and Marcus, 2007). Due to this sequential and well mapped outflow of sensory information, these pathways have been an attractive choice for scientists for years to study the exact hierarchical mechanics of information processing (Petersen, 2007).

A very good example is the primary somatosensory system. Tactile stimulus received at the periphery is sensed by the mechanoreceptors, and then sent either through the primary fibres, gracile and cuneate funiculus, to the nuclei located in the dorsal columns, respectively the gracile and the cuneus nucleus, or through the infraorbital branch of the trigeminal nerve to the sensory cranial nerve nuclei in the brainstem, i.e. the trigeminal nuclei. Second order projections from the dorsal column nuclei, in the form of the medial lemniscus, decussate or cross over to the contralateral side. Together with the secondary fibres from the trigeminal nuclei, the former end up somatotopically at the thalamic nuclei. The fibres from the trigeminal nuclei serve to connect the medial part of the ventral posterior thalamic nucleus, while those of the medial lemniscus connect the lateral part of the ventral posterior thalamic nucleus (Fox, 2008).

The thalamus is described as the 'gateway to sensory perception' as its neurons are known to change their firing modes believed to be dependent on the different attentive states of the animal (McCarley et al., 1983, McCormick and Feeser, 1990, Steriade et al., 1993, Guido and Weyand, 1995, Ramcharan et al., 2000). To complete this elegant tri-synaptic arrangement, the third order neurons from the ventral posterior thalamic nucleus finally project through the thalamocortical fibres to the primary somatosensory cortex, preserving the somatotopic representation all the way (Fox, 2008).

1.2 Columnar organisation of the sensory cortex

Cells having similar receptive field properties are organized in vertical columns in the cortex. Sensory cortices are made up of columns, constituting of many *minicolumns*, bound together by dense short-ranged horizontal connections (figure 1-1). A minicolumn is the smallest basic unit constituting the neocortex and consists of a narrow chain of about 80-100 neurons extending vertically across the layers II-VI. So the cortical columns are practically composed of a vertical array of cells that runs orthogonal to the layered structure of the cortex. They are known to vary from 300-500 μm in width across species. They serve as complex processing and distributing units that interleave several inputs with several outputs via processing pathways internal to the columns. Cortical columns are thus modularly organised and hence are sometimes called *modules* (Mountcastle, 1998). First discovered in the somatosensory cortex by Mountcastle in cats (Mountcastle et al., 1957), it was also found to be true for the visual cortex (Hubel and Wiesel, 1962).

Mountcastle described the encounter with neurons with similar properties of *place* (peripheral receptive field) and *modality* (nature of the stimulus evoking a response and the rate of adaptation to a steady stimulus) in each cell layer when penetrated with electrodes perpendicular

to the pial surface. When electrode penetrations were made parallel to the pial surface and perpendicular to the vertical axis of the cortex, he encountered similar cells in blocks of tissue 300-500 µm in width (Mountcastle, 1998).

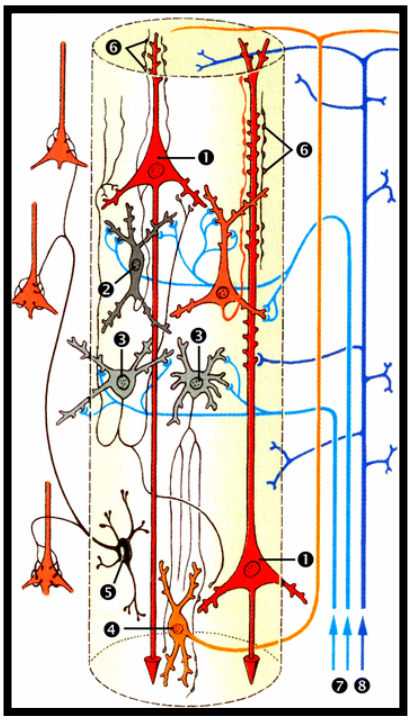

Figure 1-1: **A canonical column.** Simplified schemata showing a cortical column showing different excitatory and inhibitory cells as well as axons and afferent fibres numbered 1-8. Of particular interest are the pyramidal cells (1) in layer V. Figure adapted from Lubke and Feldmeyer (2007).

Therefore he quipped, "The data reported… support the view that there is an elementary unit of organization in the somatic cortex made up of a vertical group of cells extending through all the cellular layers. The neurons of such a group are related to the same or nearly the same peripheral receptive field upon the body surface" (Mountcastle, 1957). However, apart from place and modality, other properties such as the afferent inflow pattern or intracortical connections also define a column. Thus, a cortical column is a stereotypical circuit that is essentially repeated all over the neocortex, but differ in that they receive discrete functional thalamic input (Mountcastle, 2003).

Similarly, Hubel and Wiesel first described the presence of cortical columns in the primary visual cortex of monkeys and cats, when they found that neurons in the visual cortex were preferential in their response to the place and modality of the stimulus (Hubel and Wiesel, 1959, 1968, 1977). Such cortical columns are known as ocular dominance columns in the visual cortex, because cells responding to one particular eye are grouped together. Formation of ocular dominance columns takes place very early in development in monkeys (Rakic, 1976) and cats (Crair et al., 2001), even before eye opening in ferrets (Crowley and Katz, 2000), and thus, precludes the requirement of visual experience (Crowley and Katz, 1999). Evidences of columnar organisation in other cortical areas such as the auditory and motor cortices, homotypical cortical areas and even across species also abound (Mountcastle, 2003).

Wiesel and Hubel demonstrated that plasticity of the ocular dominance columns can be manipulated using experimental paradigms like monocular deprivation, where one eyelid is sutured closed (Hubel et al., 1977, Wiesel, 1982). In a series of elegant experiments during the 1960s, they demonstrated that starting from eye opening, there exists a *critical period*, across which, the closing of an eye to restrict the patterned retinal input to that eye, produces changes in the ocular dominance patterns in the form of weakening of the projections from the sutured eye and the reverse effect in those from the normal eye. In other words, this leads to the shrinkage of the ocular dominance columns of the closed eye and expansion of the same of the open eye (Wiesel and Hubel, 1963). However, monocular deprivation carried out outside this critical period is not as effective in inducing such structural changes (Hubel and Wiesel, 1970).

1.3 The curious case of rodent somatosensory cortex

A fascinating peculiarity, worthy of mentioning here, is that of the rodent primary somatosensory cortex. Rodents, especially rats and mice, on virtue of being nocturnal animals living in tunnel environments, have an extensively developed somatic sensory system to compensate for the lack of richness of visual information (Petersen, 2007, Aronoff et al., 2010). The whiskers on the snouts of rats and mice serve as highly sensitive tactile sense organs that, on active palpation at frequencies of 5-20 Hz (Carvell and Simons, 1990, Bermejo et al., 2005, Mitchinson et al., 2011) in rats and up to 25 Hz in mice (Jin et al., 2004, Voigts et al., 2008), can provide information about the spatial map of the external environment, can locate objects, and discriminate texture (Guic-Robles et al., 1989, Arabzadeh et al., 2005, Knutsen et al., 2006, Celikel and Sakmann, 2007, Mehta et al., 2007). A striking feature of this somatosensory system is that at all the levels of afferents stations, e.g., the brainstem, the thalamus and finally, in layer IV of the primary sensory cortex, the neurons exhibit the previously discussed modular arrangement. These modular structures in cortical layer IV are called *barrels* and were first described by Woolsey and van der Loos in 1970 (Woolsey and Van der Loos, 1970). Each whisker on the snout is represented by one barrel and the barrels are laid out in the exact somatotopic one-to-one fashion as the whiskers on the snout of the animal (figure 1-2) (Woolsey and Van der Loos, 1970). They are markedly prominent in the posteromedial barrel subfield, PMBSF, a subfield of the rodent primary somatosensory cortex (Frostig, 2006), representing the large whiskers on the contralateral face, and are easily visible in living and stained brain slices (Finnerty et al., 1999, Petersen and Sakmann, 2000).

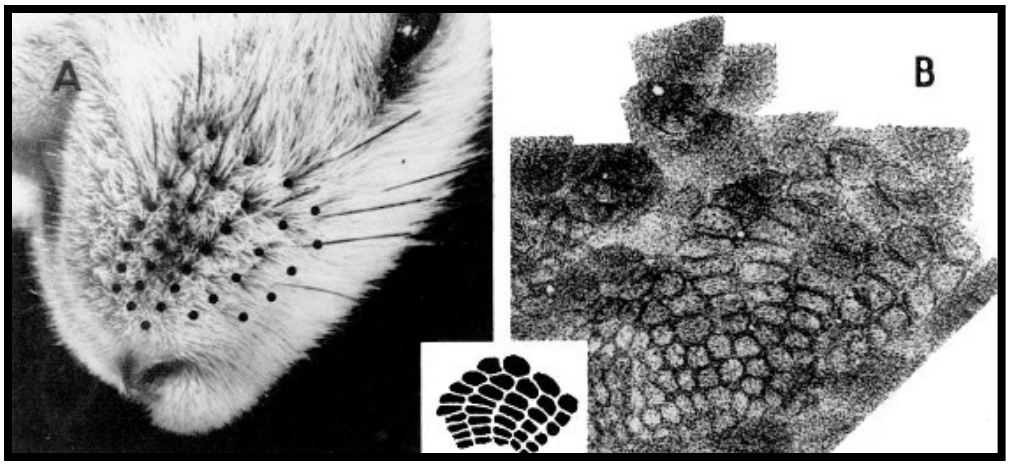

Figure 1-2: **Somatotopic organisation of whiskers representation.** The whiskers on the right mystacial pad of a mouse (A) are represented in a one-to-one manner in the contralateral (left) somatosensory cortex posteromedial barrel sub-field, PMBSF, (B). Inset shows the arrangement of the PMBSF barrels as a copy of the mystacial whisker arrangement. Figure modified from Woolsey and Van der Loos (1970).

1.4 From whiskers to the somatosensory cortex

Sensory innervation of the whisker follicles on the snouts of rodents is very high and multivarious (Ebara et al., 2002). In rats, about 200 trigeminal ganglion cells innervate the larger follicles, whereas the smaller follicles are served by about 50 of them (Fox, 2008). In keeping with this trend, the area of cortex devoted to whisker-related information is also high. Barrel cortex in mice forms about 69% of the total somatosensory cortex area (Lee and Erzurumlu, 2005). The whisker follicles are rich in vascular supply from the follicle *sinusse*; increased blood circulation leads to stiffening of individual vibrissae within their respective follicles. This results in the mechanoceptors sitting tighter on the whiskers, and thus, increasing the sensitivity of the receptors to given mechanical stimuli. A deflection of a whisker triggers the opening of the mechanoceptive sensory channels gating the endings of the sensory innervation to the follicles. A single sensory neuron responds to stimuli from only one specific whisker (Fox, 2008).

The resultant depolarization travels through the infraorbital branch of the trigeminal nerve to reach the corresponding nuclei of the trigeminal nerve in the brainstem. The neurons in the trigeminal nuclei at the level of the brainstem are somatotopically arranged into *barelletes*, the brainstem-equivalent of barrels and get strong input from one single whisker (Kossut, 1992, Veinante and Deschenes, 1999, Petersen, 2007). The trigeminal nuclei are organised into four groups: the *principalis nucleus*, the *oralis nucleus*, the *interpolaris nucleus* and the *caudalis nucleus*.

All four nuclei groups preserve the somatotopic representation of the whiskers described above (Fox, 2008).

Principalis and interpolaris nuclei form the main projections to the somatosensory thalamic nuclei. The neurons from the principalis nucleus project mainly to the ventral posteromedial nucleus, VPM, and sparsely to the posteromedial nucleus, POm, of the thalamus. The interpolaris nucleus, on the other hand, projects exclusively to the POm nucleus. The conserved somatotopic organisation of the neurons here results in the anatomical barrel-equivalents, named *barelloids* (Land and Simons, 1985, Kossut, 1992, Petersen, 2007, Fox, 2008, Aronoff et al., 2010).

The thalamic afferents from the individual barelloids of the VPM nucleus, which otherwise innervate the primary sensory cortex uniformly, form dense clusters of innervation in layer IV (Petersen, 2007), separated by gaps marked by reduced innervation. The dense clusters of innervation form the *core* of the barrels, where cells are sparse. The layout of the barrels in the layer IV of the primary sensory cortex is identical in a one-to-one way to the spatial distribution of the whiskers on the snouts of the animal (Woolsey and Van der Loos, 1970). Cell density profoundly increases in the barrel walls from where they tend to orient their dendrites towards the barrel core (Simons and Woolsey, 1984). The gaps of sparse innervation mentioned above, surround the barrels and are called *septae*. Septae can span about 50 μm in width in between barrels in rats, although, they are less well defined in mice (Woolsey and Van der Loos, 1970, Petersen, 2007). In the latter, the barrels are tightly apposed to each other. The barrels themselves range about 200 μm in diameter and about 100 μm along the axis of the row in mice. In rats, however, the same barrels can range up to 400 μm in diameter. The difference in cell densities between the barrel core and the barrel walls are much higher in mice than in rats. Nevertheless, owing to the difference in *refractive indices* caused by the relative richness of myelinated fibres in the barrel core, the barrels are usually visible in an unstained brain slice under microscope (Finnerty et al., 1999, Petersen and Sakmann, 2000, Fox, 2008). However, owing to this spatial pattern of cell body and fibre localisation, other ways to visualise barrels involve staining for mitochondrial *succinate dehydrogenase*, *cytochrome oxidase* or using a *Nissl stain* (Belford and Killackey, 1979). Mitochondria are numerous in synapses, sites of energy-intensive activity. Therefore, staining for cytochrome oxidase labels the barrel centres or cores up until the inner boundaries of the barrel walls. Contrastingly, using a Nissl stain would result in the cell-rich walls of the barrels to show up more prominently than the cell-sparse cores (Fox, 2008).

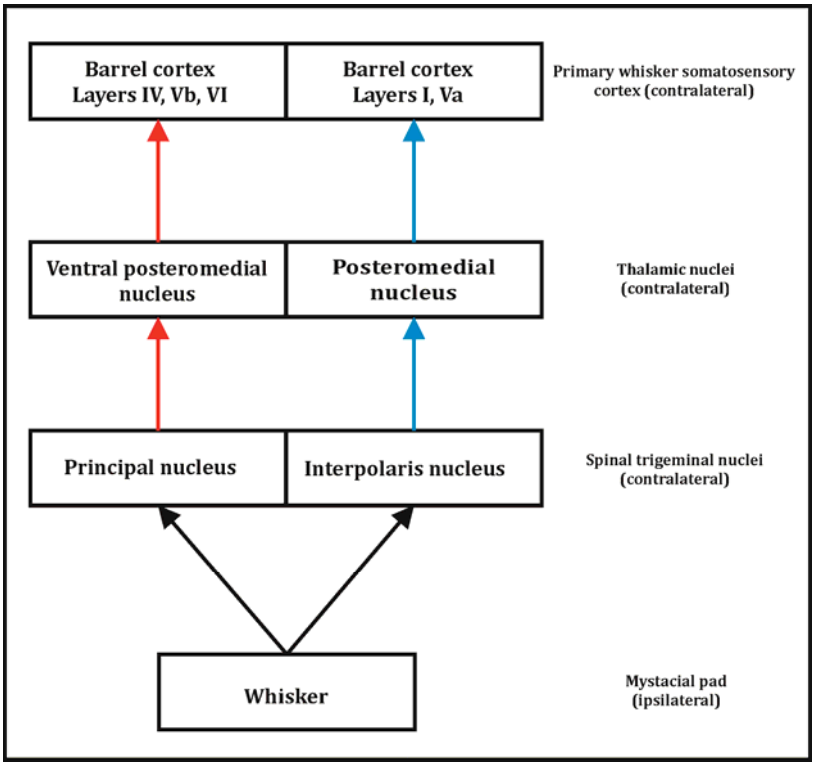

Figure 1-3: **Trisynaptic pathway from whisker to the barrel.** The trigeminal nerve brings whisker information to the nuclei at the level of the spinal cord (two of which are shown here). From there, the information travels to the two thalamic nuclei, via the lemniscal pathways (red) to the ventral posteromedial thalamic nucleus and via the paralemniscal pathway (blue) to the posteromedial thalamic nucleus. The final station for the information train is the barrel cortex where the two different pathways serve specific cortical layers (the directions of the arrows are by no means the only direction in which information flows).

There are two separate projection systems to the barrels carrying barrel-related information from the thalamic nuclei to the cortex (figure1-3) (Bureau et al., 2006, Brecht, 2007, Petersen, 2007, Aronoff et al., 2010). The *lemniscal pathway* arises from the neurons of the prinicipalis nucleus and course their way up to the VPM nucleus in the thalamus. Next order neurons from this thalamic nucleus course up to innervate primarily layer IV barrels in the cortex. In addition, they also connect the upper layer VI and layer Vb (Bureau et al., 2006, Petreanu et al., 2009, Cruikshank et al., 2010). The *paralemniscal pathway*, on the other hand, arises from the interpolaris nucleus in the brainstem and innervates the POm nucleus in the thalamus, which in turn, innervates the layer I and layer Va of the primary somatosensory cortex, avoiding the layer IV barrels altogether (Bureau et al., 2006, Petreanu et al., 2009). Moreover, the projections from the POm also innervate the secondary somatosensory cortex and the motor cortex (Petersen, 2007). Several other parallel pathways, arising from the subdivisions of the thalamic nuclei and projecting to both primary and secondary somatosensory cortices, have been recently discovered (Pierret et

al., 2000, Deschenes, 2009, Furuta et al., 2009). It is believed that these parallel processing pathways are involved in different aspects of sensorimotor information in rats (Yu et al., 2006); in mice however, the nature of information carried through these pathways have not yet been completely delineated (Aronoff et al., 2010).

Taken together, because of the added aspect of motor control of the whisker movements, the rodent whisker system is ideal in many ways to investigate multimodal sensory processing leading to perception (Kleinfeld et al., 2006, Diamond et al., 2008, O'Connor et al., 2009). Furthermore, over the years, it has served as a useful model to study cortical plasticity and regeneration following injury, due to the numerous advantages to the respective fields this system has to offer (Fox, 2008, Wu et al., 2011).

1.5 Intracortical connections in the barrel cortex

Given the complexity and multi-modal nature of whisker-sensory information and its triggered goal-directed behaviour, it follows intuitively, that vibrissal sensory perception and its resulting behaviour is a consequence of activity in multiple brain areas and not just primary somatosensory cortex (Aronoff et al., 2010). Precisely because of this multi-loci cortical processing of sensorimotor information, it is important to take into consideration the intracortical connectivity between the primary and secondary somatosensory cortices (S1 and S2 respectively) and the vibrissa motor cortex (vM1; mentioned briefly in the last section), in order to understand the underlying mechanisms. Especially, given the direct involvement of the motor cortex in the use of vibrissae, one can strongly argue for the possible existence of strong connections between the primary somatosensory cortex and the motor cortex.

Indeed, using anatomical tracers, functional imaging using voltage sensitive dyes and similar techniques, it has been established, that apart from the axonal innervations across a cortical column in the barrel cortex, the primary somatosensory cortex neurons (both barrel- and septa-related) also project to the secondary somatosensory cortex, S2 (Welker et al., 1988, Hoffer et al., 2003, Chakrabarti and Alloway, 2006), and that these connections are reciprocal

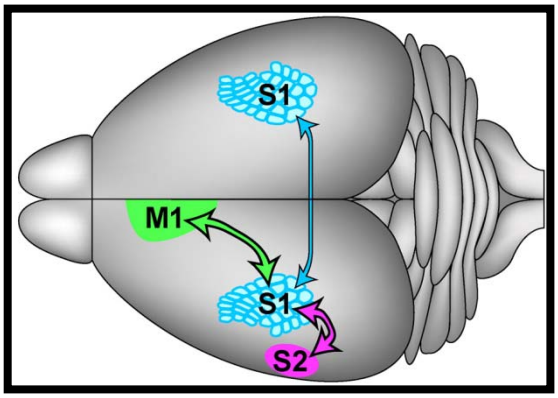

Figure 1-4: **Intracortical connectivity of barrel cortex.** The primary somatosensory cortex (S1) is reciprocally connected to the ipsilateral primary motor cortex (M1) and secondary somatosensory cortex (S2), as well as the contralateral primary somatosensory cortex. Figure modified from Petersen (2007).

(Petersen, 2007, Aronoff et al., 2010). Consequently, activity within an individual barrel column spreads to neighbouring areas rapidly within 10-20 ms (Ferezou et al., 2007). This is assumed to help integrate whisker information from several whiskers to build a representation of the environment (Aronoff et al., 2010).

Further, activity in the primary somatosensory cortex in response to whisker stimulation also spreads with a 10-20 ms delay to a specific region of the motor cortex, that is, the vibrissa motor cortex (Ferezou et al., 2007). This spread of the response to the motor cortex is, of course, dependent on the activity in the primary somatosensory cortex (Chakrabarti et al., 2008). Labelling studies have been able to identify direct and reciprocal projections from the barrel cortex to the vibrissa primary motor cortex (Welker et al., 1988, Hattox et al., 2002, Hoffer et al., 2003, Alloway et al., 2004). It is known that the superficial cell layers of the primary somatosensory cortex project to the deeper layers of the vibrissa motor cortex while the deeper layer cells of the former project to the superficial cell layers of the latter (figure 1-4) (Mao et al., 2011). In addition, the barrel cortex also projects to other cortical areas like temporal association cortex, contralateral somatosensory and motor cortices, etc. (Fox, 2008).

1.6 The vibrissa motor cortex

The motor representation of the vibrissae in the motor cortex, named the vibrissa motor cortex (vM1), is the largest of its kind in the rodent brain. The vibrissa motor cortex takes up about 45% of the primary motor cortex in rats (Brecht et al., 2004a). Through surface stimulation, and later, through microstimulation studies, it has been possible to describe the functional localization of the vibrissa motor cortex. Unlike previously thought, the vibrissa motor cortex turned out to be bigger than just a narrow strip extended along the anterior-posterior axis. This might have been due to the mapping techniques used at the time that failed to take into consideration the strongly curved rat motor cortex (Brecht et al., 2006). A gamut of studies now indicates that the vibrissa motor cortex is located in the posteromedial part of the frontal agranular cortex, anteromedial to the barrel cortex (Neafsey et al., 1986, Brecht et al., 2004a, Ferezou et al., 2007). However, despite a general agreement on the spatial layout of the vibrissa motor cortex, the functional topographic representation of the body in the motor cortex remains unclear.

The vibrissa motor cortex corresponds to the agranular medial area or AG_m as shown in figure 1-5. An expanded layer Vb and VI, compressed layers II/III and Va, a lack of a distinct granular layer IV, strong myelination, among others, characterize it. Additionally, layer I is observed to be thicker than in other areas (Brecht et al., 2006).

Worthwhile to note here is that the vibrissa motor cortex lacks any somatotopic representation of whiskers in the form of barrel-equivalents, although projections from the primary somatosensory cortex are topographical. The vibrissa motor cortex receives strong projections from extragranular cells above and below the septal areas (columns of neurons aligned with septa regions) of the primary somatosensory barrel cortex and these projections are bidirectional in nature (Welker et al., 1988, Hoffer et al., 2003, Alloway et al., 2004, Chakrabarti and Alloway, 2006, Petersen, 2007). In addition, the thalamic nucleus POm, but not VPM, also projects to the vibrissa motor cortex (Cicirata et al., 1986, Aldes, 1988, Hoffer and Alloway, 2001). Because the POM mainly projects to the septal regions of the primary somatosensory cortex (Koralek et al., 1988, Lu and Lin, 1993), it is believed that the POm nucleus acts with the primary somatosensory cortex to provide vibrissa motor cortex with sensory information regarding whisking frequency (Ahissar and Zacksenhouse, 2001, Kleinfeld et al., 2002).

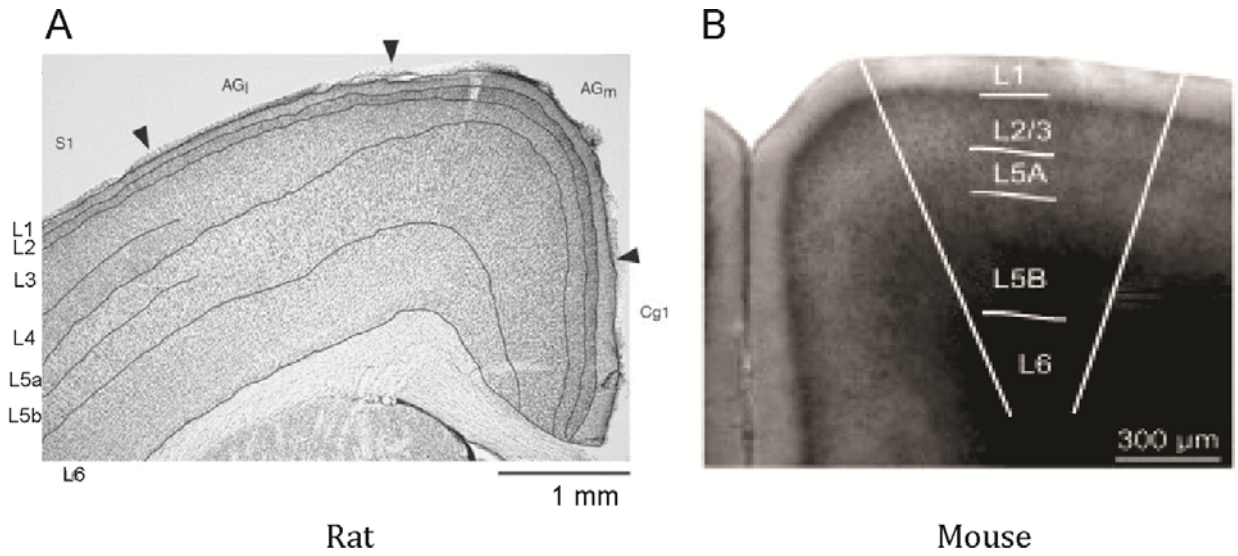

Figure 1-5: **Vibrissa related primary motor cortex in rodents. A.** Nissl stained coronal slice of rat primary motor cortex. Cell layers are indicated. The agranular medial area, AG_m and not the agranular lateral area, AG_l, contains the cells related to whisker movement; modified from Brecht et al. (2004a). **B.** Coronal slice of mouse primary motor cortex with the cell layers indicated. The vertical lines show the approximate range of vibrissa motor cortex; modified from Mao et al. (2011).

1.7 Experience-dependent cortical plasticity

The brain is able to constantly adapt to new information acquired during the lifetime of an individual (Buonomano and Merzenich, 1998). This is possible because of the unique ability of the

neurons, the cellular building blocks, to produce various changes, among others structurally, in order to realise the altered functionality (Feldman and Brecht, 2005, Fox and Wong, 2005, Sur and Rubenstein, 2005). The ability of neurons to scale their output at a particular synapse according to the history of activity at that synapse, Hebbian plasticity, was first reported in the hippocampus (Andersen and Lomo, 1967), and was later also found in the neocortex (Artola and Singer, 1987).

It is widely accepted that the relatively unspecific neuronal circuitry at the time of birth is sculpted into its present form by experience, that is, sensory information that it receives, a process aptly described by John Locke's metaphor of the *tabula rasa.* While there is evidence, that the blueprint to the basic neuronal geometry vis-à-vis its circuitry is laid out in the genome (Daw, 2009), there is reason to believe that the ultimate hard-wiring of the neurons is not entirely dependent on the genetic program, and that environmental inputs to the neurons also play an extensive role (Wiesel, 1982).

Plasticity during development, combined with experimental manipulations of environment or sensory inputs, have been amply demonstrated (Hubel and Wiesel, 1970, Van der Loos and Woolsey, 1973, Killackey et al., 1976, Hubel et al., 1977, Simons and Land, 1987). In the visual cortex, neo-natal deprivation of normal visual experience was shown to alter visual cortical circuitry and functions (Hubel and Wiesel, 1970, Hubel et al., 1977). At the same time, the idea of a critical period was suggested by Hubel and Wiesel, during which the circuitry is especially vulnerable to environmental alterations (Hubel and Wiesel, 1970, Hensch, 2004). Similarly, destruction of vibrissal follicles was shown, by Van der Loos and Woolsey, to alter cortical representations of barrels (Van der Loos and Woolsey, 1973). However, this sort of manipulation was successful only shortly after birth, before the formation of barrels, and did not affect the barrels if carried out later in life (Weller and Johnson, 1975). For a long time since, it was widely believed that adult cortical circuits were incapable of plasticity due to the expiry of the critical period.

However, studies over the next decades have undone this idea for good and it is now widely believed that cortical cells are fully capable of plastic changes throughout life (Kossut, 1992, Fu and Zuo, 2011). For example, pairing of two neighbouring whiskers and clipping the rest (whisker pairing) in adult rats caused potentiation of the spared inputs and depression of the deprived ones (Diamond et al., 1993, Diamond et al., 1994). Similar potentiation of the spared input also occurs when all but one whisker are clipped off (Kossut et al., 1988, Kossut, 1992). However, following a host of studies in this field, it seems to be a widespread belief, that geometry of a neuronal dendritic tree is an early developmental phenomenon and is fixed until adulthood (Harris and Woolsey, 1981, Greenough and Chang, 1988, Katz and Constantine-Paton, 1988, Kossel et al., 1995); so much so

that, apart from small tip extensions and retractions, dendritic morphology (especially apical arborisations of pyramidal neurons) remains stable unless dramatic interventions like peripheral lesions are in play (Grutzendler et al., 2002, Trachtenberg et al., 2002, Mizrahi and Katz, 2003, Hickmott and Steen, 2005, Tailby et al., 2005). This is partly because although the existence of functional plasticity, due to experimental manipulations or sensory deafferentation caused by injuries, had been confirmed in adult animals, experimental evidence for correlative structural changes in the gross dendritic architecture has been scarce (Tailby et al., 2005). Several investigations have looked at spine dynamics, dendritic polarity, axonal restructuring during adult plasticity, as well as cortical representational map alterations, but rarely dendritic structural changes (Trachtenberg et al., 2002, Hickmott and Steen, 2005, Tailby et al., 2005, De Paola et al., 2006, Frostig, 2006, Holtmaat et al., 2006, Wimmer et al., 2010, Fu and Zuo, 2011, Oberlaender et al., 2012). However, caution must be exercised in extending these findings to all cell types across cortical layers as experience-dependent structural plasticity varies between cell types (Fu and Zuo, 2011). Moreover, most of these studies did not look at cell types in deeper layers because current imaging techniques are limited to superficial layers; they also did not look at full dendritic arborisations, choosing instead to look at small stretches of dendrites at a time. Currently published studies that have investigated plasticity of adult dendritic architecture have come up with conflicting results (Tailby et al., 2005, Chen et al., 2011), and this field would therefore be subject to further investigations until consensus is reached.

1.8 Aim of this thesis

The responses of sensory cortical neurons are known to be layer and cell specific (Brecht and Sakmann, 2002, de Kock et al., 2007). This might suggest that cells that are genetically identical and share the same morphological characteristics are functionally identical and connect similarly. However, apart from some basic properties like place and mode, other properties vary between cells across the layers, even within the same minicolumn (Mountcastle, 2003). The identification of genetically identical cell types throughout the cortical areas may help answer the question whether morphology, connectivity, and response properties of cells with the same genetic identity are preserved throughout the cortical areas or whether they are dependent on the areas of the cortex and/or their sensory inputs. In other words, do incoming thalamic sensory input properties customize the properties of similar cells located in various cortical areas or are these cell properties preserved across the cortex?

Two such identified cell types in the infragranular cortical layer V are the thick-tufted and thin-tufted neurons, the thick-tufted being in layer Vb while the thin-tufted in layer Va, that respond differentially to sensory stimuli (Hallman et al., 1988, Larkman and Mason, 1990, Groh et al., 2010). The thin-tufted neurons are striatum-projecting, while the thick-tufted neurons project to the brainstem, pons, posterior nucleus of thalamus, and superior colliculus (Alloway, 2008, Groh et al., 2008, Aronoff et al., 2010). These two cell types comprise the main output sources of a cortical column (Meyer et al., 2010), and are known to occur throughout several cortical areas (Hubener et al., 1990, Brecht et al., 2004b, Morishima and Kawaguchi, 2006, Larsen et al., 2007, Sakata and Harris, 2009). The recent availability of genetically-labelled cell populations of the thick-tufted and thin-tufted neurons in separate mouse lines from the GENSAT project at the Rockefeller University, New York (www.gensat.org), has made it possible to test the aforementioned issues (Gong et al., 2003, Heintz, 2004, Fu and Zuo, 2011). One of these mouse lines, carrying bacterial artificial chromosomes, *BAC*, expresses enhanced green flouorescent protein, EGFP, in thick-tufted neurons under the control of a promoter of a *glycosyltransferase*, *glycosyltransferase 25 domain containing 2* or GLT or glt25d2. Layer V, of the six layered neocortical organization, is a major cortical output source for the subcortical structures (Alloway, 2008, Groh et al., 2008, Aronoff et al., 2010), and studying the plasticity mechanisms of layer V cells stands to give an insight into the sensory modality-specific information processing in the brain.

Using the mouse line with the selective labelling of thick-tufted cells throughout the neocortex, I have investigated the extent of sensory input driven (experience-dependent) dendritic plasticity in the whisker-representative cortex in adult animals. Due to a distinct topographic arrangement of the whiskers and their representation in the cortex, coupled with the ease with which whiskers can be manipulated, the barrel cortex has proven to be a system of choice for experimental studies on plasticity or effect of environment on circuit rearrangements (Buonomano and Merzenich, 1998).

To this end, I employed targeted patch-clamp based biocytin filling of thick-tufted pyramidal cells in cortical layer V of mice that express GFP in the same cells. *Post-hoc* staining of these cells for biocytin renders the fine dendritic morphology of these cells visible for manual reconstruction. The whole study bases on the comparison of the dendritic morphologies of genetically identical cells in whisker-related cortical areas in control animals with those in sensory deprived animals (somatosensory deprivation by whisker trimming). The studied cortical regions are the whisker-related primary somatosensory cortex (S1) or barrel cortex, and whisker-related motor cortex or vibrissal motor cortex (vM1).

2 Materials and Methods

2.1 Materials

2.1.1 Chemicals

3, 3-diaminobenzidine-4-hydrochloride (DAB), Serva Electrophoresis GmbH, Heidelberg, Germany

4-(2-hydroxyethyl)-1-piperazineethanesulfonic acid (HEPES), Biomol GmbH, Hamburg, Germany

Adenosine 5'-triphosphate magnesium salt (ATP-Mg), Sigma-Aldrich Chemie GmbH, Steinheim, Germany

Biocytin, Sigma-Aldrich Chemie GmbH, Steinheim, Germany

Calcium chloride, Merck, Darmstadt, Germany

Catalase, Sigma-Aldrich Chemie GmbH, Steinheim, Germany

Chloral hydrate, Sigma-Aldrich Chemie GmbH, Steinheim, Germany

Choline chloride, Sigma-Aldrich Chemie GmbH, Steinheim, Germany

Cytochrome C, Sigma-Aldrich Chemie GmbH, Steinheim, Germany

D-Glucose, Merck, Darmstadt, Germany

Disodium hydrogenphosphate, Merck, Darmstadt, Germany

Glycerol, Sigma-Aldrich Chemie GmbH, Steinheim, Germany

Guanosine 5'-triphosphate sodium salt (GTP-Na), Sigma-Aldrich Chemie GmbH, Steinheim, Germany

Hydrogen peroxide, Merck, Darmstadt, Germany

Isoflouran CP (Isoflurane), CP-Pharma, Burgdorf, Germany

Magnesium chloride, Merck, Darmstadt, Germany

Mowiol 4-88, Carl Roth GmbH + Co. KG, Karlsruhe, Germany

Paraformaldehyde, Merck, Darmstadt, Germany

Phosphocreatine disodium salt, Sigma-Aldrich Chemie GmbH, Steinheim, Germany

Poly-d-lysine hydrobromide, Sigma-Aldrich Chemie GmbH, Steinheim, Germany

Potassium Chloride, Merck, Darmstadt, Germany

Potassium d-gluconate, Sigma-Aldrich Chemie GmbH, Steinheim, Germany

Sodium ascorbate, Sigma-Aldrich Chemie GmbH, Steinheim, Germany

Sodium bicarbonate, Merck, Darmstadt, Germany

Sodium Chloride, Merck, Darmstadt, Germany

Sodium dihydrogenphosphate, Merck, Darmstadt, Germany

Sodium pyruvate, Sigma-Aldrich Chemie GmbH, Steinheim, Germany

Tris-hydrochloric acid, Sigma-Aldrich Chemie GmbH, Steinheim, Germany

Triton X-100, Merck, Darmstadt, Germany

2.1.2 Computers

Dell Optiplex 760, Dell Computers, Germany

Dell Precision 690 Workstation, Dell Computers, Germany

2.1.3 Electrophysiological instruments and accessories

Axon headstage, Axon Instruments, Germany

Axopatch 200B, Axon Instruments, Germany

Borosilicate glass capillaries (outer diameter 0.02 cm, length 0.75 cm, wall thickness 0.005 cm, ends firepolished, filamented), Hilgenberg, Germany

coolSNAP HQ2 CCD camera, Photometrics, USA

Hitachi IR-DIC New Vicon video monitor, Hitachi, Japan

HM 303-6, 35 MHz analog oscilloscope, Hameg Instruments, Mainhausen, Germany

Luigs and Neumann SM III Manipulator, Luigs and Neumann, Ratingen, Germany

Manual seal sucker and temperature controller, MPI for Medical Research, Heidelberg, Germany

Olympus BX51WI microscope, Olympus, Japan

Olympus LUM Plan Fl objective (40X/0.80 WI), Olympus, Philippines

Olympus Plan CN objective (4X/0.10), Olympus, Philippines

precisExcite Flourescence Imaging system, CoolLED Microscopy, UK

Sutter P-97 Flaming/Brown micropipette puller, Sutter Instrument Co., California, USA

VX44-PCO CCD Imaging video camera, PCO Imaging, Germany

2.1.4 Other Materials

2 ml reaction tubes, Eppendorf, Hamburg, Germany

24 well cell culture plate, Costar, Corning Incorporated, USA

3ml glass vials, VWR, Germany

Cover slip “000”, Menzel Gläser, Thermo Scientific, Germany

Cover slip, 15mm diameter, Menzel Gläser, Thermo Scientific, Germany

Glass slides (76 X 26 mm), Menzel Gläser, Thermo Scientific, Germany

Nalgene cellulose acetate 4 mm syringe filters with 0.2 µm pore size, Nalgene Nunc International Corporation, USA

2.1.5 Reconstruction tools

Olympus BX61 microscope, Olympus, Japan

Olympus BX-UCB (100W mercury lamp), Olympus, Japan

LEP MAC 5000 PS-System (microscope stage system), Ludl Electronic Products Ltd., Hawthorne, USA

Olympus UPlan Fl objective (4X/0.13), Olympus, Japan

Olympus Plan objective (100X/1.25), Olympus, Japan

2.1.6 Slicing instruments and accessories

10° ramp with horizontal slits at 45° to x-axis, MPI for Neurobiology, Martinsried, Germany

Gillette shaving blade, Gillette, Germany

Microm HM650V, Microm International GmbH, Walldorf, Germany

Paintbrush “00”, VWR, Germany

UHU Sekundenkleber (Cyanoacrylate glue), UHU GmbH, Bühl, Germany

2.1.7 Software

Amira, Visage Imaging GmbH, Berlin, Germany

Adobe Illustrator, Adobe Systems GmbH, Germany

CorelDRAW X5, Corel Corporation, Germany

Corel PHOTO-PAINT X5, Corel Corporation, Germany

Matlab, Mathworks, Natick, USA

Neurolucida Explorer (for reconstruction analysis), MicroBrightFields Inc., USA

Neurolucida Software (for 3D reconstructions), MicroBrightField Inc., USA

NeuronRegistrator, MPI for Medical Research, Heidelberg, Germany

SigmaPlot, Systat Software GmbH, Erkrath, Germany

Visiview (image acquisition software), Visitron Imaging GmbH, Puchheim, Germany

2.1.8 Surgical Instruments

1 ml syringe, Braun, Melsungen, Germany

10 ml syringe, Braun, Melsungen, Germany

Forceps, VWR, Germany

Neolus 23 gauge needle, Terumo Corporation, Leuven, Belgium

Neolus 26 gauge needle, Terumo Corporation, Leuven, Belgium

Scissors FST 14094-11, Fine Science Tools, Germany

Scissors FST 14130-17, Fine Science Tools, Germany

Spatula, VWR, Germany

2.1.9 Water bath

Julabo U3, Julabo Labortechnik GmbH, Seelbach, Germany

2.2 Methods

2.2.1 Recipes of solutions

Table 2.1: Choline ACSF for slicing

Substance	Molarity (mM)	Concentration (g l^{-1})
Choline chloride	110	15.36
Potassium chloride	2.5	0.19
Sodium carbonate	25	2.10
Sodium biphosphate	1.25	0.17
Calcium chloride	0.5	0.07
Magnesium chloride	7	1.423
D-Glucose	25	4.95
Sodium ascorbate	11.6	2.30
Sodium pyruvate	3.1	0.341

The solution was adjusted to pH 7.4 and osmolarity was ~305 mOsm.

Table 2.2: HEPES ACSF for incubation

Substance	Molarity (mM)	Concentration (g l^{-1})
Sodium chloride	125	7.3
Potassium chloride	2.5	0.19
Sodium carbonate	20	1.68
Sodium biphosphate	1.25	0.17
Calcium chloride	1	0.15
Magnesium chloride	2	0.41
D-Glucose	25	4.95
HEPES	5	1.19

The solution was adjusted to pH 7.4 and osmolarity was ~305-320 mOsm.

Table 2.3: Pipette Internal Solution

Substance	Molarity (mM)	Concentration (g l^{-1})
Potassium gluconate	135	31.68
Sodium phosphocreatine	10	2.52
Potassium chloride	4	0.30
ATP – Magnesium salt	4	2.02
GTP	0.3	0.146
HEPES	10	2.38

The solution was adjusted to pH 7.2 and the osmolarity was ~210 mOsm.

2.2.2 Experimental protocol

All experiments were conducted according to the German animal welfare regulations and that of the Max Planck Institute of Neurobiology, Martinsried. Mice of both sex and post natal age 28 days were either divided into control group or whisker trimmed group. GLT mice, described previously, were used for the studies on layer Vb neurons. A schematic of the experimental protocol is shown in figure 2-1.

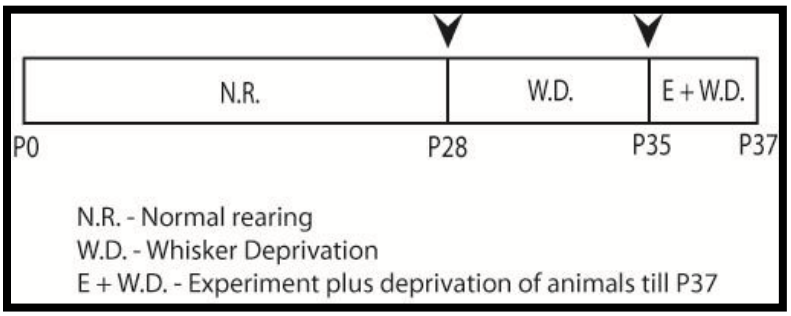

Figure 2-1: **The experimental protocol.** GLT mice were used for this study. The animals were allowed normal rearing till the age of post-natal day 28 (P28) and then divided into either the control group or the whisker trimmed group. Whiskers on both mystacial pads of animals from the control group were trimmed till P35-37. The control animals were allowed undisturbed normal rearing till P35-37. All animals were sacrificed within the age window of P35-37.

2.2.3 *BAC*-transgenic mice

Glt25d2 BAC-EGFP transgenic mice, that expressed EGFP in a subpopulation of layer Vb thick-tufted neurons using the well-established bacterial artificial chromosome (BAC) method (Gong et al., 2002, Gong et al., 2007, Gong et al., 2010), were obtained from the GENSAT project at the Rockefeller University, New York (Gong et al., 2003, Heintz, 2004). These mice were used for studying layer Vb cells in the barrel cortex and the vibrissal motor cortex. More information on the expression of EGFP in these mice and their genetic make-up is available on the GENSAT project website (www.gensat.org). Experiments were performed on the offsprings of BAC-EGFP positive parents.

2.2.4 Whisker trimming

The animals in the trimmed group were deprived of their whiskers on both mystacial pads starting P28 days of age. The mystacial hairs were cut down as close to the skin as possible with a

pair of small scissors. The animals were grabbed at their neck in order to carry out the trimming of whiskers. The whole process was carried out in sterile conditions with controlled laminar airflow. Trimming was carried out for 8-10 days. No anaesthesia was used during the trimming process. The trimmed animals were housed with their trimmed littermates in cages with a maximum of six animals per cage.

2.2.5 Control animals

Glt animals that comprised the control group were likewise housed with their control littermates in cages with a maximum of six animals per cage. They were not subjected to sham trimming but were handled identically as the trimmed animals.

2.2.6 Preparation of biocytin solution

2mg biocytin powder was added to a 2ml reaction tube containing 1 ml of pipette internal solution followed by a brief vortexing. Then it was placed in an ultrasonographic cleaner machine for about a minute at 37 °C. This was usually enough for the biocytin powder to be dissolved in the internal solution. Subsequently, the solution was filtered through 0.2 μm cellulose acetate filters and kept wrapped in aluminium foil for use during the experiment.

2.2.7 Preparation of acute brain slices

2.2.7.1 Thalamocortical slices for barrel cortex

Animals in the age group of P35-P37 were sacrificed for slice preparation. The mice were put in a 3l bell jar with about 0.4 ml isoflurane to anaesthetise them sufficiently for the subsequent procedures. When the mice stopped moving, a quick intra-peritoneal injection of 7% chloral hydrate solution was administered taking care not to puncture any internal organs. Ideally about 300 mg Chloral hydrate per kilogram body weight was used. The mice were then laid on their backs in the cage and constantly checked for the disappearance of the toe reflex on pinching. When the toe reflex was totally abolished, the animal was transferred to the dissecting platform made of styrofoam. Next, the limbs were tightly pinned to the platform using dissecting pins. The skin was cut open along the longitudinal axis near the thoracic cavity just enough to allow hindrance-free perfusion. A very quick opening in the thoracic cavity was made taking care not to puncture either the heart or the lungs. A quick cut of the vein supplying the blood back to the heart was made to drain out the blood. Immediately, 10 ml of ice-cold choline-ACSF (for slicing) pre-bubbled with 95% O_2 and 5% CO_2 (carbogenated) was then injected into the right ventricle at a steady rate taking care not to move the needle much during the process. A successful perfusion was accompanied by an involuntary twitching of the tail of the animal.

The animal was then decapitated and the brain was swiftly dissected out of the skull cavity. The brain was then placed on an elevated 10° ramp with horizontal slits at an angle of 55° to the right of the anterior-posterior axis of the brain (or simply 45° to the horizontal x-axis) for a shaving blade to pass through. A blade was used to cut away the anterior one-third of the brain at an angle of 45° to the horizontal axis (figure 2-2). The plane of the cut was thus determined by both the 10° tilt of the ramp and the blade angle of 45°. The posterior two-third of the brain was then glued to the slicing platform with the cut-face down using cyanoacrylate glue. The platform was then transferred to the slicing chamber containing ice-cold carbogenated choline-ACSF.

Thalamocortical slices of the right hemisphere containing the somatosensory cortex and the thalamus were obtained with a thickness of 300 µm with a vibrotome according to established procedure (Agmon and Connors, 1991).

The vibrotome blade had an inclination of 15° and was set to a forward velocity of 1.2 mm/s and an oscillation of 75 Hz. The amplitude of vibration was set to 1.2 mm. The slicing plane was parallel to the barrel arcs. The slices were kept for experiments only after cutting away 2.3 mm of

tissue. Thereafter, 4 slices were accepted for experiment out of which only the first three were mostly used for experiment.

2.2.7.2 Coronal slices of vibrissa motor cortex

The initial procedure was the same as described above. After removal, the brain was placed on a 10° ramp with the anterior face uphill to optimise alignment of the apical dendrites with the slice surface (figure 2-2). This is necessary because of the location of vibrissa motor cortex at the bend of cortical convexity. A handheld razor blade was then used to make a cut through the tissue at an angle of 90° to the posterior-anterior axis of the brain, intersecting this axis at about its anterior two-third. The tissue rostral to the cut was used for slicing with the cut surface glued onto the vibrotome stage with the pia (dorsal surface) facing the blade.

Figure 2-2: **The cutting ramps.** 10° ramp top (used for motor cortex slices) and 10° ramp with 45° to x-axis slits for thalamocortical slices (of barrel cortex).

Starting from the topmost surface (rostro-caudal axis), 1.2 mm of tissue was cut off to expose the primary motor cortex area of interest. Subsequently, three slices of 300µm width were used for experiments. Both hemispheres were used. The third pair of slices was seldom used as usually, the first two pairs sufficed. This corresponded to ≈ 0.7-1.3 mm anterior to *bregma* and the slices typically had a fused *corpus callosum* (Hooks et al., 2011, Mao et al., 2011). The range of the vibrissal motor cortex was from ≈ 0.5-1.75 mm lateral of the midline (Hooks et al., 2011).

2.2.8 Cell filling using voltage clamp configuration

Layer Vb thick tufted neurons in both barrel cortex and the vibrissal motor cortex of Glt mice were readily identified because of their EGFP fluorescence when exposed to 488 nm light. Identified cells were then approached using patch pipettes (tip resistance ideally between 2-5 MΩ) filled with internal solution and biocytin under diffraction interference contrast optics (DIC). Under voltage clamp, whole cell configuration was first achieved along with the establishment of a giga-seal, following which the cell membrane patch was broken through to let the cell get loaded with biocytin.

Having achieved the membrane break-in, the cells were allowed to be loaded with the biocytin by passive diffusion for 20-30 minutes. It was usual for the cell body to become visually unclear under DIC optics upon successful filling possibly owing to the change in refractive index of the cell. After the desired filling time, the patch pipette was slowly but steadily withdrawn from the cell body taking care to allow the membrane of the cell to snap shut again. Following the withdrawal of the pipette, the slices containing the cells were washed in the chamber off the superfluous biocytin for about 15-30 minutes.

2.2.9 Slice fixation

After wash-off of the excess extrastitial biocytin, the slices were carefully retrieved from the patching chamber and put in a 3 ml glass vial with 1.5-2 ml 4% paraformaldehyde solution in 0.1 M phosphate buffer and stored at 4°C for 1-2 days. Only one slice was stored per vial. Subsequently, the slices were removed from the fixative and stored in a 24 well cell culture plate immersed in 0.1 M phosphate buffer until staining.

2.2.10 Staining for cytochrome oxidase to visualize barrels

Staining for the mitochondrial enzyme cytochrome oxidase is a commonly used method to visualize the barrels in the rodent somatosensory cortex. For this, the slices were washed thoroughly in phosphate buffer (0.1 M) thrice and for ten minutes each time. A mixture of 2-3 mg cytochrome C and 2 mg catalase was prepared in 10 ml of 0.1 M phosphate buffer. To this 0.286 ml of DAB solution was added from a stock solution containing 17.5 mg per ml DAB. 1.5 ml of this final mixture was then added to each well of the culture plate containing a slice and incubated at 37° C till the barrels became visible. Normally this took between 1-6 h depending on individual slices. Finally, each slice was washed in phosphate buffer for ten minutes and this step was repeated up to four times.

2.2.11 Staining for biocytin and mounting

The slices were stained using the DAB-avidin-biotin complex protocol (Horikawa and Armstrong, 1988) Before staining the slices for biocytin, each slice was washed in 0.1 M phosphate buffer three times for ten minutes each. The slices were then incubated in a 3% solution of H_2O_2 in 0.1 M phosphate buffer for 15 min, all the while keeping the culture plate containing the slices on a stirrer. After 15 minutes, the slices were washed thoroughly in phosphate buffer till the bubbles

from the peroxide reaction stopped appearing. The wash was repeated 6-8 times and for 10 min each time. Alongside this process, a solution containing the Vectastatin ELITE ABC system was prepared in a 1:100 dilution with 0.5% Triton in 0.1 M phosphate buffer. This would translate to one drop (~50 µl) each of the Vectastatin 'A' and 'B' reagents in 5 ml of the solution. This solution needed to be stirred for at least 30 min before use. Subsequently, the slices were incubated with 1.5 ml of solution per slice overnight at 4° C.

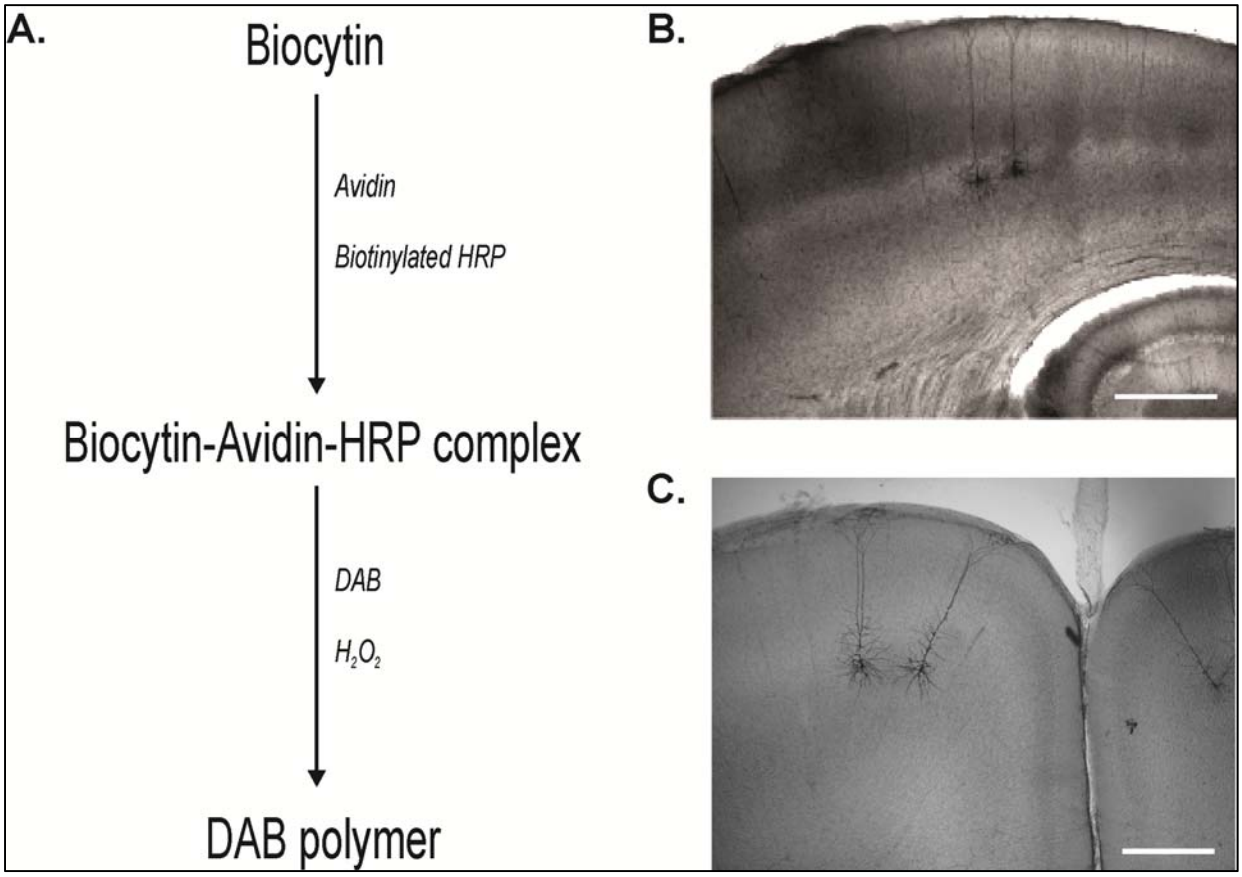

Figure 2-3: **The DAB-avidin-biotin staining reaction and its end product. A.** Schematic showing the chemical reactions during the DAB-ABC staining for biocytin resulting in darkly stained cells on a clear background as shown in adjacent photographs (*HRP* and *DAB* abbreviated in the figure stand for respectively *horseradish peroxidase* and 3,3'-Diaminobenzidene). **B.** An example of biocytin stained cells in thalamocortical slice of mouse vibrissa somatosensory cortex (scale bar 500 µm). **C.** An example of biocytin stained cells in mouse vibrissa motor cortex (scale bar 500 µm).

The next step of staining began with the washing the slices well with phosphate buffer at room temperature. This was repeated about six times with 10-15 min each time. The slices were then immersed in 1.5 ml each of a DAB solution containing 0.7gm/ml DAB and incubated in the dark for exactly 25 minutes. Following incubation, 3.3 µl of H_2O_2 from a 1:100 dilute solution was added to each well containing a slice and incubated till the cells appeared stained against a not too

dark background (Figure 2-3). Lastly, each slice was washed thoroughly with phosphate buffer multiple times. Next, the slices were mounted on a glass slide and covered with an ultra-thin cover slip using Mowiol as mounting medium.

2.2.12 3D reconstructions of cells

Reconstructions of biocytin stained cells were made using the Neurolucida software under 100X magnification. Neurolucida is a computer based tracing software along the lines of the manually operated *Camera Lucida*, except that it is semi-automated and does not involve a pen and paper based tracing. One can see the filled cell on the computer monitor through a live camera feed and use the mouse to trace the processes of the cell by virtue of an interactive interface on the computer monitor. Apart from the cell, the approximate contours of the slice as well as layer IV boundaries were also traced. Consequently, the final raw tracing consisted of the cell body, the basal and the apical dendrites, the pia, the white matter, and the layer IV border with layer V. Also in cases of the somatosensory cortex cells, the barrel borders, wherever clearly visible, were traced to show the location of the cell relative to the barrel. In order to rule out experimenter bias in reconstructions, a random subset of cells were reconstructed double blind by two different experienced investigators and these values were then later compared with the original values.

Following Neurolucida reconstructions, the files were rotated so that the portion of the pia directly over the soma remained horizontal. Using the custom-made software NeuronRegistrator 1D, the files were then converted into a form readable by Amira to be used for 3D representation.

A summary of all the experimental steps is illustrated in the following schemata (figure 2-4).

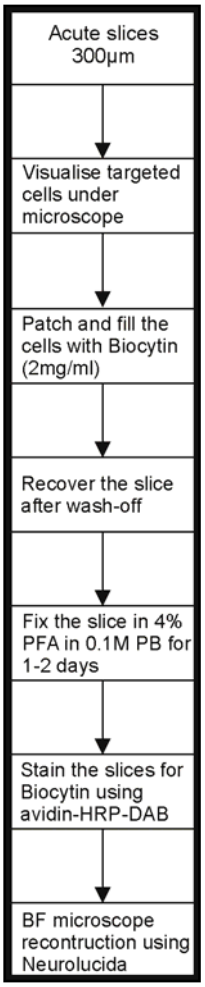

Figure 2-4: Schemata outlining the experimental steps involved.

2.2.13 Analysis of cell parameters

2.2.13.1 NeuroExplorer

The reconstructed cells in 3D were then analysed for the dendritic parameters using the NeuroLucida Explorer, the accompanying data analysis tool with Neurolucida.
Morphological parameters based on observed geometry, like, dendritic lengths, numbers of dendrites, branch points, endings and branch order were evaluated. The results were tabulated in an MS Office Excel file to be further evaluated and their mean values calculated and compared.

2.2.13.2 NeuronRegistrator2D

Following primary analyses with Neuroexplorer, the '*.asc*' format cells from Neurolucida were converted into '*.hoc*' file format using a custom-written MATLAB-based programme, *NeuronRegistrator2d*. Using an inbuilt converter called *NeuroConv*, this programme, apart from converting the file formats, could also align the cells, either with their soma referenced as the origin or the pia referenced as the origin. This was respectively called, soma-centred or pia-centred. This programme also has the ability, on being fed with soma depth and contour measurements, to scale the cells (thereby converting them to registered 2D .hoc files) to mean pia-WM distances or using scale factors provided by the user.

2.2.13.3 Rembrandt3D v1.0

Once the cells were converted into appropriate formats compatible with the custom-written programme, Rembrandt, the next step was to analyse the dendritic lengths of the cells. Rembrandt achieved this by calculating the quantity of dendrites in a bin volume of 50 μm^3 along the entire length of a cell. It could do this for each individual cell or for a pool of cells grouped together. What resulted was a linear two column output Microsoft Excel sheet containing the dendritic length contained in every 50 μm^3 bin size. It also generated and integral value of the all the bin-wise dendritic lengths to give the total length of dendrites for every cell. However, Rembrandt was unable to distinguish between dendrite sub compartments, e.g. basal, apical or oblique.

2.2.13.4 Rothko v041

To visualise the quantitative dendritic distribution of a cell along the vertical span of the cell, it's 2D dendritic profile (also called the *dendritic z-profile*), the result/output sheet generated with Rembrandt was fed to another custom-written MATLAB based programme Rothko, which spewed line plots and grayscale colour plots of the z-profiles after linear interpolation and a sliding mean filter based smoothing of the plots.

2.2.14 Statistical analyses

All statistical analyses used in this study like, T-test, one-way analysis of variance (ANOVA), Mann Whitney rank sum test (in case of non-normal distributions) were performed using SigmaPlot 11.0 software. The dendritic parameters were imported from Microsoft Excel files into SigmaPlot data sheet and could be then used for statistical analyses. All data were displayed as the mean values with the standard deviation. A p-value of $p \leq 0.05$ was considered to be significant.
All data were plotted into vertical dot plots also using the software SigmaPlot.

3 Results

In order to investigate the role of sensory information in the shaping of an adult neuronal network, or the extent of experience-dependent structural plasticity in adult networks, I proceeded with the study of the dendritic patterns of an identified cell genotype in control animals. Using the well-established bacterial artificial chromosome (BAC) method (Gong et al., 2002, Gong et al., 2007, Gong et al., 2010), in the GLT mouse line with a C57Bl/6 background (developed under the GENSAT project at the Rockefeller University, USA; www.gensat.org), EGFP was expressed under the control of the promoter for the enzyme glycosyltransferase 25 domain containing 2 (GLT or glt25d2), characteristically found in a subpopulation of the thick-tufted neocortical pyramids occurring in layer Vb (Gong et al., 2003, Heintz, 2004). The GLT-pyramidal cells constituted about 12% of all neurons in layer Vb (Groh et al., 2010). These cells are typified by a thick apical tuft, which eventually fans out wide on reaching the piamater. Hence, the name thick-tufted pyramidal cell is interchangeably used for these cells in this thesis.

In the initial part of the results section, I would present the individual cell galleries along with their depth parameters and contour measurements. Subsequently, I would present the morphological differences at the level of the dendrites between the different experimental conditions and cortical regions.

3.1 Depth distributions and cell galleries

Following the filling, staining and embedding methods described in chapter 'Materials and Methods', the cells were placed under a light microscope and reconstructed using the tracing software Neurolucida. Thus, complete datasets were established for the layer Vb thick-tufted GLT cells from the primary somatosensory cortex in animals both from control and whisker trimmed (sensory deprived) groups. Similarly, datasets of GLT cells were accumulated from the vibrissal motor cortex of both control and whisker trimmed cells. The final datasets of primary somatosensory cortex cells from control and trimmed groups consisted of respectively 31 cells (14 animals) and 36 cells (7 animals). The data set of GLT cells from vibrissa motor cortex comprised of 28 cells (9 animals) from the control group and 29 cells (7 animals) from the trimmed group.

However, after the cells were reconstructed and their depth distributions along with the contours measured, it was evident that the cells differed considerably from each other in terms of soma depth, cortex thickness (pia-white matter distance) and layer IV (L4) depth. Plots of the depth

distributions of the various cell groups along with their contour distances are shown below. It might be worthwhile to note here that the motor cortex is characterized by the lack of a distinctive layer IV, which is why the layer IV distances in the corresponding plots are missing.

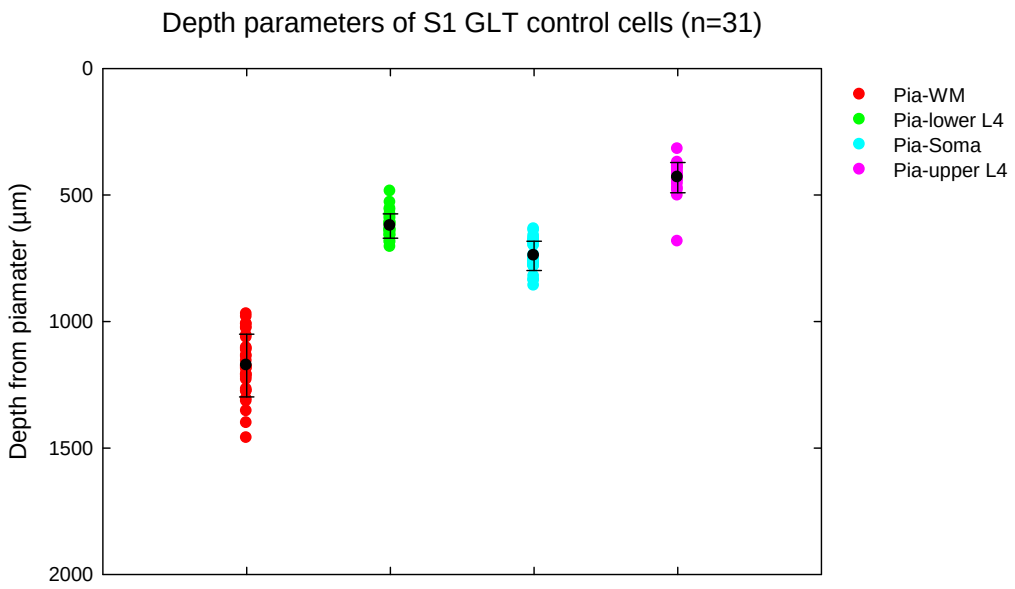

Figure 3-1: **Depth distributions of primary somatosensory cortex control cells.** The means are indicated by black circles and the standard deviations are shown by the tails.

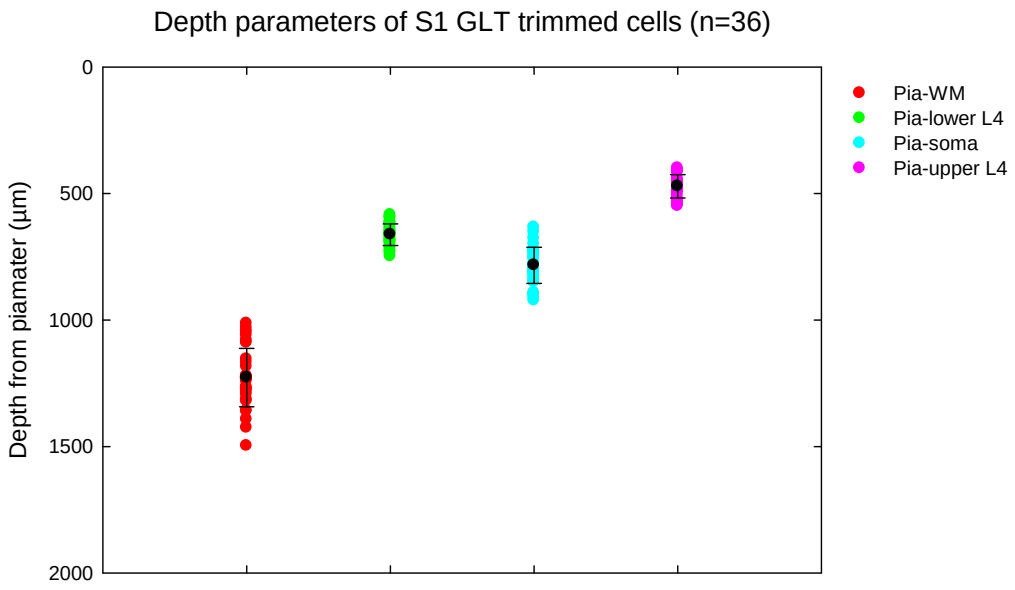

Figure 3-2: **Depth distributions of primary somatosensory cortex trimmed cells.** The means are indicated by black circles and the standard deviations are shown by the tails.

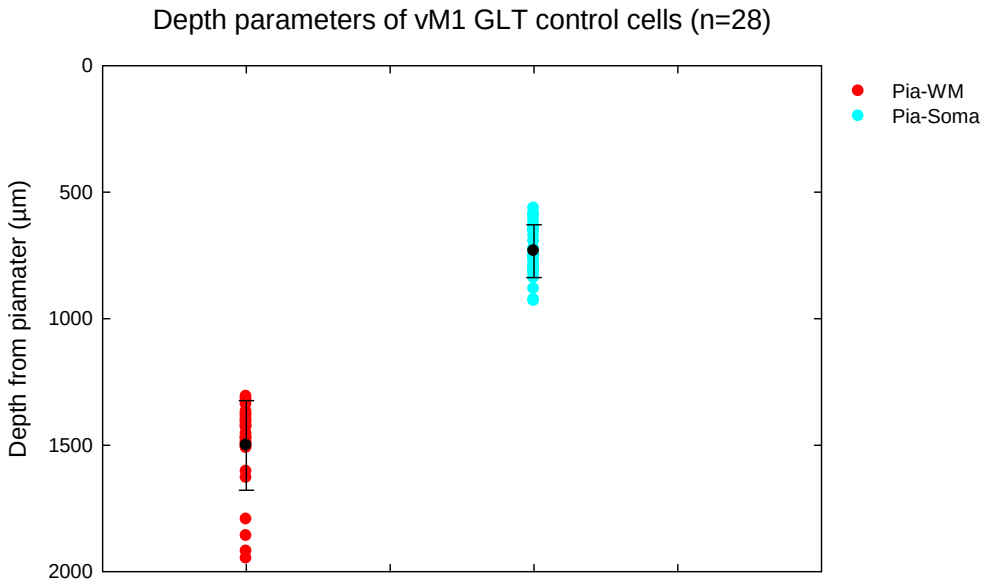

Figure 3-3: **Depth distributions of vibrissa motor cortex control cells.** The means are indicated by black circles and the standard deviations are shown by the tails.

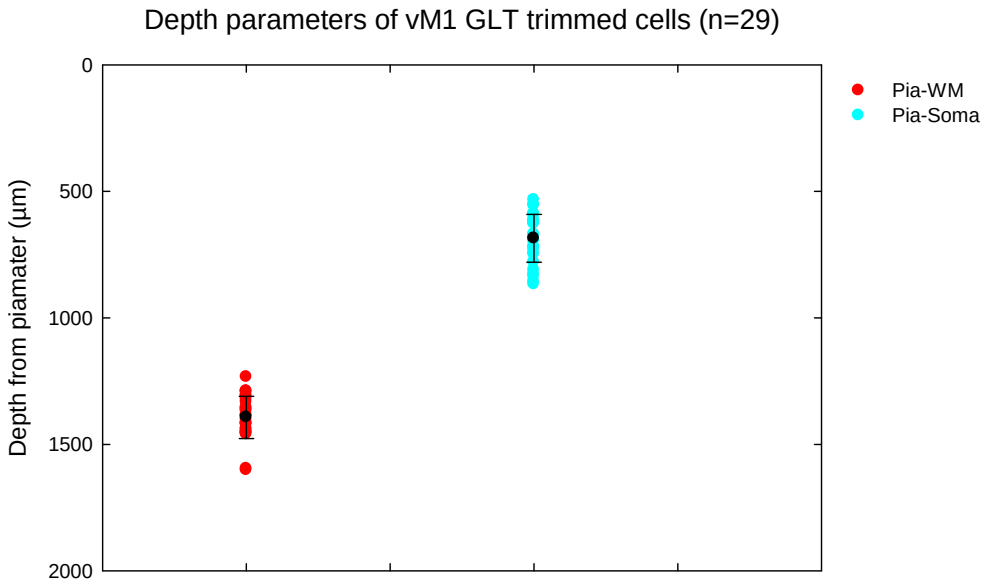

Figure 3-4: **Depth distributions of vibrissa motor cortex trimmed cells.** The means are indicated by black circles and the standard deviations are shown by the tails.

On average, the S1 GLT control cells had a soma depth of 741 ± 58 µm, pia-upper layer IV distance of 425 ± 39 µm, pia-lower layer IV distance of 629 ± 42 µm and pia-WM distance of 1174 ± 124 µm. On the other hand, the S1 GLT trimmed cells had a mean soma depth of 784 ± 72 µm, mean pia-upper layer IV distance of 472 ± 46 µm, mean pia-lower layer IV distance of 663 ± 42 µm and mean pia-WM distance of 1228 ± 116 µm.

The vibrissa motor cortex had a diffuse layer V distribution leading to a mean soma depth of 730 ± 107 µm for the control group of cells and 686 ± 95 µm for the trimmed group of cells. The average pia-WM distance for the control group was 1501 ± 177 µm and 1393 ± 83 µm for the trimmed group. However, in both the groups from vibrissa motor cortex, a pattern could be noticed: even while sometimes having similar pia-WM distances, some cells could have very variable soma depths. Thus, in-order to reduce this variability, I sub-divided the vM1 cells into two groups: upper and lower, depending whether their soma depths lay above or below 630 µm from the pia surface. Their depth distributions are shown separately in the figures (figures 3-5, 3-6, 3-7, 3-8) below. The average soma depths of the upper vM1 cells were respectively, 625 ± 25 µm and 609 ± 46 µm for control and trimmed groups while the respective pia-WM distances were 1417 ± 64 µm and 1367 ± 68 µm. In case of the lower vM1 cells, the soma depths and pia-WM distances were respectively, 809 ± 68 µm and 1564 ± 208 µm for the control group, while those for the trimmed cells were 757 ± 68 µm and 1418 ± 91 µm.

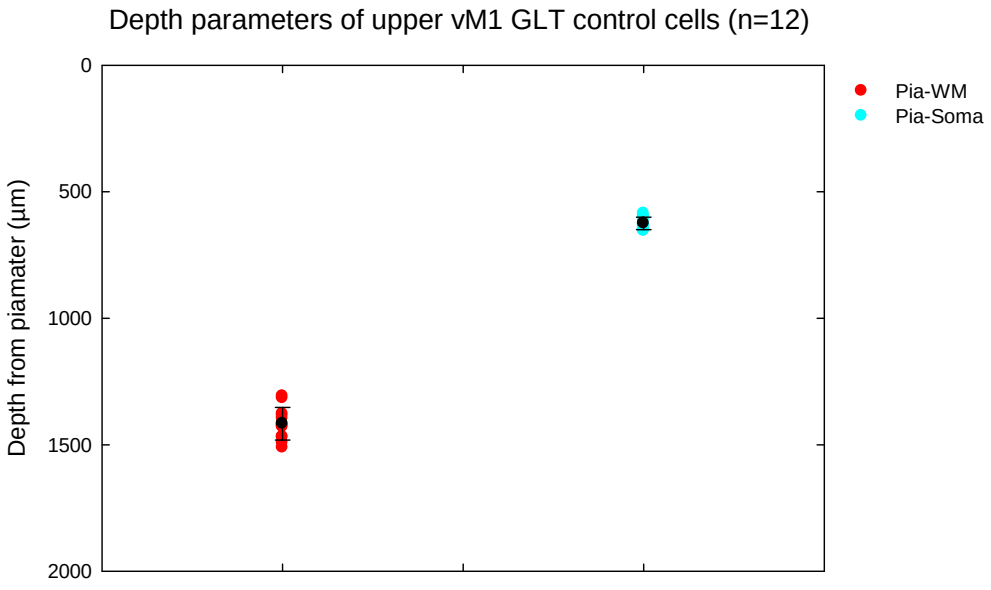

Figure 3-5: **Depth distributions of upper vibrissa motor cortex control cells.** The means are indicated by black circles and the standard deviations are shown by the tails.

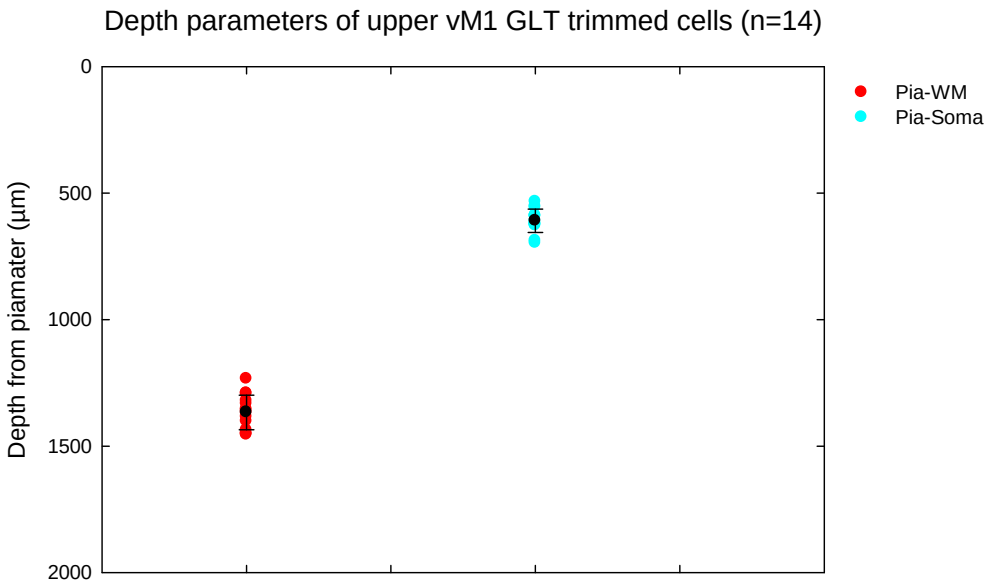

Figure 3-6: **Depth distributions of upper vibrissa motor cortex trimmed cells.** The means are indicated by black circles and the standard deviations are shown by the tails.

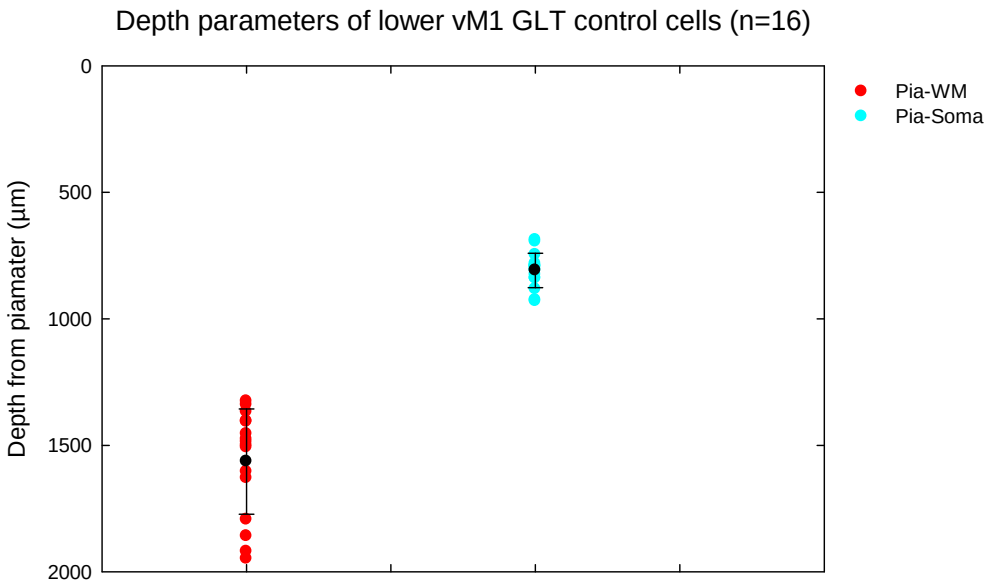

Figure 3-7: **Depth distributions of lower vibrissa motor cortex control cells.** The means are indicated by black circles and the standard deviations are shown by the tails.

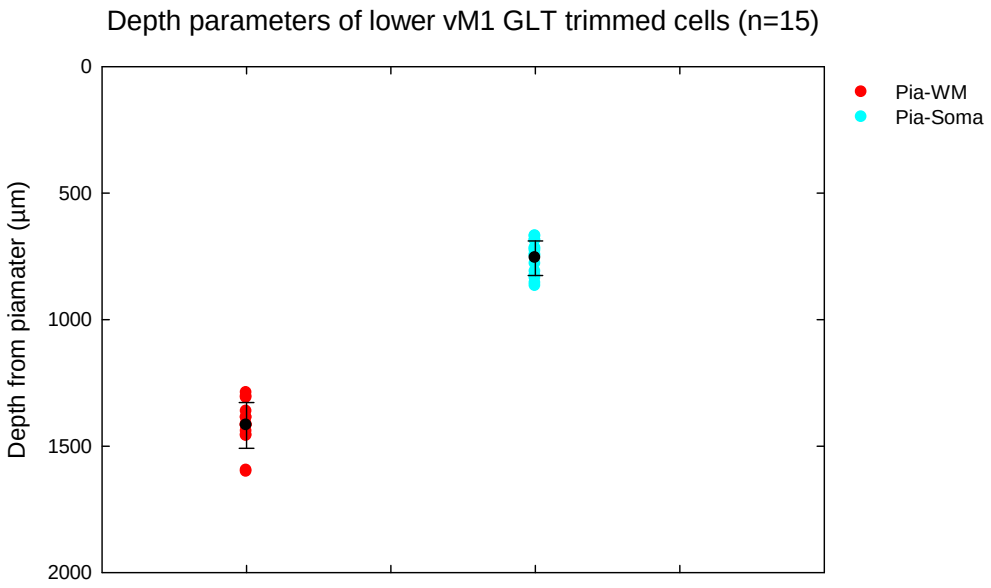

Figure 3-8: **Depth distributions of lower vibrissa motor cortex trimmed cells.** The means are indicated by black circles and the standard deviations are shown by the tails.

Thus, in order to buttress any analysis carried out on the original cells and to rule out any false-positive differences between groups, the cells were also normalized to the group-average pia-white matter (WM) distance. These normalisations were carried out on each cell individually.

To scale a cell, each individual pia-WM distance was divided by the group mean pia-WM distance to obtain the corresponding scaling factor. For viewing purposes, this scaling factor was simply fed into AMIRA to obtain a 3D scaled version of the cell. Similarly, the original depth and distance measurements were multiplied by the scaling factor to obtain the scaled depths and distances. Corroborative comparisons of different kinds of scaling are shown below.

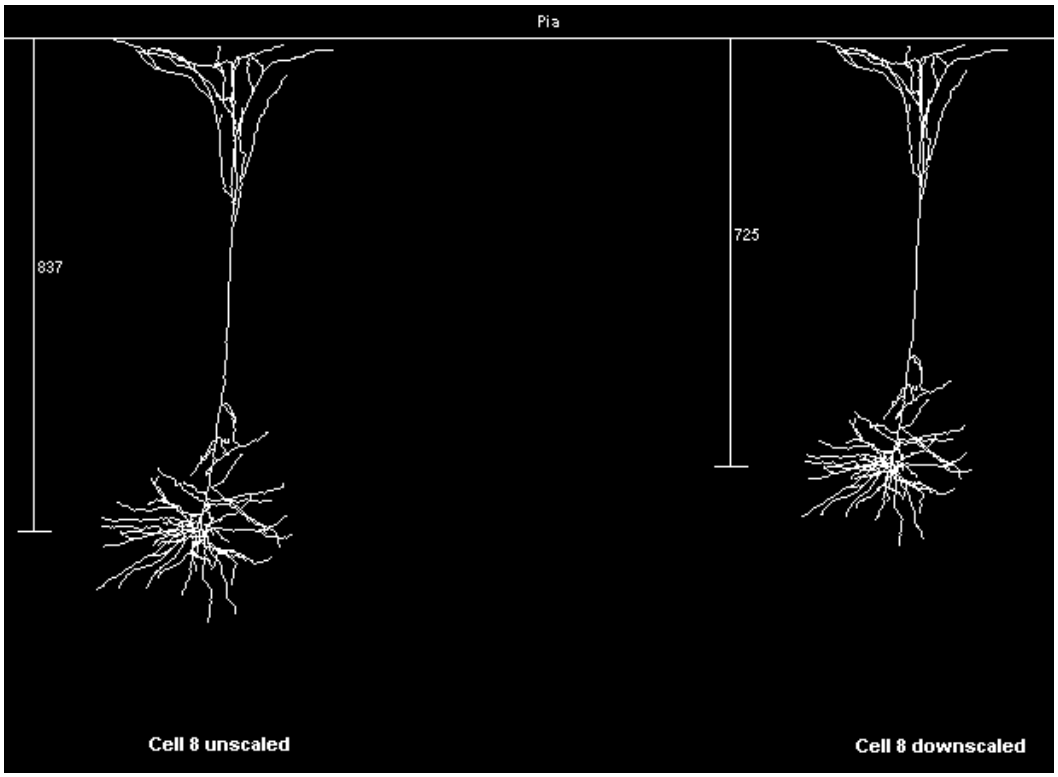

Figure 3-9: **A downscaled cell.** Comparison of an original unscaled cell with its downscaled version.

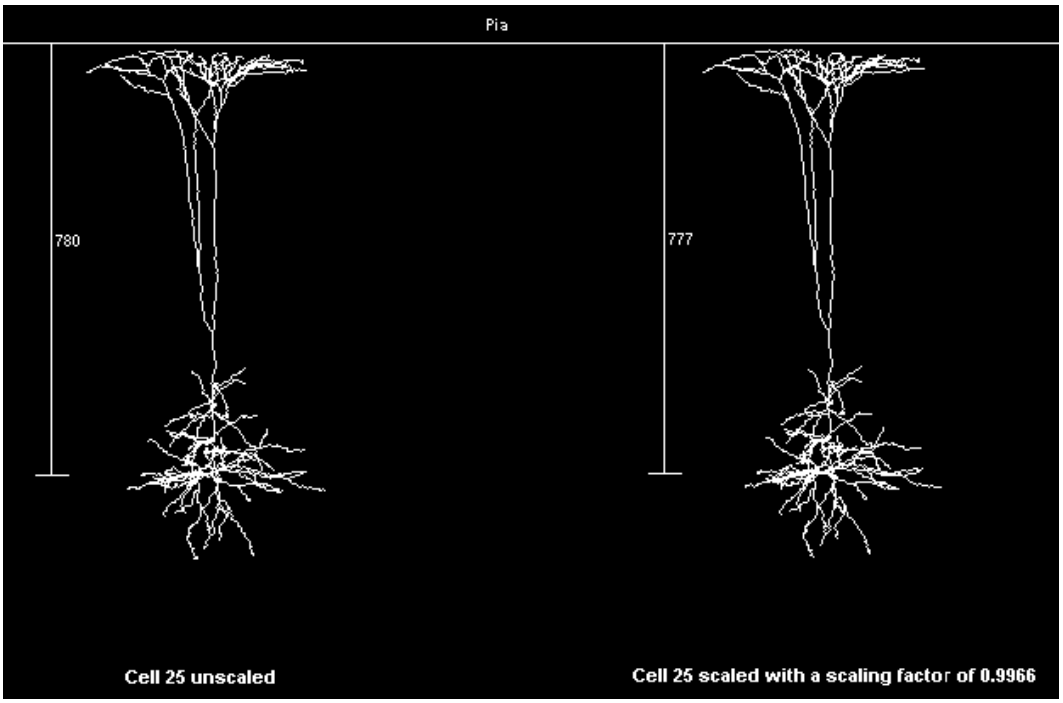

Figure 3-10: **An almost unscaled cell.** Comparison of an original unscaled cell with its negligibly scaled version.

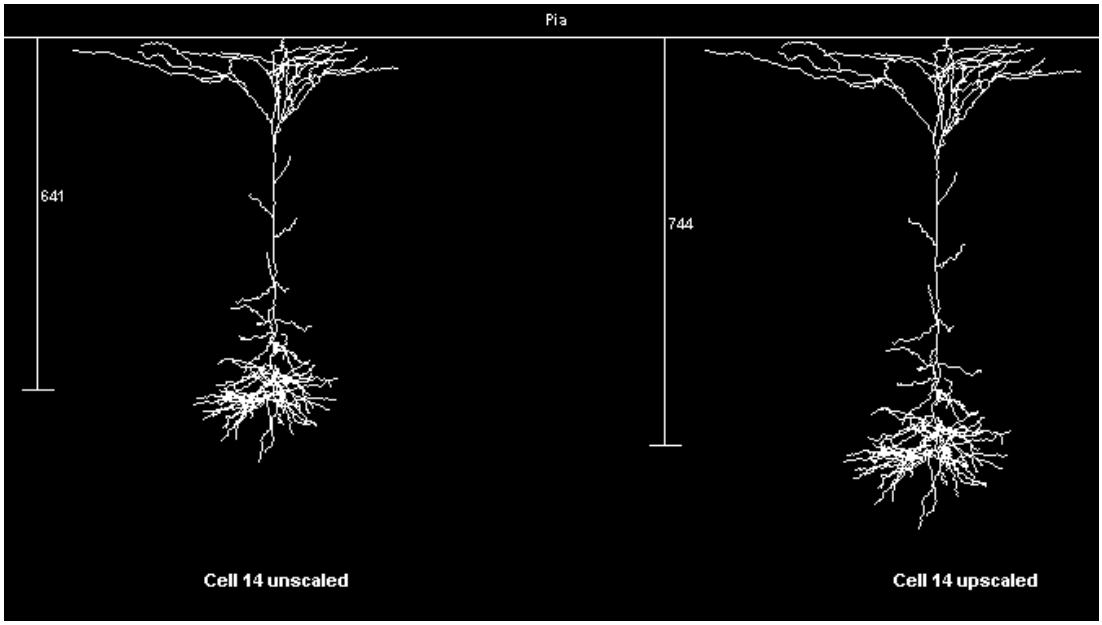

Figure 3-11: **An upscaled cell.** Comparison of an original unscaled cell with its upscaled version.

Also in order to make the analysis as accurate as possible the cells were also stripped off their apical dendrites, basal dendrites and soma, leaving just the oblique dendrites intact and ready to be analysed separately. This was necessary as the Neuroexplorer software used for the primary analyses of the dendritic parameters was unable to identify the oblique dendrites as separate entities. These oblique dendrites were then also scaled along the *x-, y-* and *z*-axes similar to the scaling of the complete cells as described above.

The following galleries (galleries 3.1.1.1 - 3.1.4.6, pages 38-73) present the original, unscaled cells comprising each cell groups from a soma-oriented and a tuft-oriented perspective. Each cell group is also shown with individual cell depths and contour distances indicated beside respective cells. Further, subsequent galleries show the scaled cells with their scaled distances indicated beside them. Lastly, the stripped oblique dendrites from each cell are also presented individually both as unscaled, originals and as scaled versions.

Gallery 3.1.1.1: Soma-centred overview of all unscaled cells comprising the primary barrel cortex (S1) GLT control data set.

(The gallery was displayed using the software AMIRA)

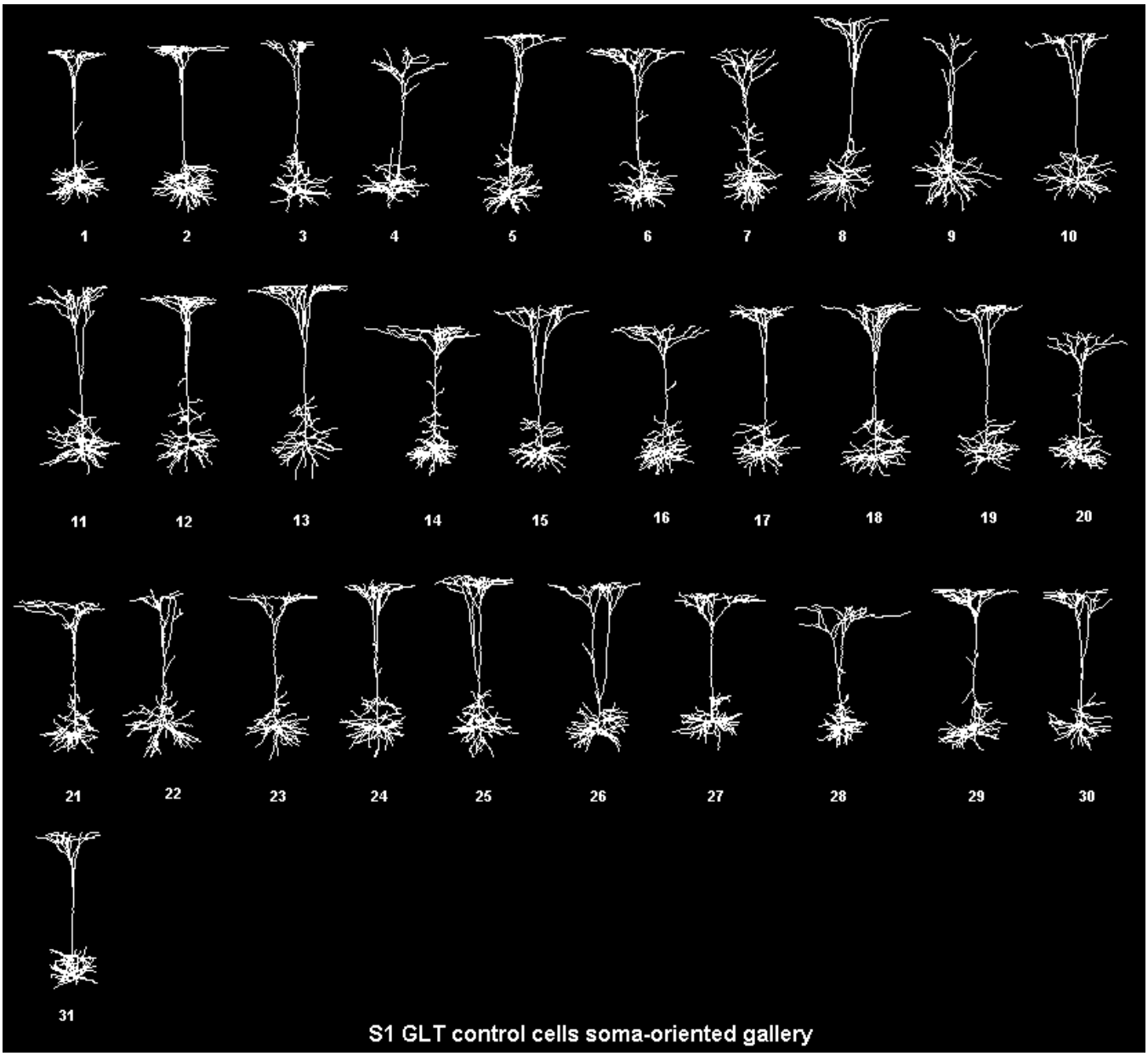

Gallery 3.1.1.2: Tuft-centred overview of all unscaled cells comprising the primary barrel cortex (S1) GLT control data set.

(The gallery was displayed using the software AMIRA)

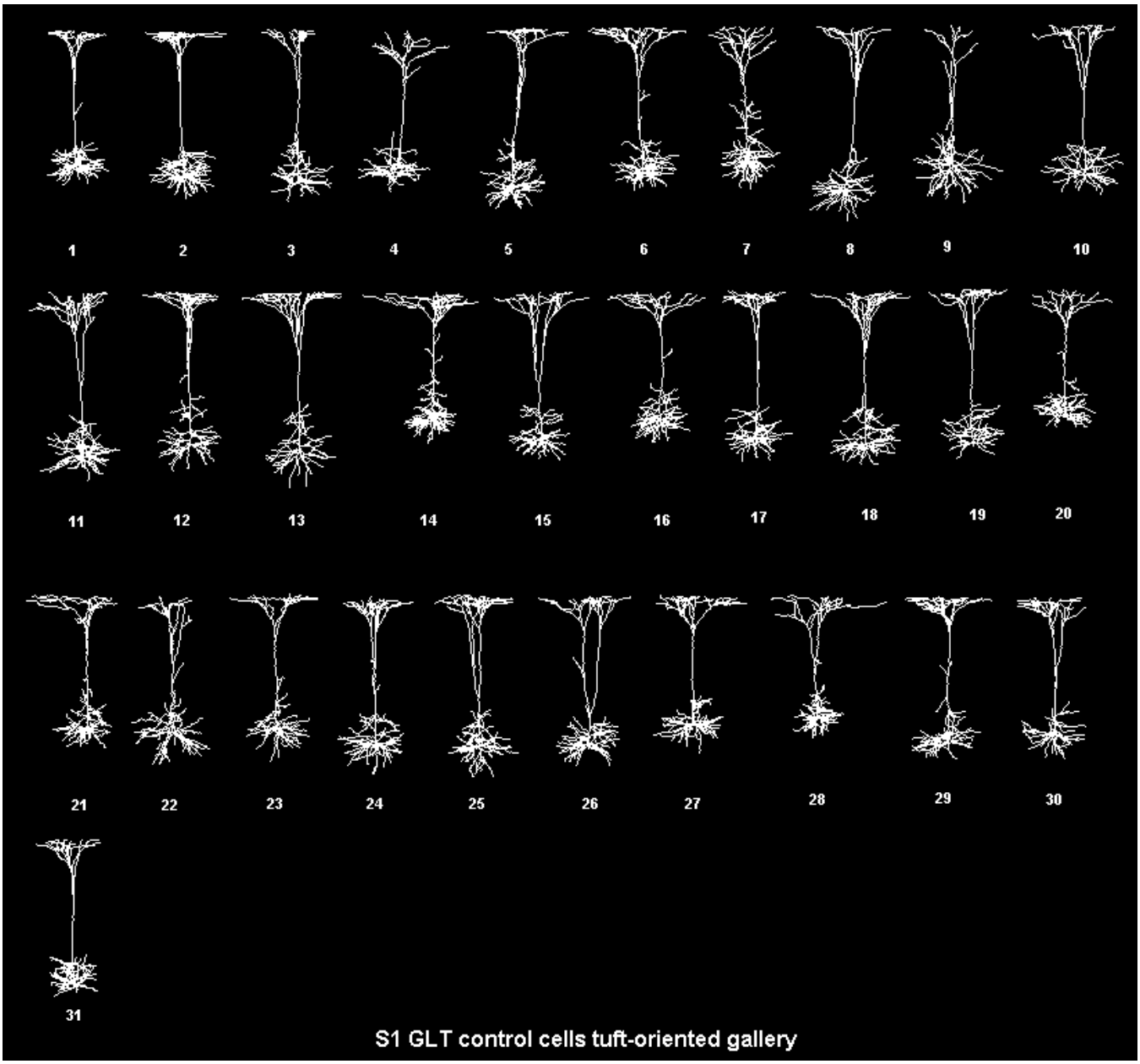

Gallery 3.1.1.3: Depiction of unscaled primary barrel cortex (S1) GLT control cells with the respective distances depicted alongside.

(The linear distances are respectively, pia-WM distance, pia-soma distance, layer IV boundaries (red) and pia-layer IV distance. The distances and gallery were displayed using the software AMIRA)

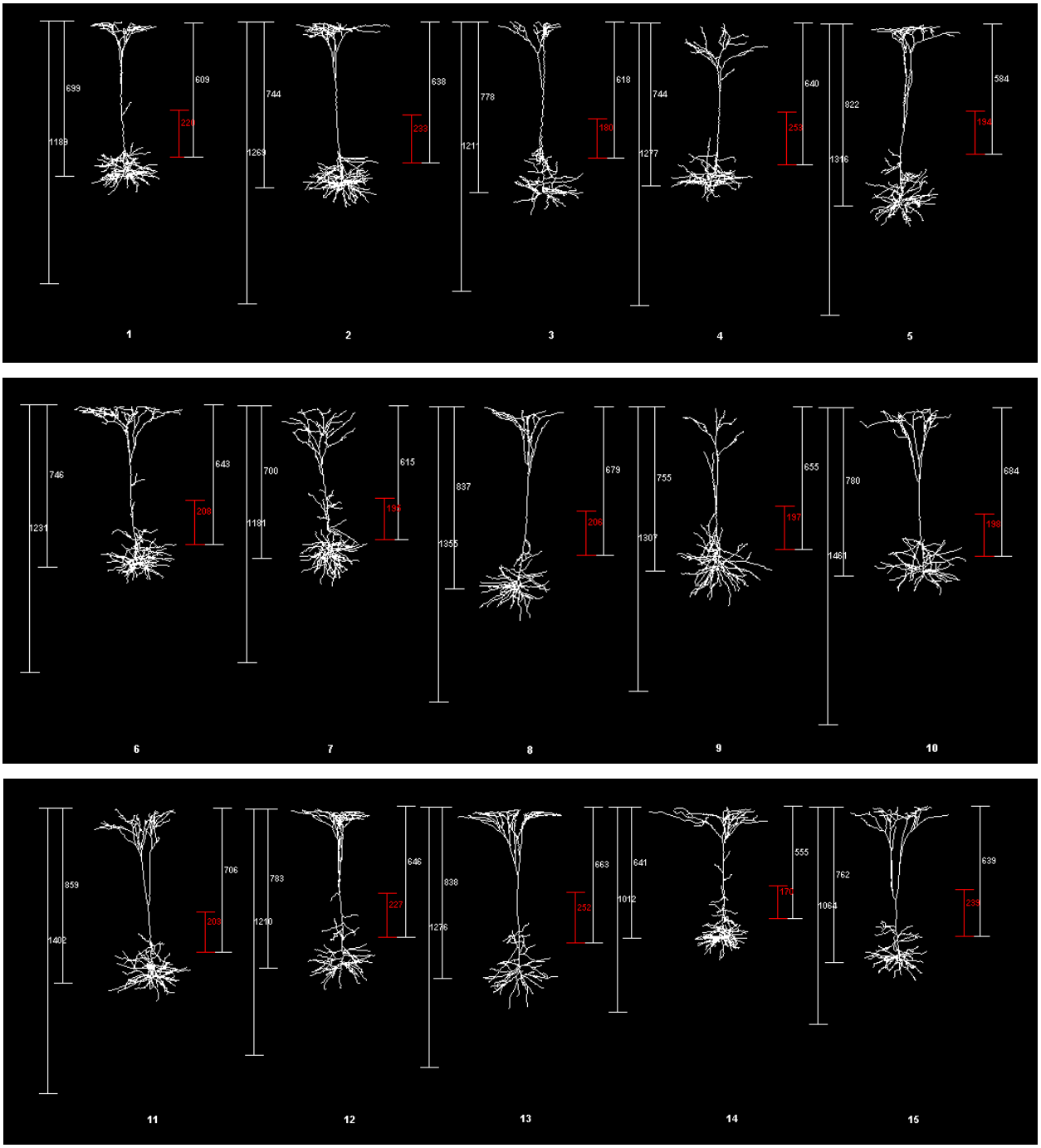

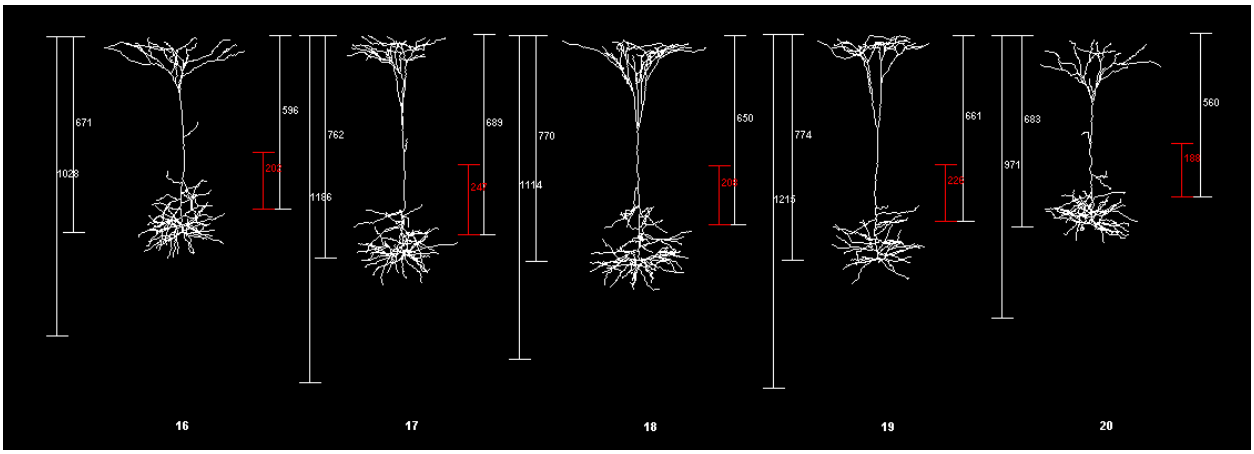
671
1028
596
203
762
1186
689
244
770
1114
650
203
774
1215
661
226
683
971
560
188
16
17
18
19
20

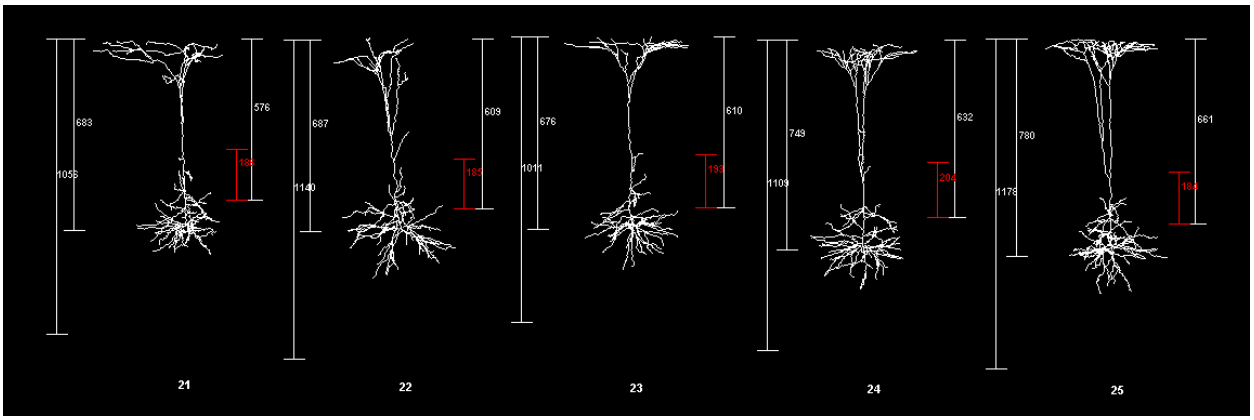
683
1056
576
188
687
1140
609
185
676
1011
610
193
749
1109
632
204
780
1178
661
188
21
22
23
24
25

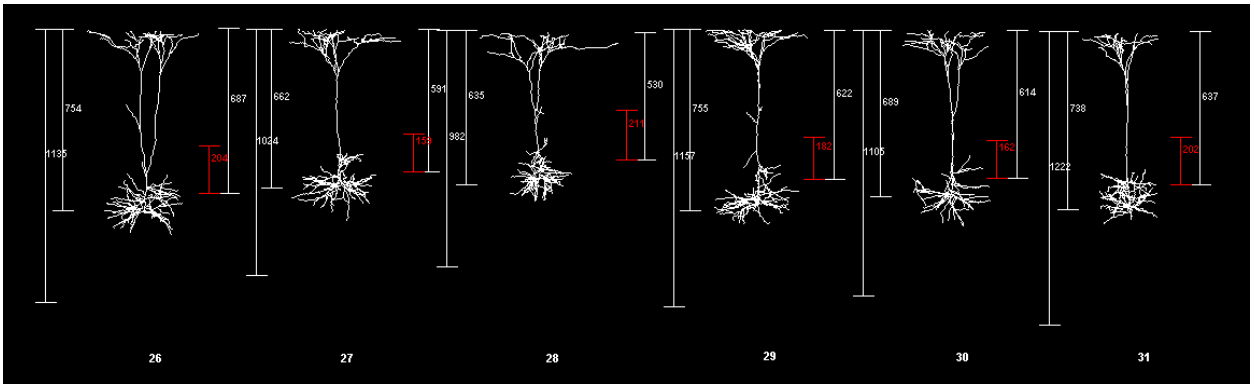
754
1135
687
204
662
1024
591
159
635
982
530
211
755
1157
622
182
689
1105
614
162
738
1222
637
202
26
27
28
29
30
31

Gallery 3.1.1.4: Depiction of scaled primary barrel cortex (S1) GLT control cells with the respective scaled distances depicted alongside.

(The linear distances are respectively, scaled pia-soma distance, scaled layer IV boundaries (red), scaled pia-layer IV distance and scaled pia-WM distance at the far right corner. The distances and gallery were displayed using the software AMIRA)

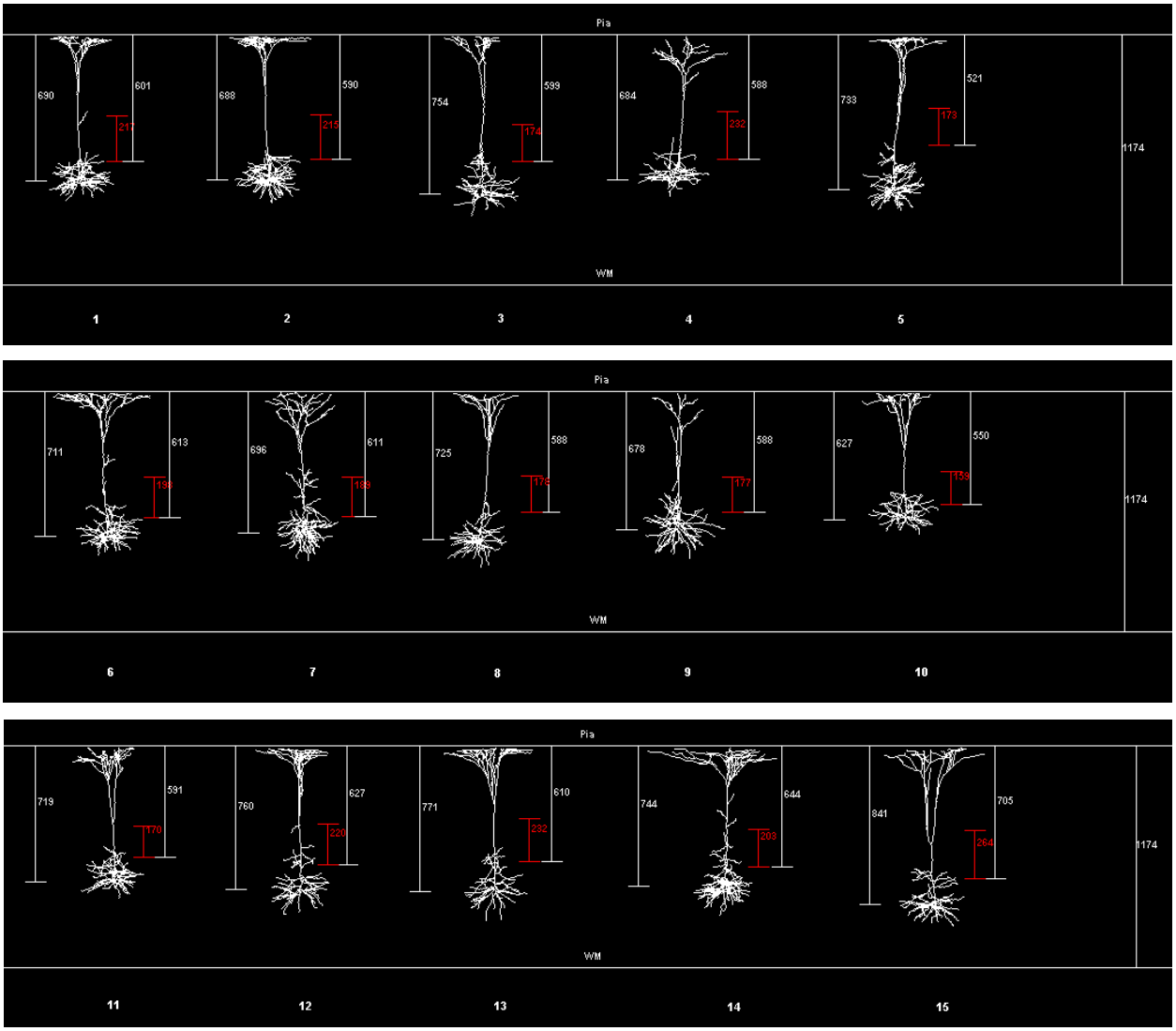

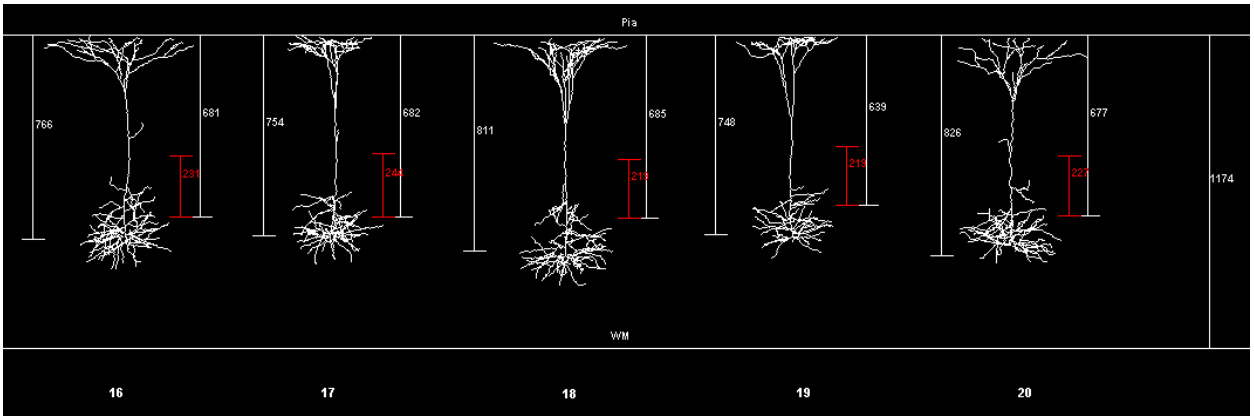
Pia
766
681
231
754
682
244
811
685
213
748
639
219
826
677
227
1174
WM
16
17
18
19
20

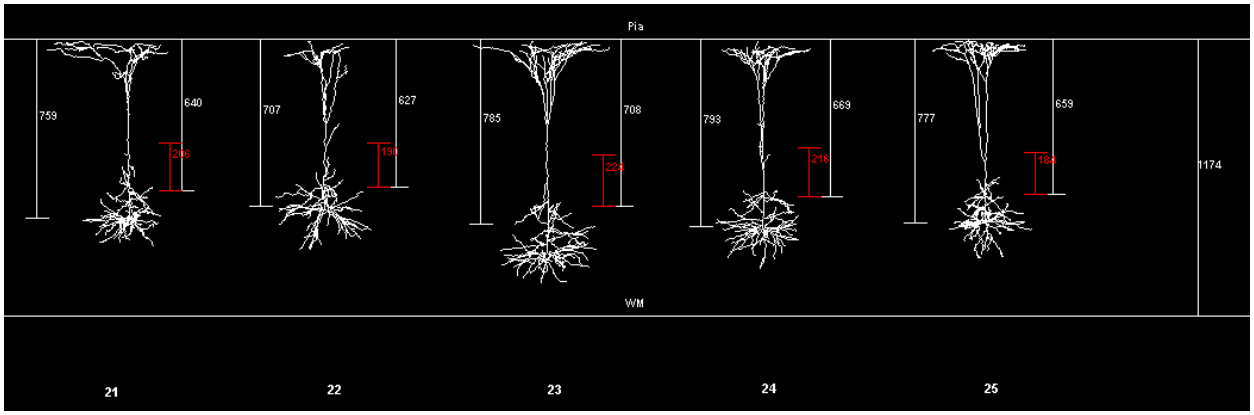
Pia
759
640
246
707
627
194
785
708
224
793
669
216
777
659
184
1174
WM
21
22
23
24
25

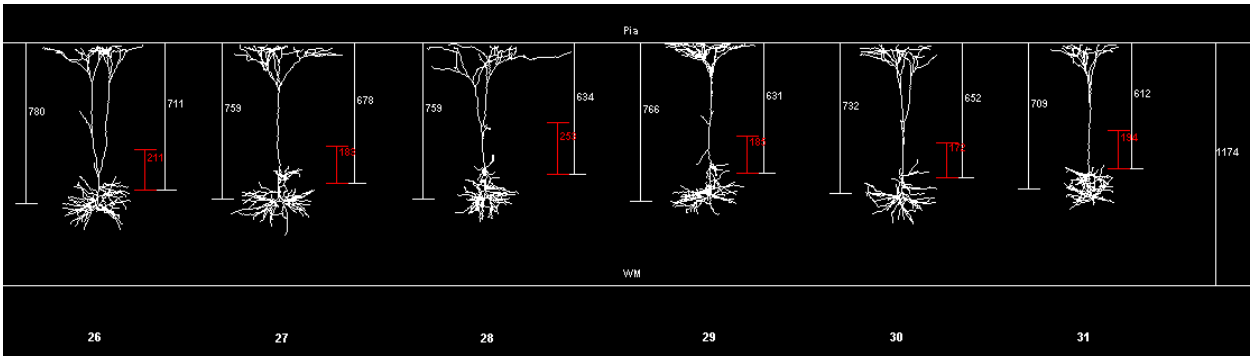
Pia
780
711
211
759
678
185
759
634
251
766
631
184
732
652
172
709
612
194
1174
WM
26
27
28
29
30
31

Gallery 3.1.1.5: Depiction of unscaled, stripped oblique dendrites of unscaled primary barrel cortex (S1) GLT control cells.

(The gallery was displayed using the software AMIRA)

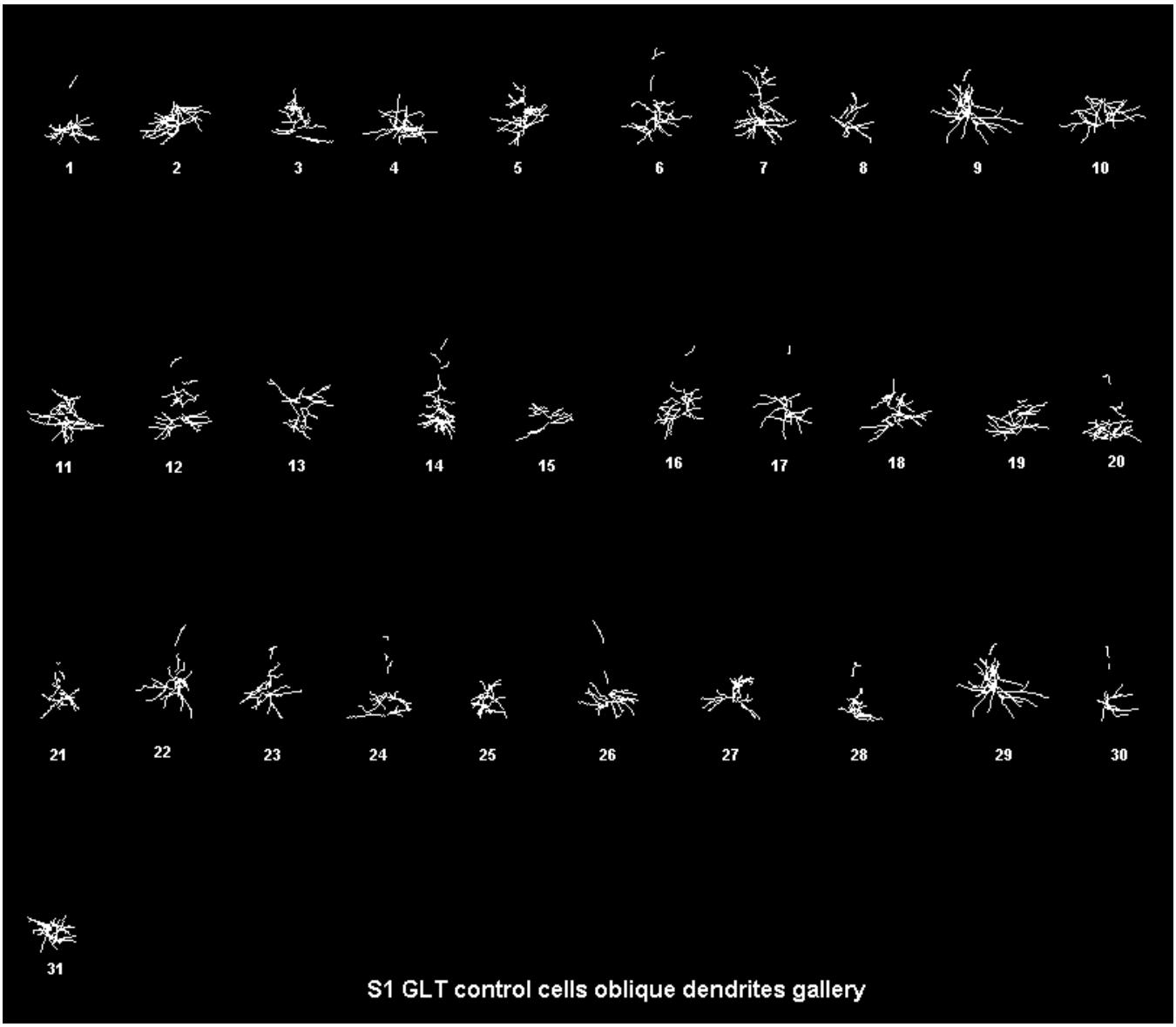

Gallery 3.1.1.6: Depiction of scaled, stripped oblique dendrites of scaled primary barrel cortex (S1) GLT control cells.

(The gallery was displayed using the software AMIRA)

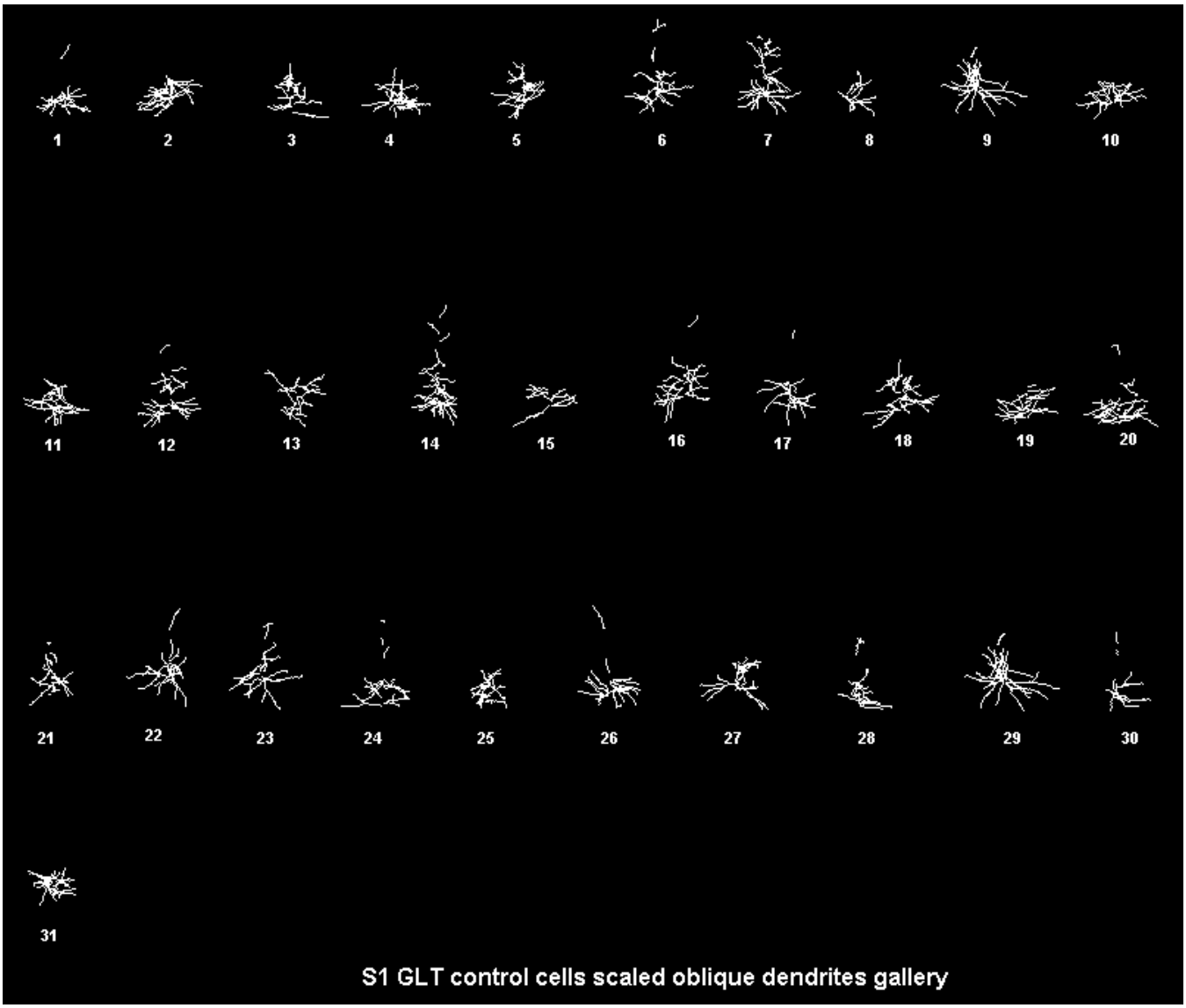

Gallery 3.1.2.1: Soma-centred overview of all unscaled cells comprising the primary barrel cortex (S1) GLT trimmed data set.

(The gallery was displayed using the software AMIRA)

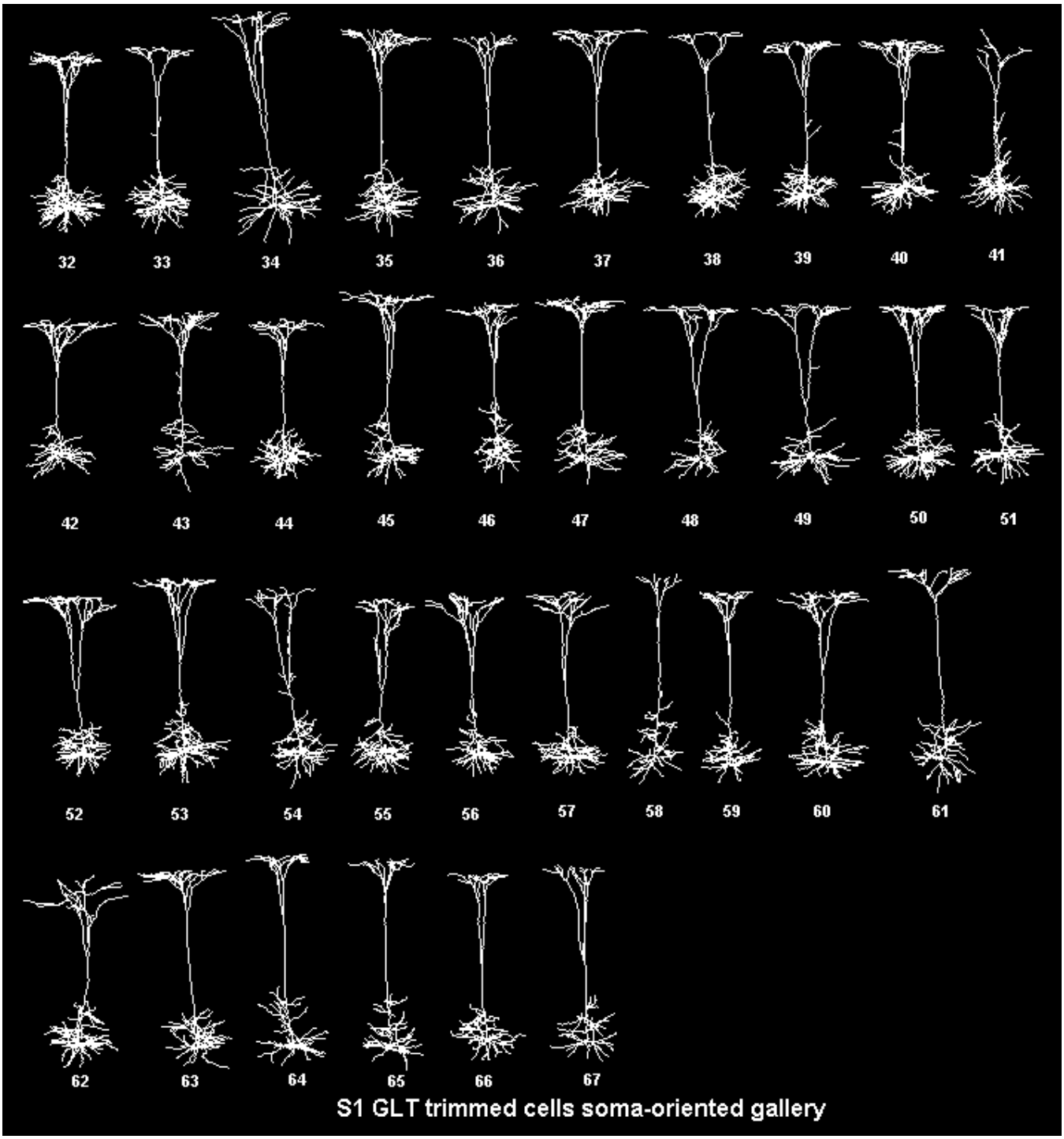

Gallery 3.1.2.2: Tuft-centred overview of all unscaled cells comprising the primary barrel cortex (S1) GLT trimmed data set.

(The gallery was displayed using the software AMIRA)

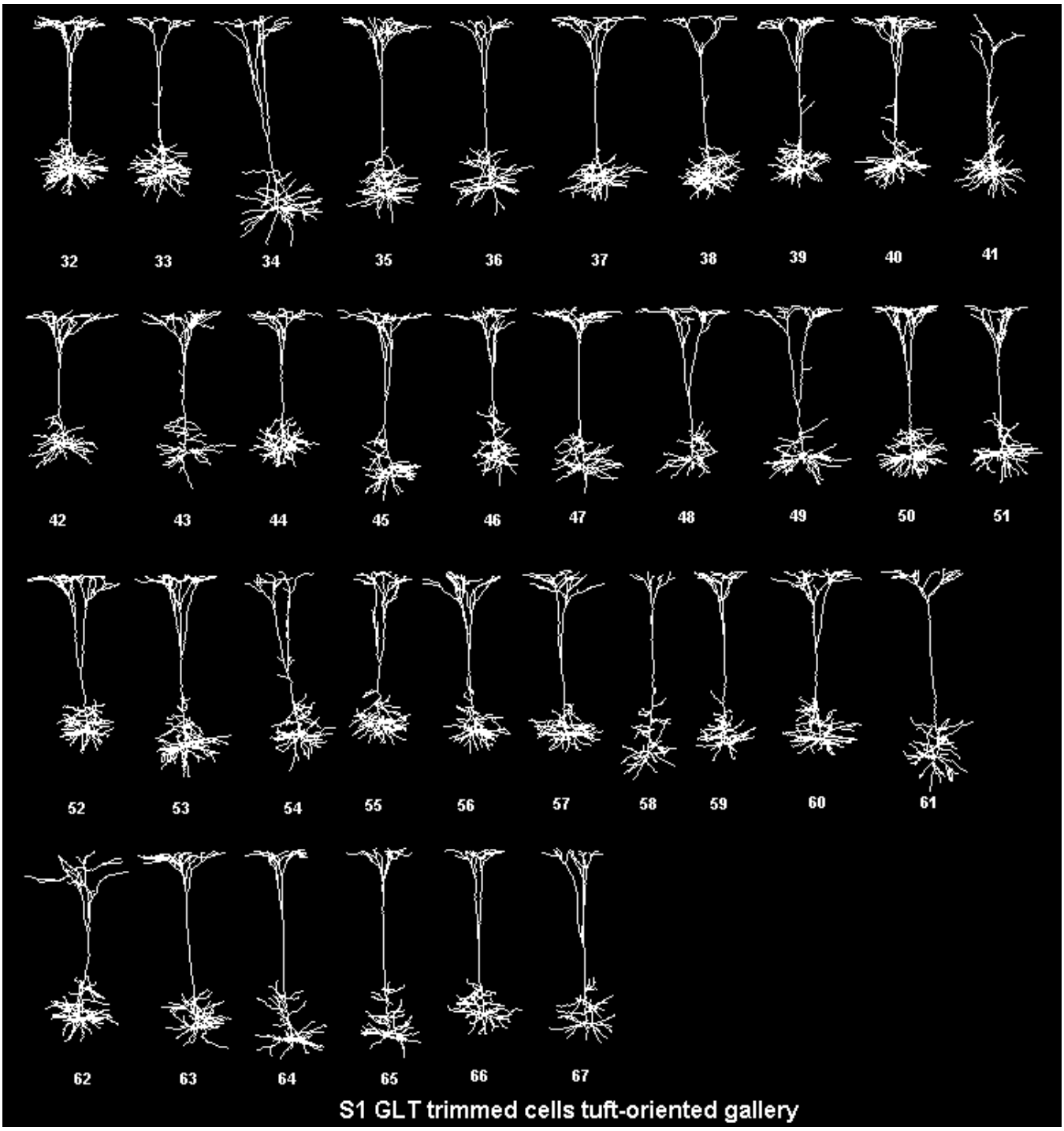

Gallery 3.1.2.3: Depiction of unscaled primary barrel cortex (S1) GLT trimmed cells with the respective distances depicted alongside.

(The linear distances are respectively, scaled pia-soma distance, scaled layer IV boundaries (red), scaled pia-layer IV distance and scaled pia-WM distance at the far right corner. The distances and gallery were displayed using the software AMIRA)

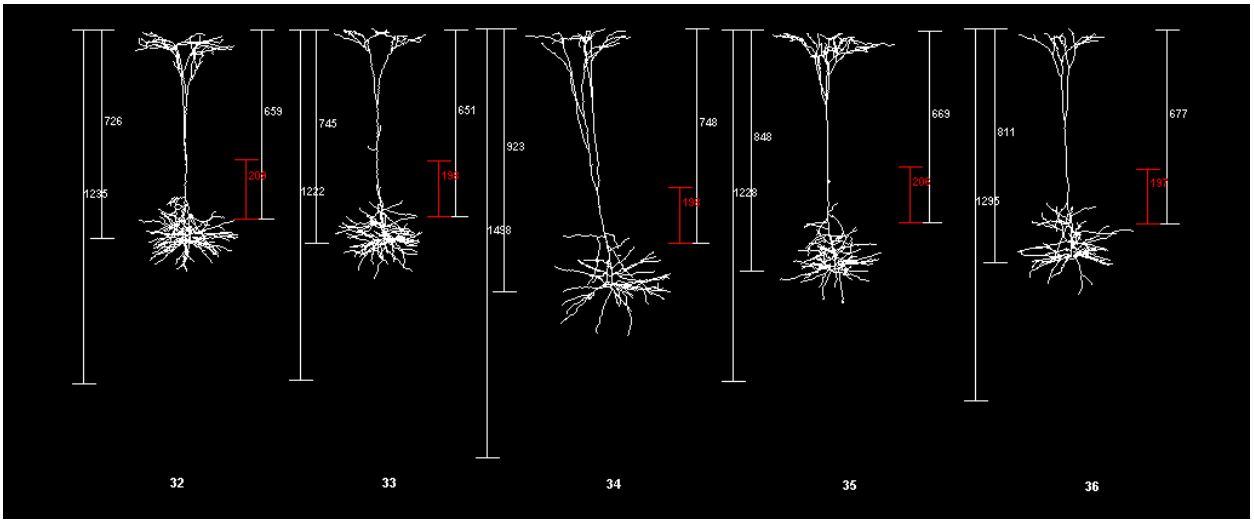

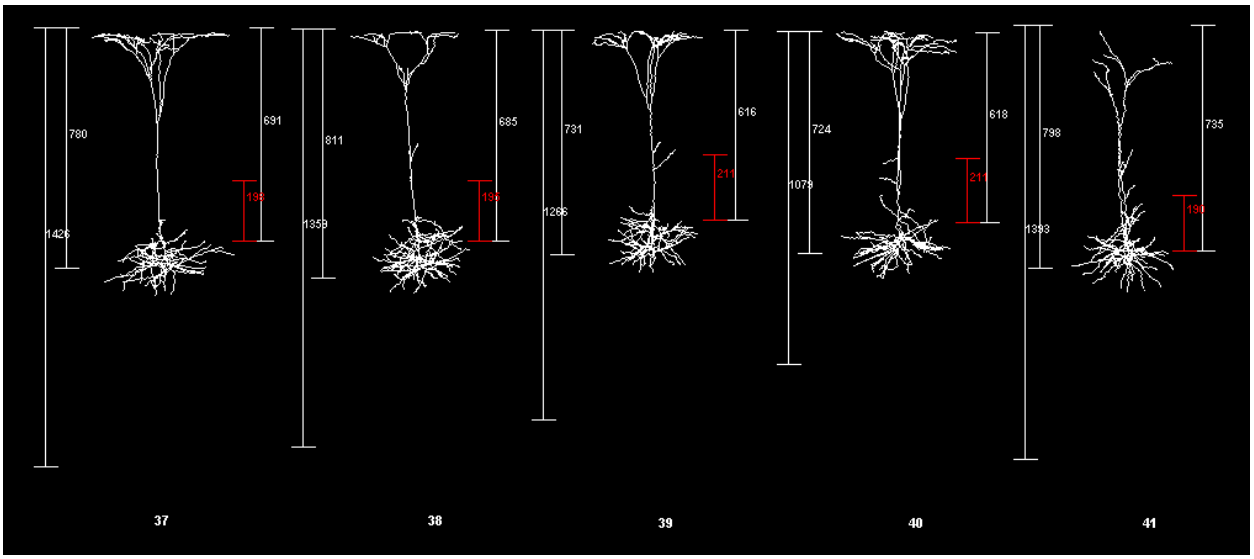

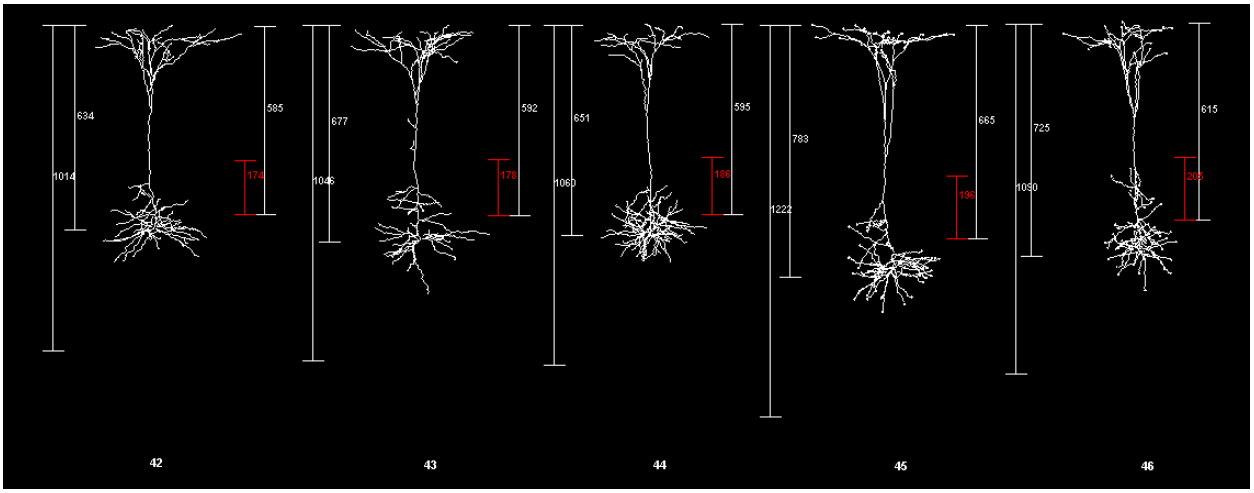
634
585
1014
174
677
592
1046
178
651
595
1060
186
783
665
1222
198
725
615
1090
205
42
43
44
45
46

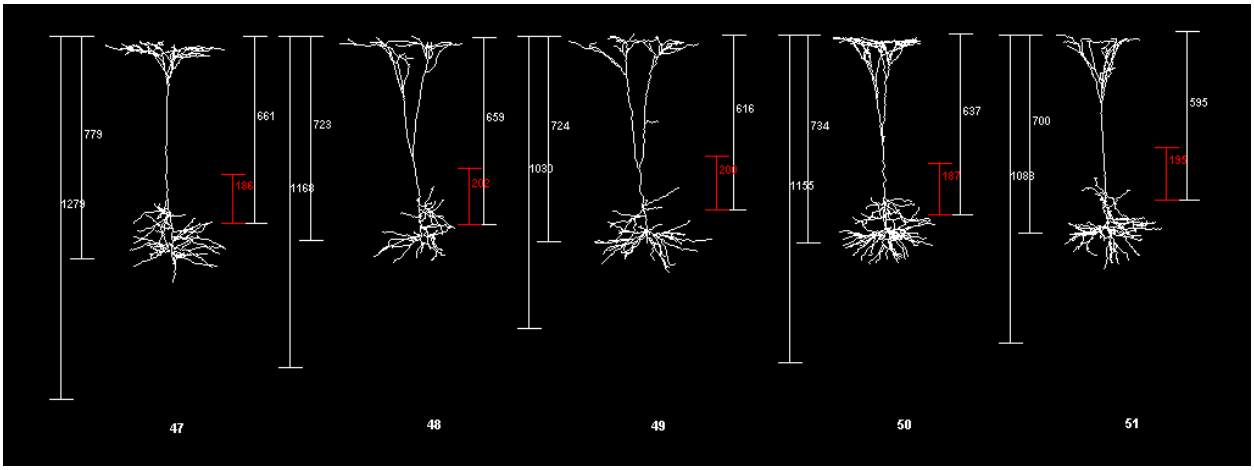
779
661
1279
188
723
659
1168
202
724
616
1030
209
734
637
1155
187
700
595
1088
195
47
48
49
50
51

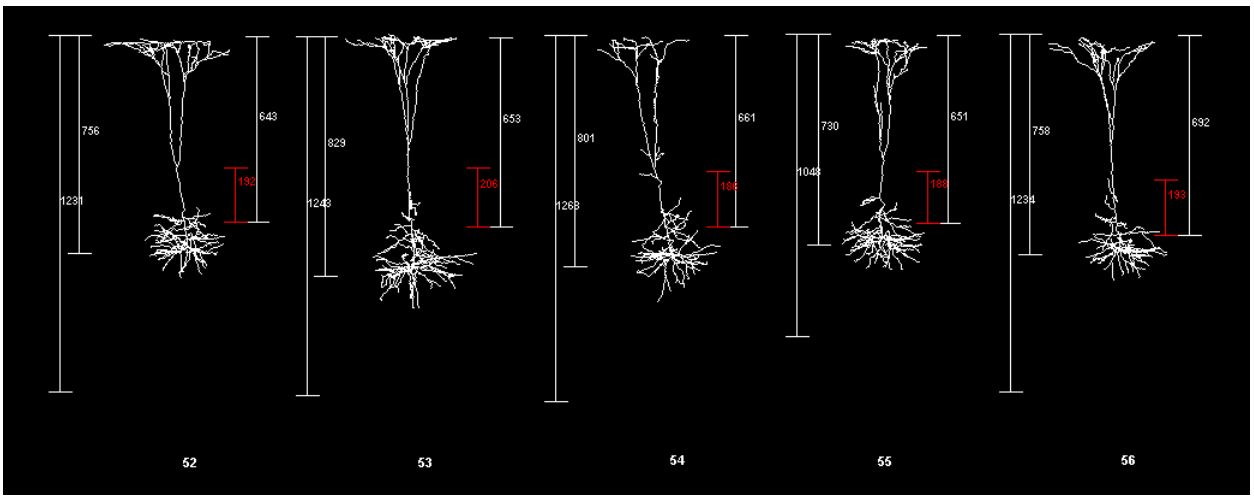
756
643
1231
192
829
653
1243
206
801
661
1263
186
730
651
1044
188
758
692
1234
193
52
53
54
55
56

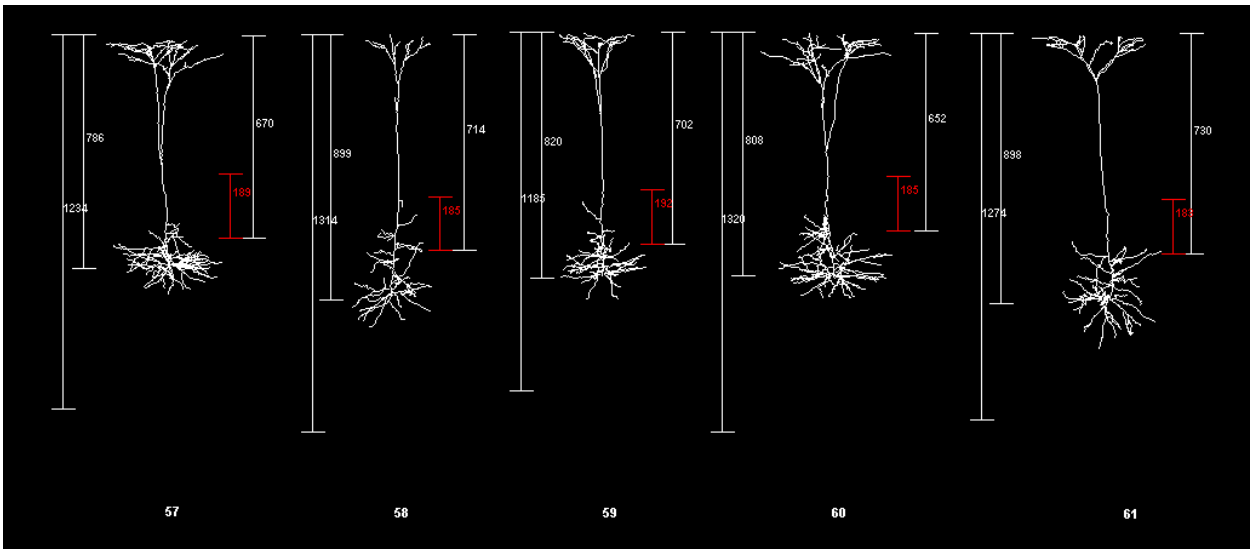
786
670
189
1234
57
899
714
185
1314
58
820
702
1185
59
808
652
185
1320
60
898
730
1274
61

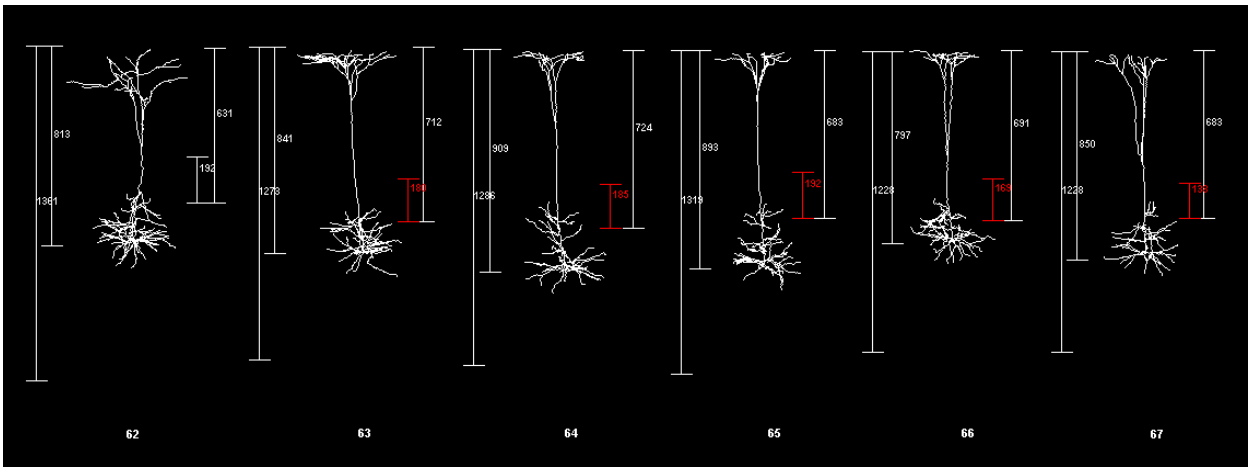
813
631
192
1361
62
841
712
1273
63
909
724
185
1286
64
893
683
192
1319
65
797
691
1229
66
850
683
1228
67

Gallery 3.1.2.4: Depiction of scaled primary barrel cortex (S1) GLT trimmed cells with the respective scaled distances depicted alongside.

(The linear distances are respectively, scaled pia-soma distance, scaled layer IV boundaries (red), scaled pia-layer IV distance and scaled pia-WM distance at the far right corner. The distances and gallery were displayed using the software AMIRA)

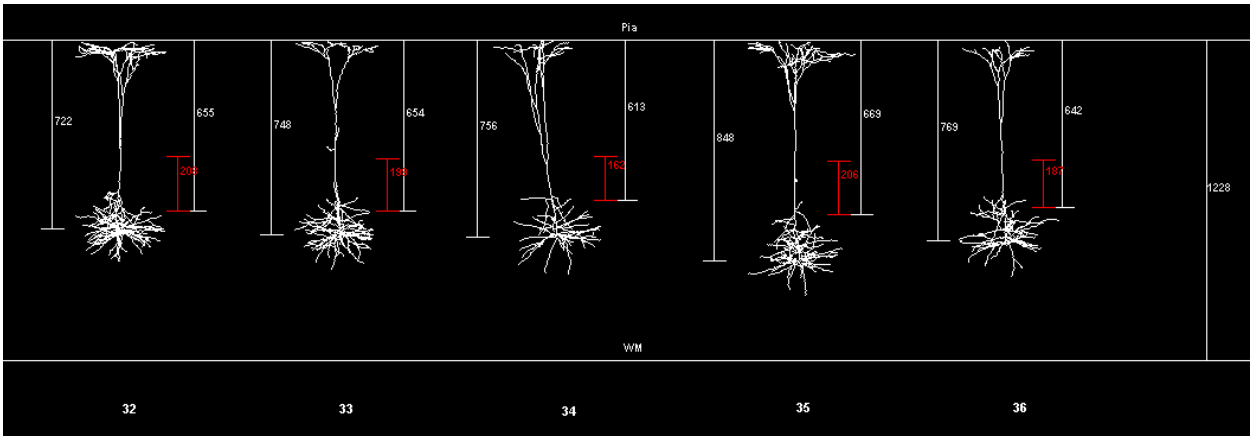

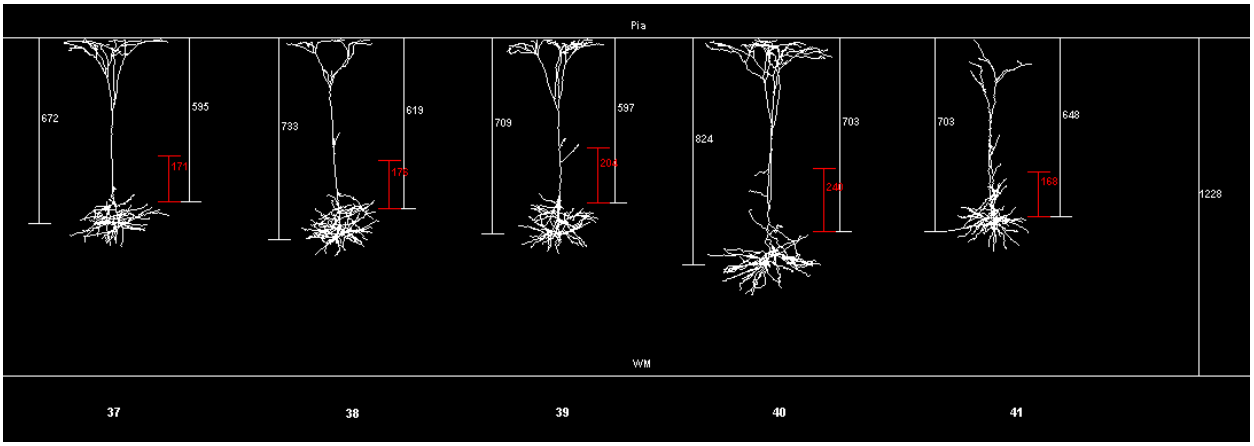

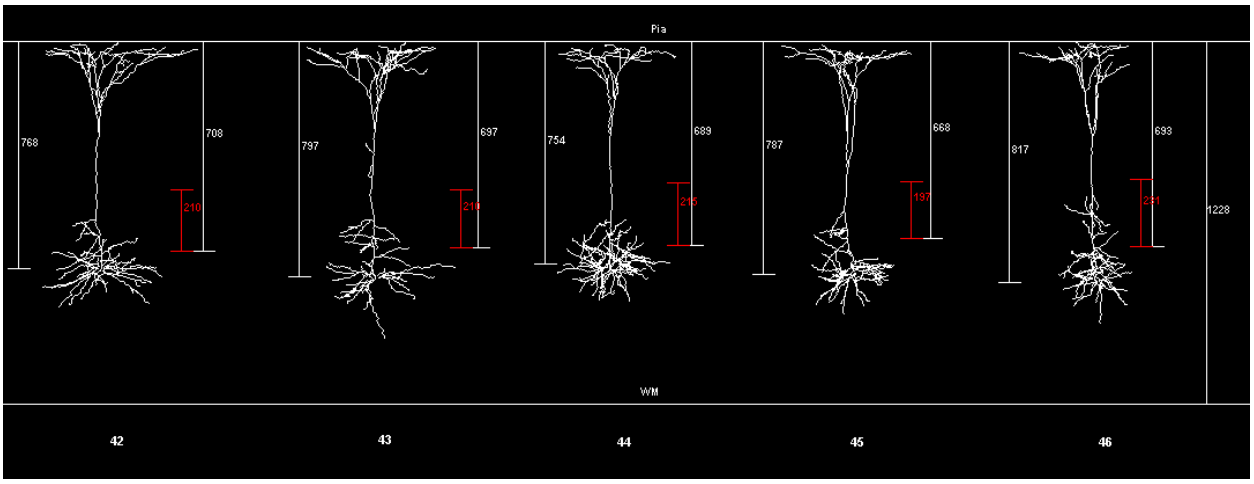

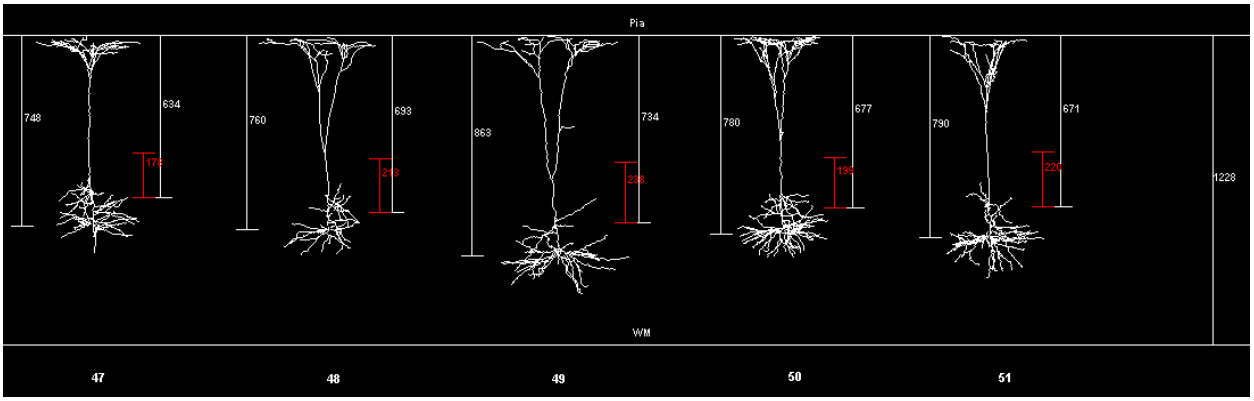
Pia
748
634
172
760
693
213
863
734
238
780
677
195
790
671
225
1228
WM
47
48
49
50
51

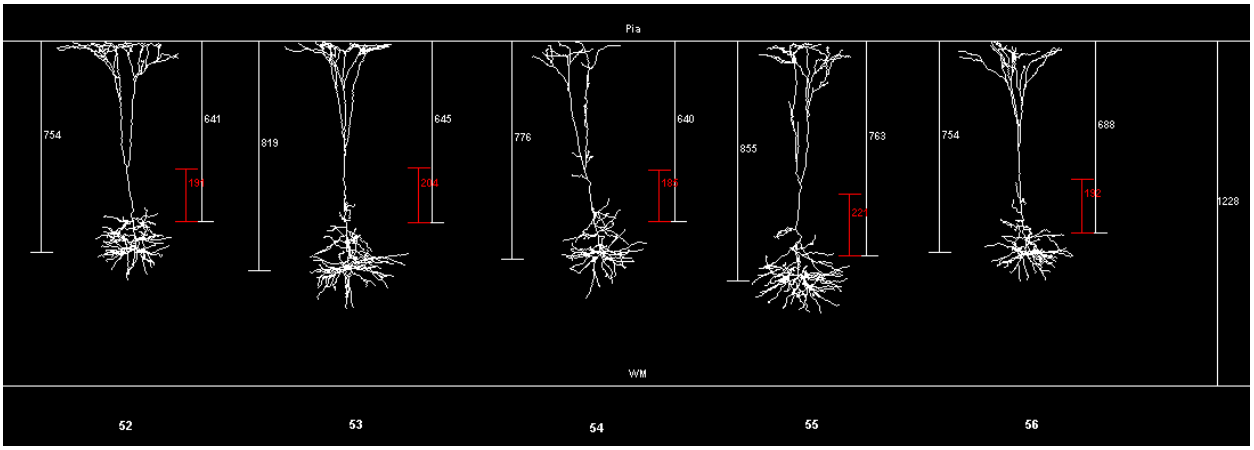
Pia
754
641
191
819
645
204
776
640
196
855
763
221
754
688
192
1228
WM
52
53
54
55
56

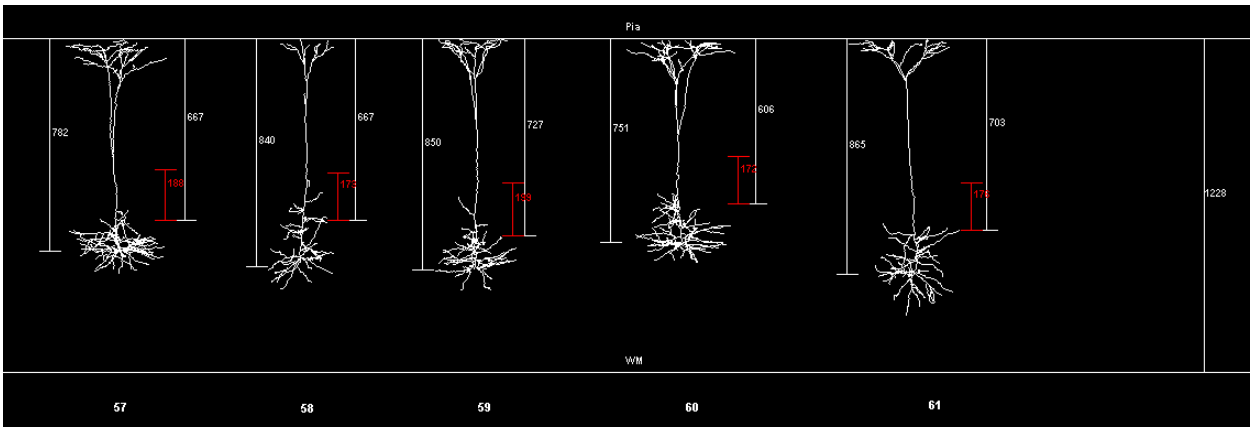
Pia
782
667
180
840
667
175
850
727
159
751
606
172
865
703
175
1228
WM
57
58
59
60
61

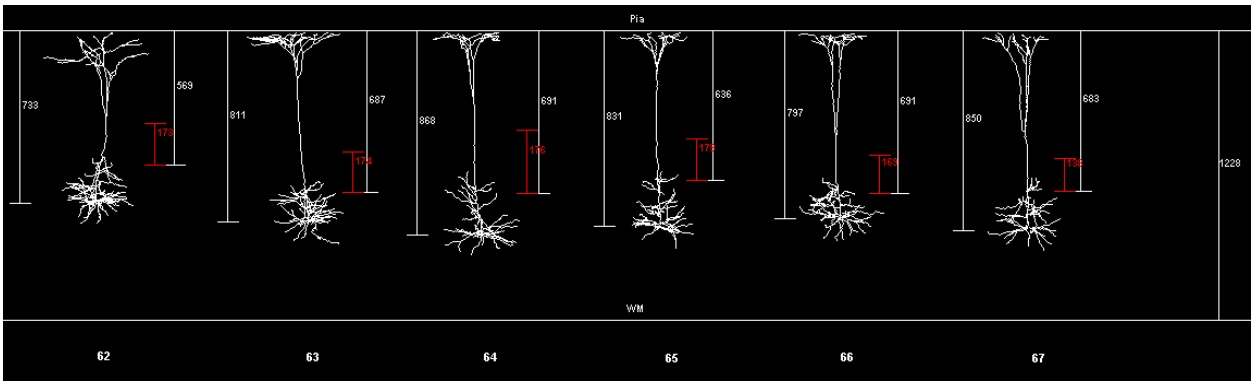
Pia
733
569
175
811
687
174
868
691
176
831
636
174
797
691
169
850
683
176
1228
WM
62
63
64
65
66
67

Gallery 3.1.2.5: Depiction of unscaled, stripped oblique dendrites of unscaled primary barrel cortex (S1) GLT trimmed cells.

(The gallery was displayed using the software AMIRA)

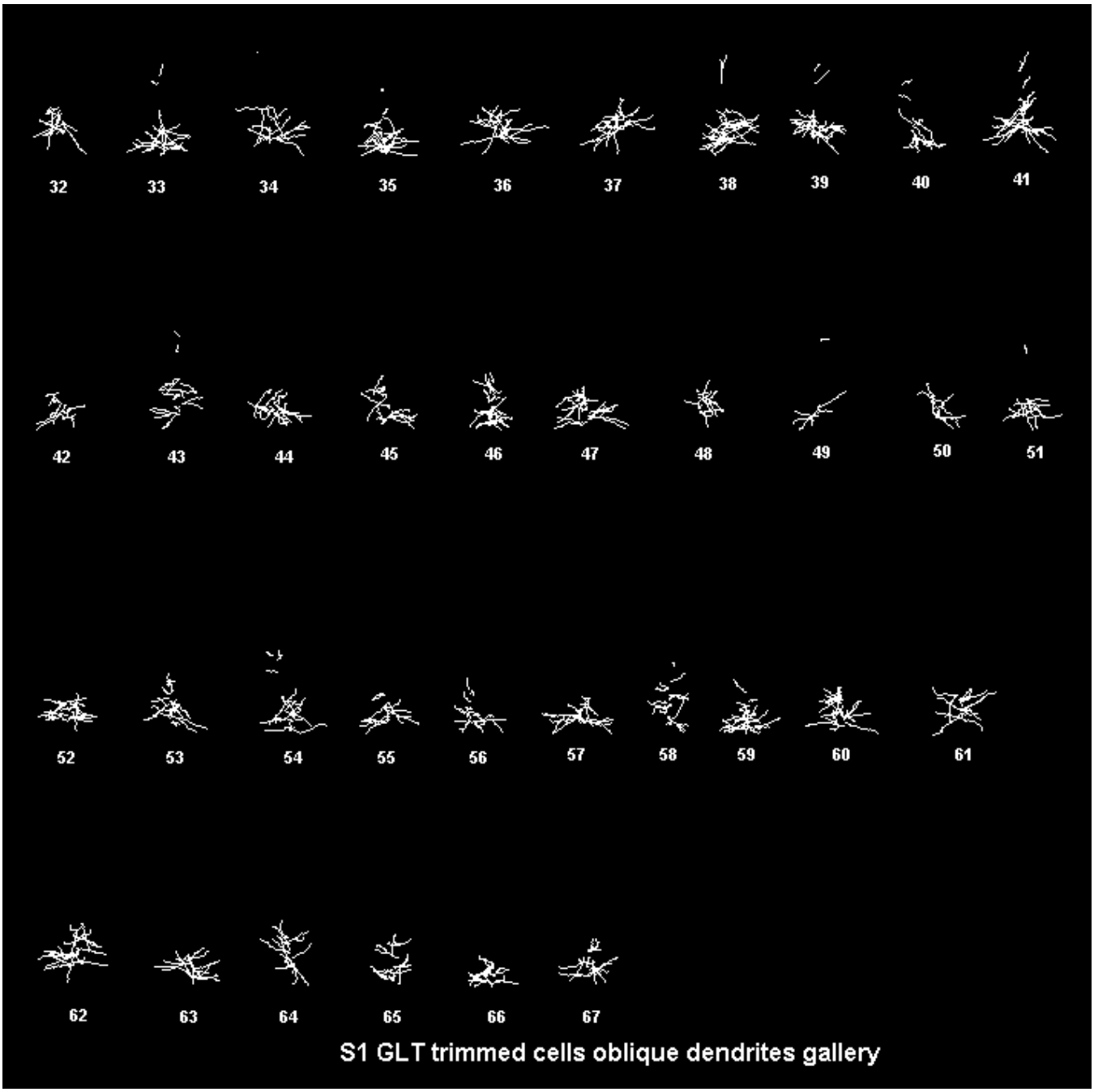

Gallery 3.1.2.6: Depiction of scaled, stripped oblique dendrites of scaled primary barrel cortex (S1) GLT trimmed cells.

(The gallery was displayed using the software AMIRA)

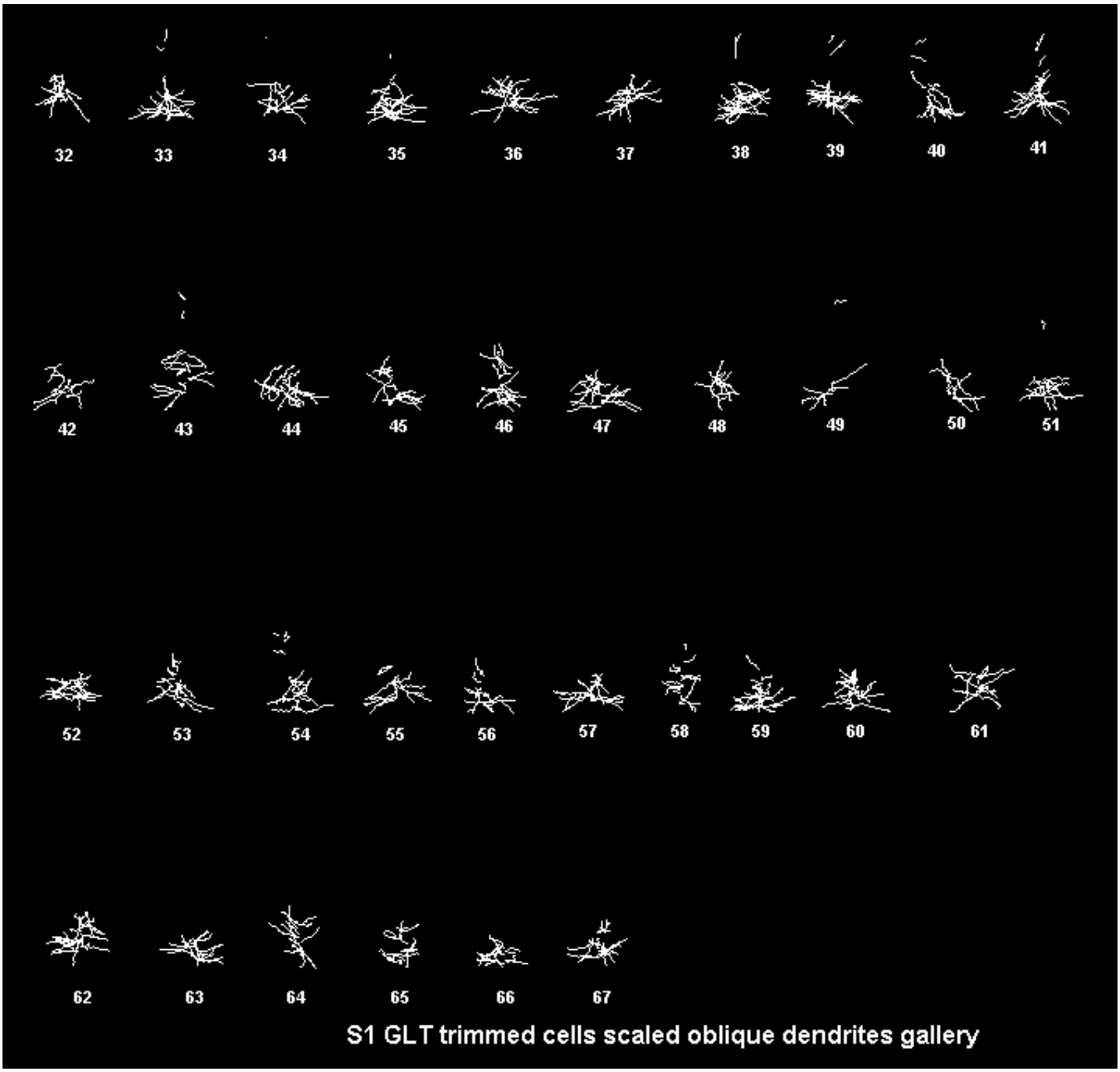

Gallery 3.1.3.1: Soma-centred overview of all unscaled cells comprising the primary vibrissal motor cortex (vM1) GLT control data set.

(The gallery was displayed using the software AMIRA)

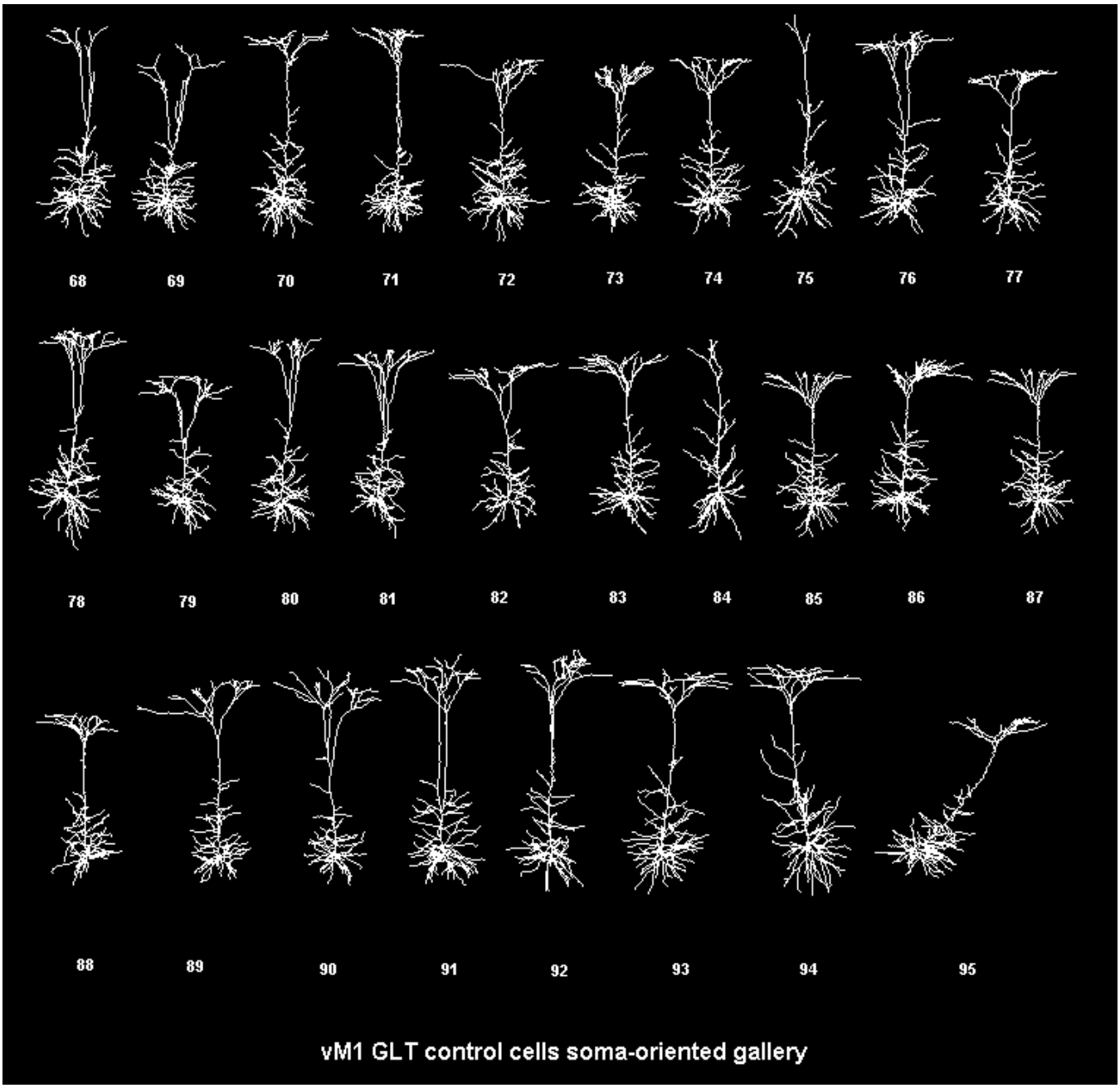

Gallery 3.1.3.2: Tuft-centred overview of all unscaled cells comprising the primary vibrissal motor cortex (vM1) GLT control data set.

(The gallery was displayed using the software AMIRA)

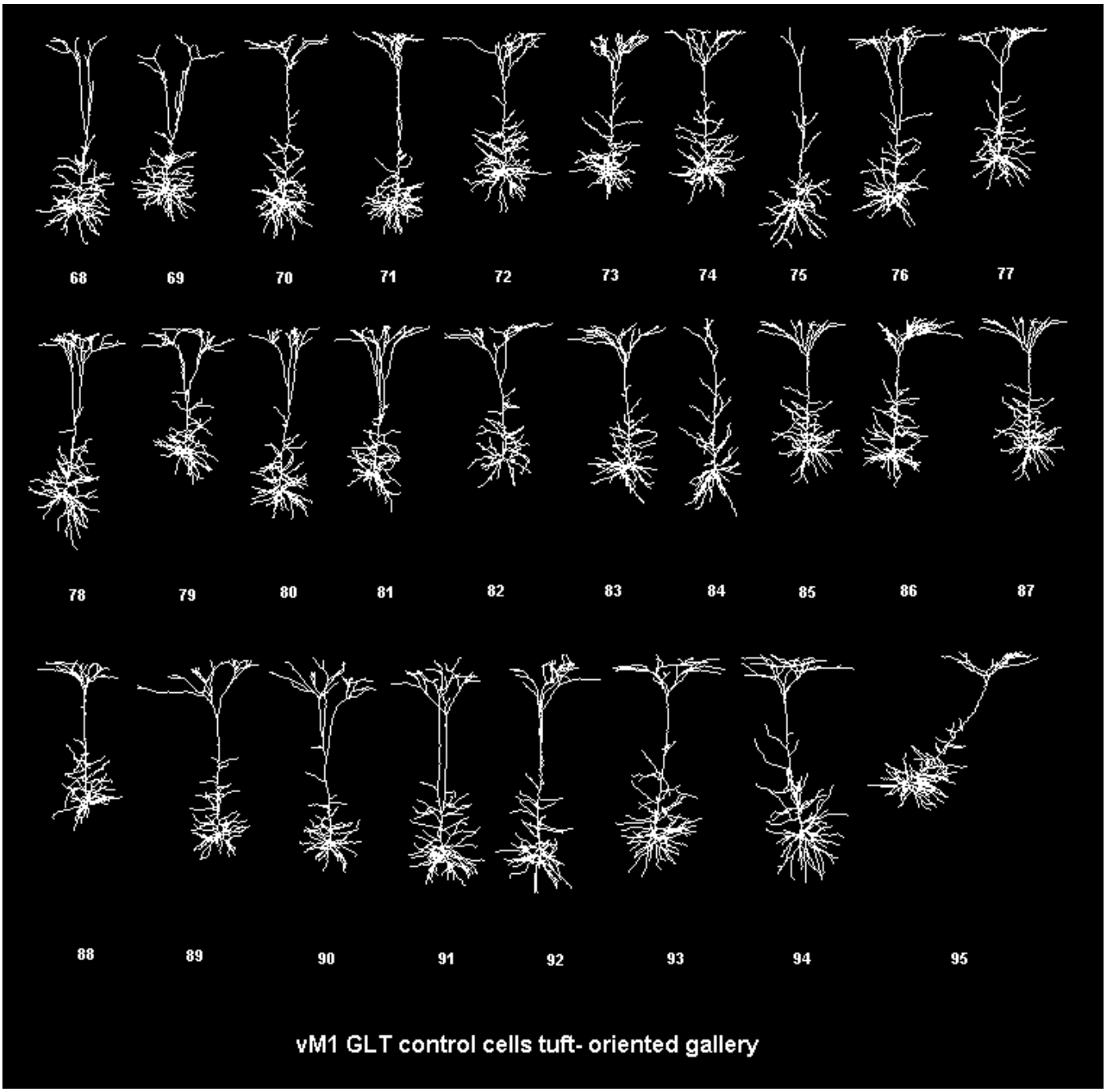

Gallery 3.1.3.3: Depiction of unscaled primary vibrissal motor cortex (vM1) GLT control cells with the respective distances depicted alongside.

(The linear distances are respectively, pia-WM distance and pia-soma distance. The distances and gallery were displayed using the software AMIRA)

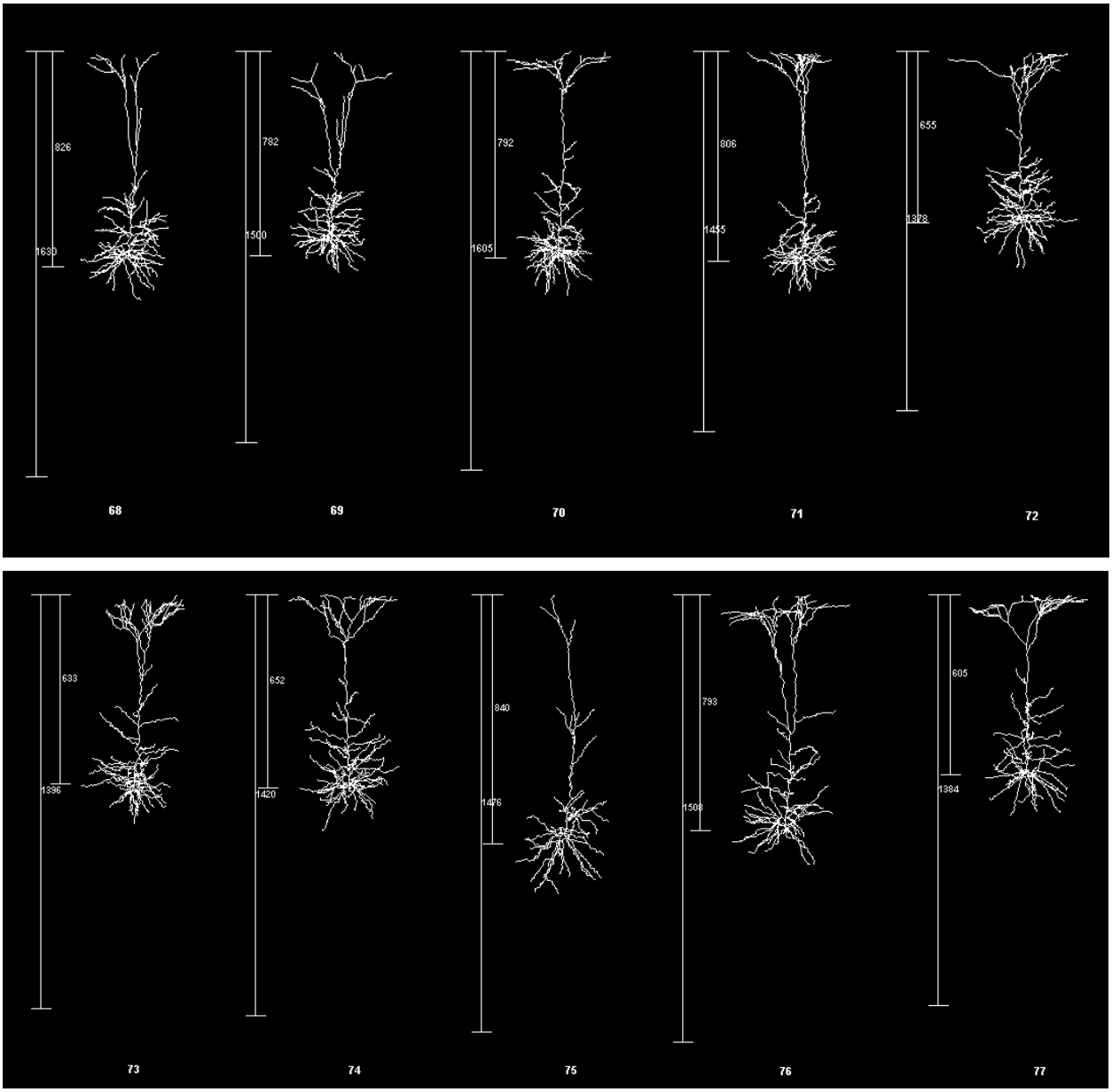


747
1407
78
594
1427
79
613
1471
80
688
1437
81
628
1493
82

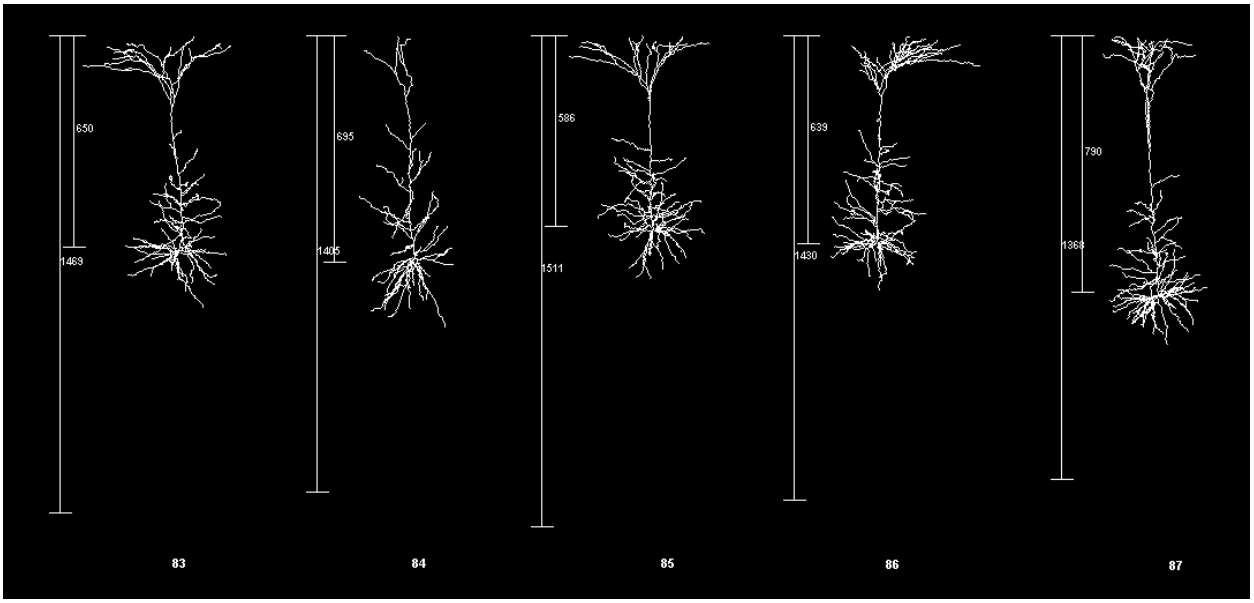
650
1469
83
695
1405
84
586
1511
85
639
1430
86
790
1368
87

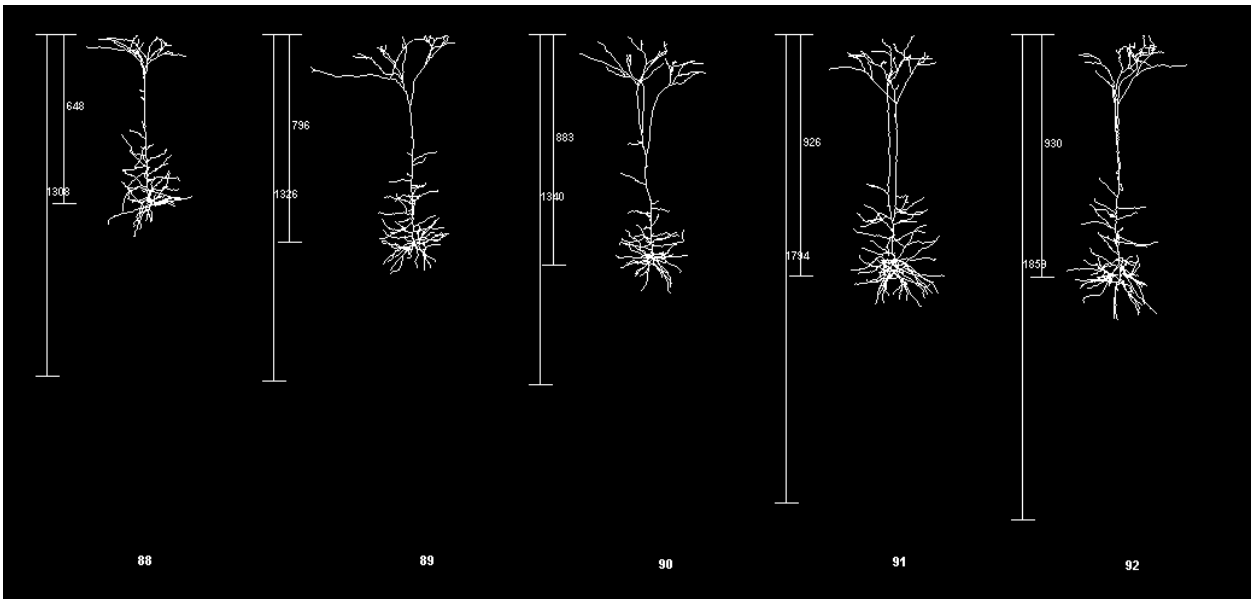
648
1308
796
1326
883
1340
926
1794
930
1859
88
89
90
91
92

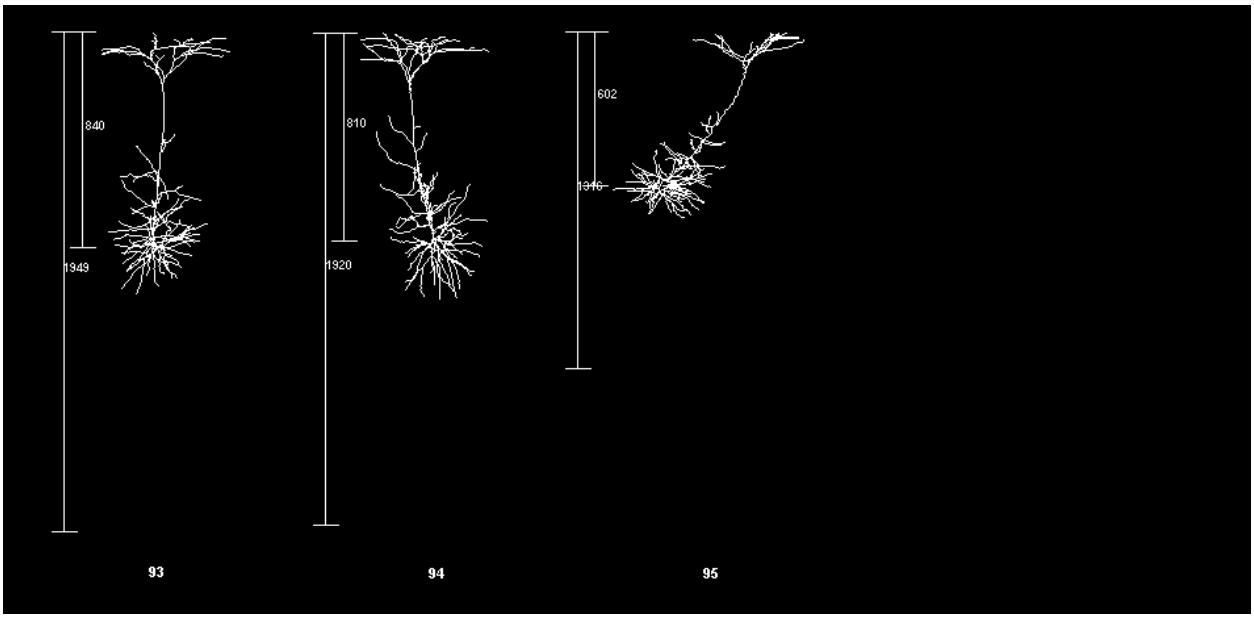
840
1949
810
1920
602
1316
93
94
95

Gallery 3.1.3.4: Depiction of scaled primary vibrissal motor cortex (vM1) GLT control cells with the respective scaled distances depicted alongside.

(The linear distances are respectively, scaled pia-soma distance and scaled pia-WM distance at the far right corner. The distances and gallery were displayed using the software AMIRA)

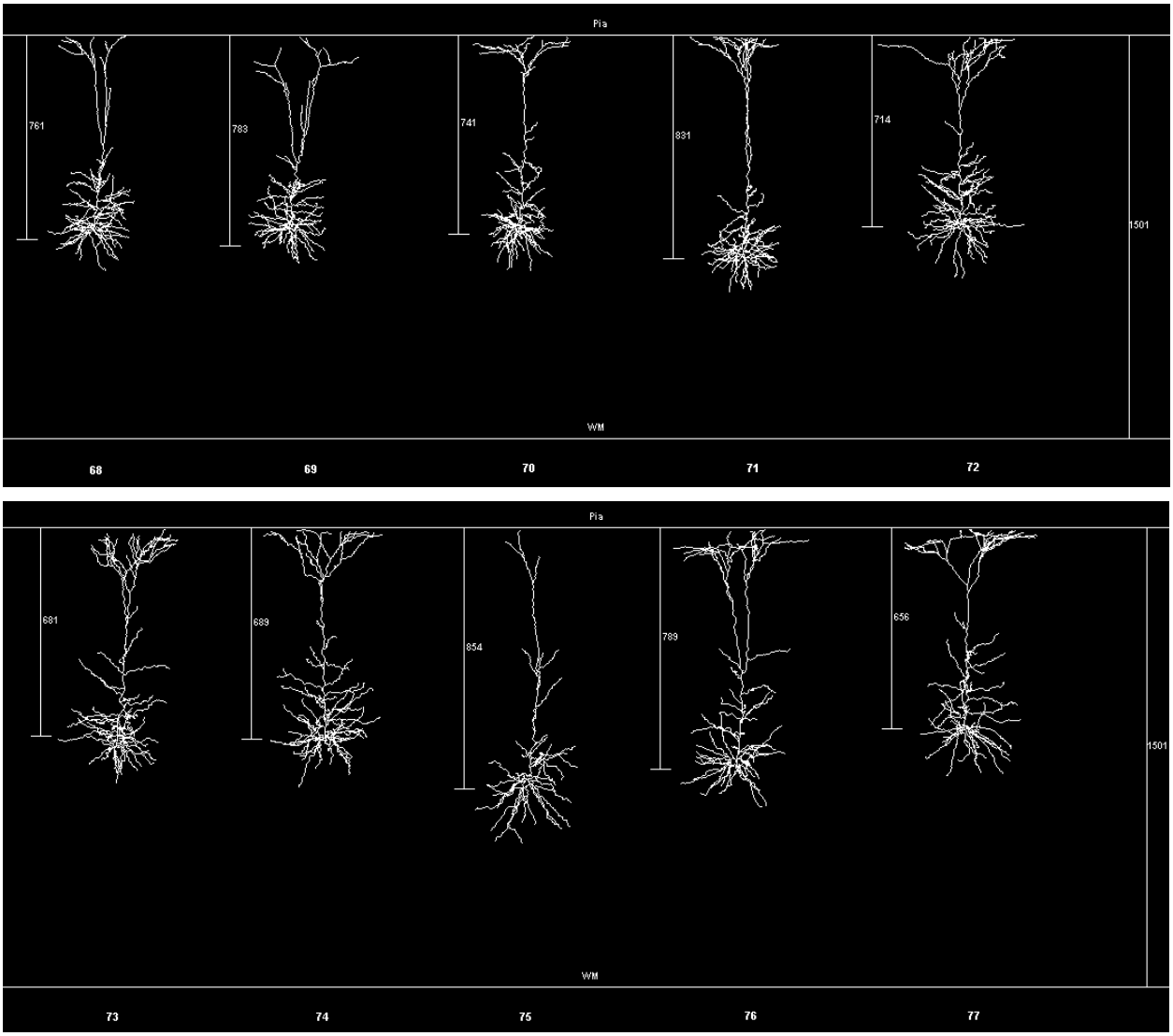

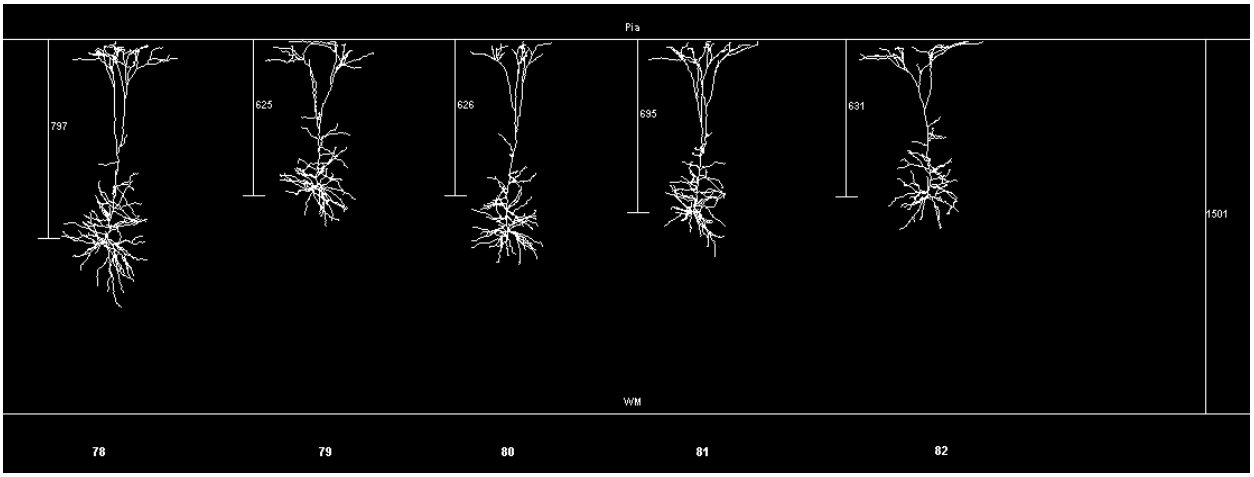
Pia
797
625
626
695
631
1501
WM
78
79
80
81
82

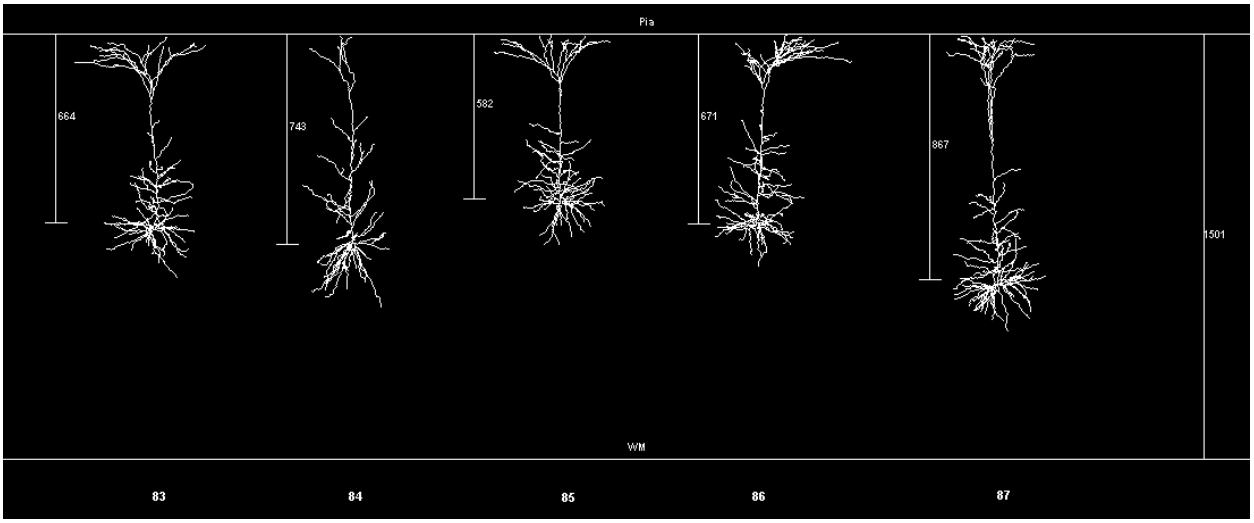
Pia
664
743
582
671
867
1501
WM
83
84
85
86
87

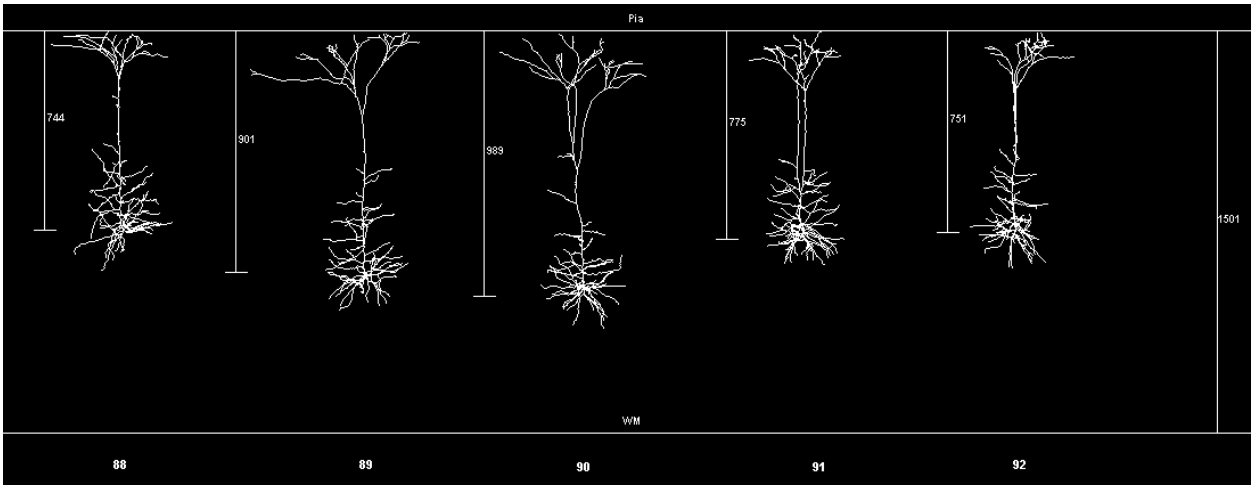
Pia
744
901
989
775
751
1501
WM
88
89
90
91
92

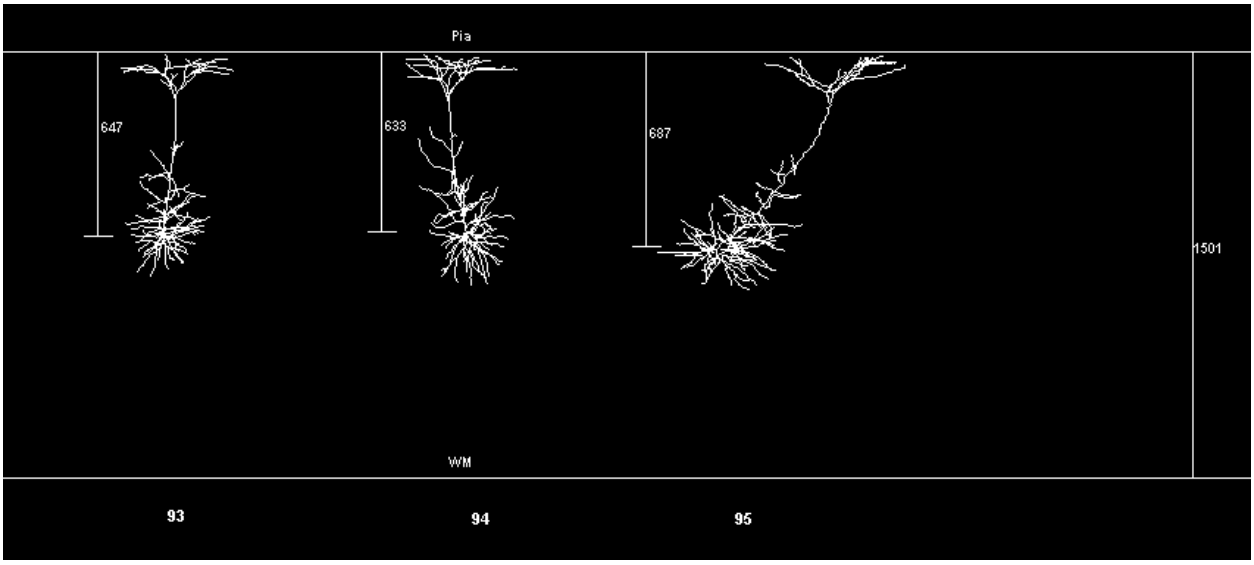
Pia
647
633
687
1501
WM
93
94
95

Gallery 3.1.3.5: Depiction of unscaled, stripped oblique dendrites of unscaled primary vibrissal motor cortex (vM1) GLT control cells.

(The gallery was displayed using the software AMIRA)

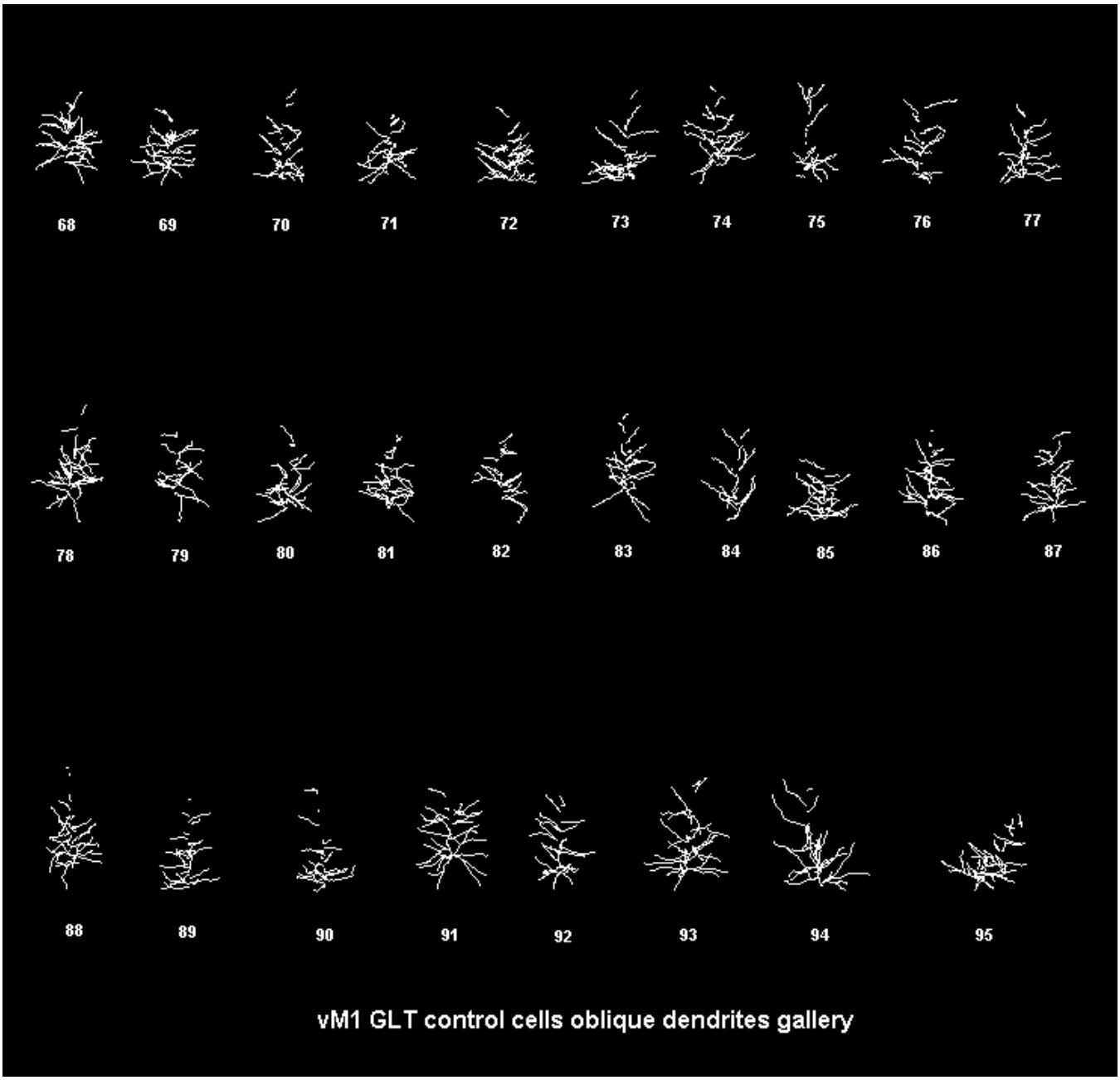

Gallery 3.1.3.6: Depiction of scaled, stripped oblique dendrites of scaled primary vibrissal motor cortex (vM1) GLT control cells.

(The gallery was displayed using the software AMIRA)

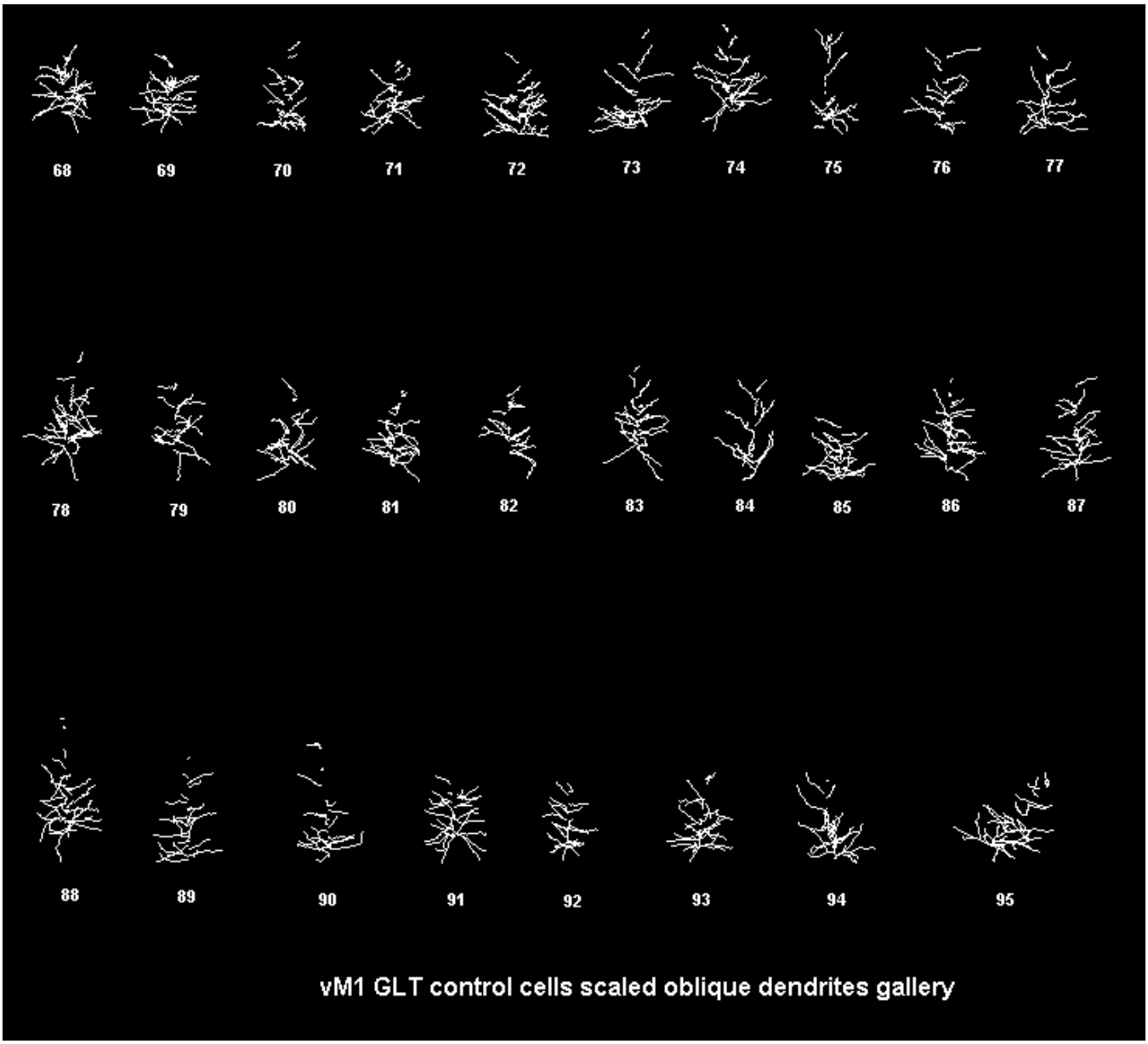

Gallery 3.1.4.1: Soma-centred overview of all unscaled cells comprising the primary vibrissal motor cortex (vM1) GLT trimmed data set.

(The gallery was displayed using the software AMIRA)

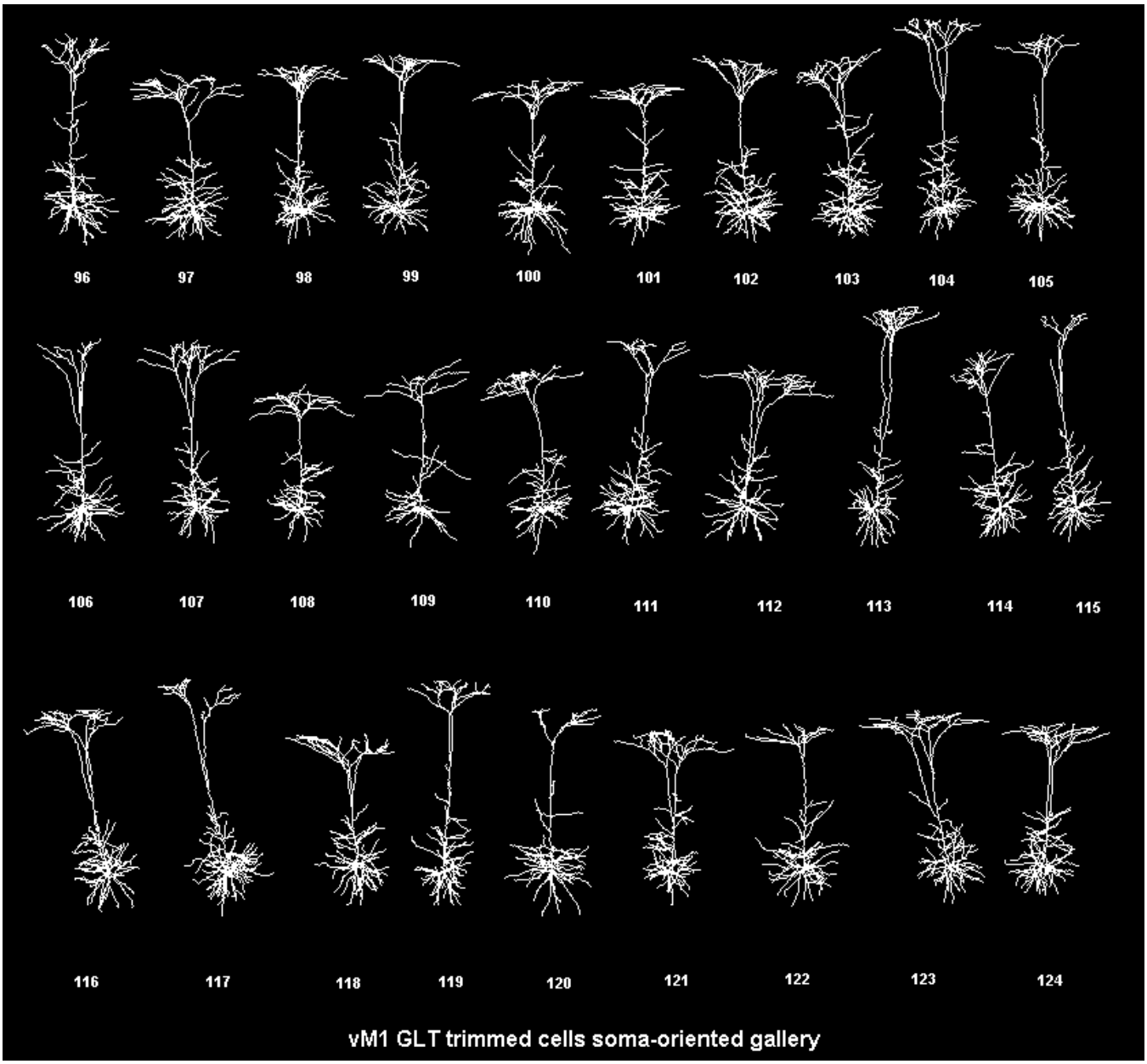

Gallery 3.1.4.2: Tuft-centred overview of all unscaled cells comprising the primary vibrissal motor cortex (vM1) GLT trimmed data set.

(The gallery was displayed using the software AMIRA)

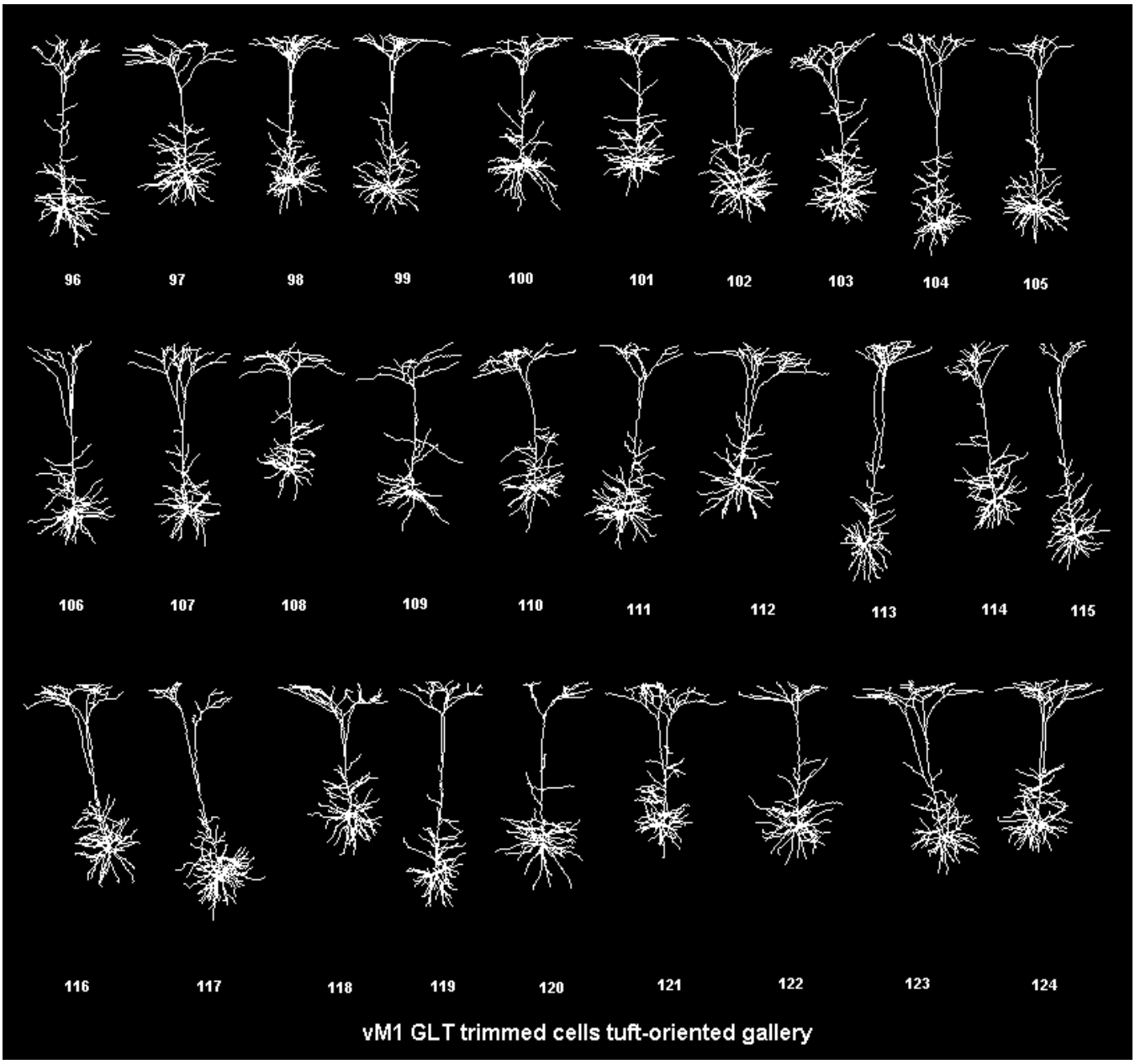

Gallery 3.1.4.3: Depiction of unscaled primary vibrissal motor cortex (vM1) GLT trimmed cells with the respective distances depicted alongside.

(The linear distances are respectively pia-WM distance and pia-soma distance. The distances and gallery were displayed using the software AMIRA)

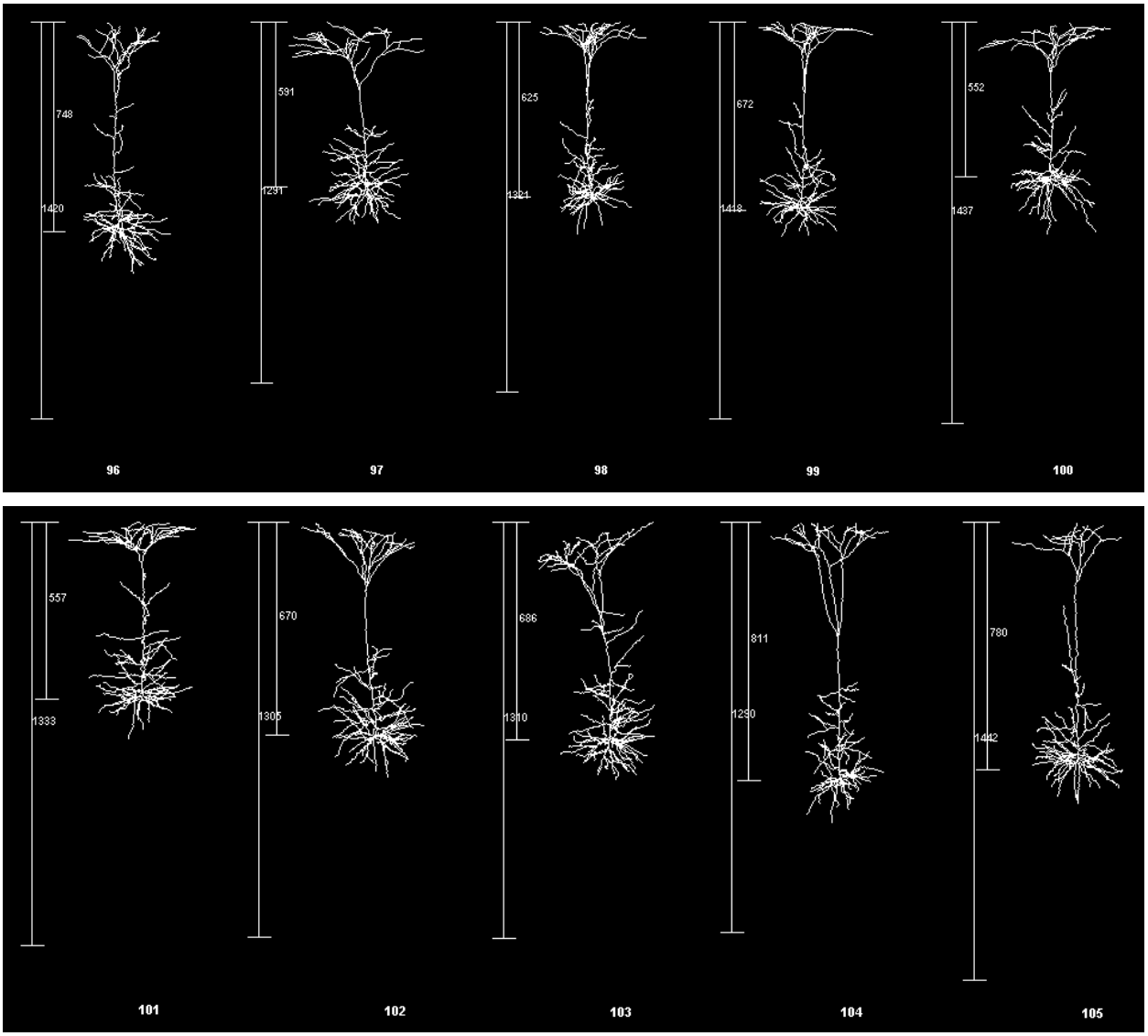

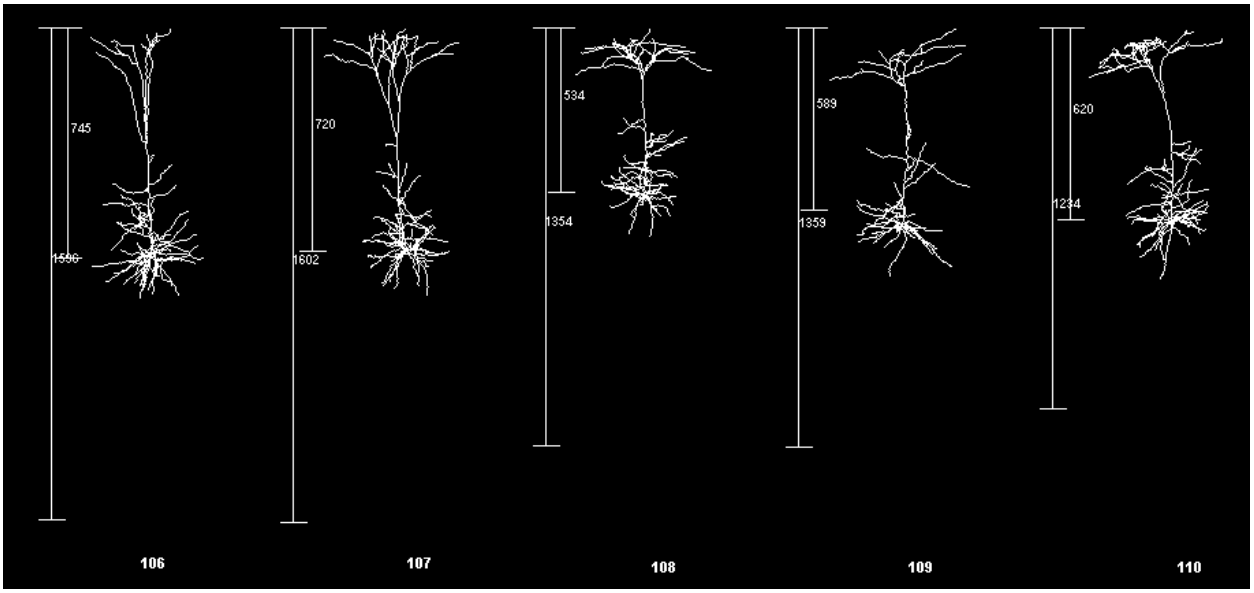
745
1556
720
1602
534
1354
589
1359
620
1234
106
107
108
109
110

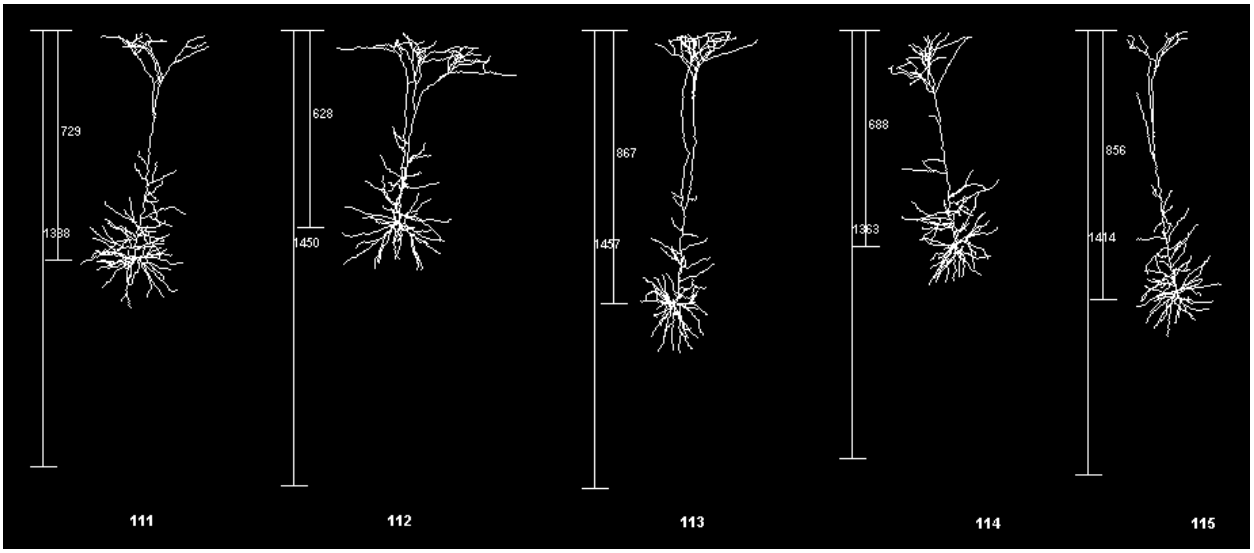
729
1388
628
1450
867
1457
688
1363
856
1414
111
112
113
114
115

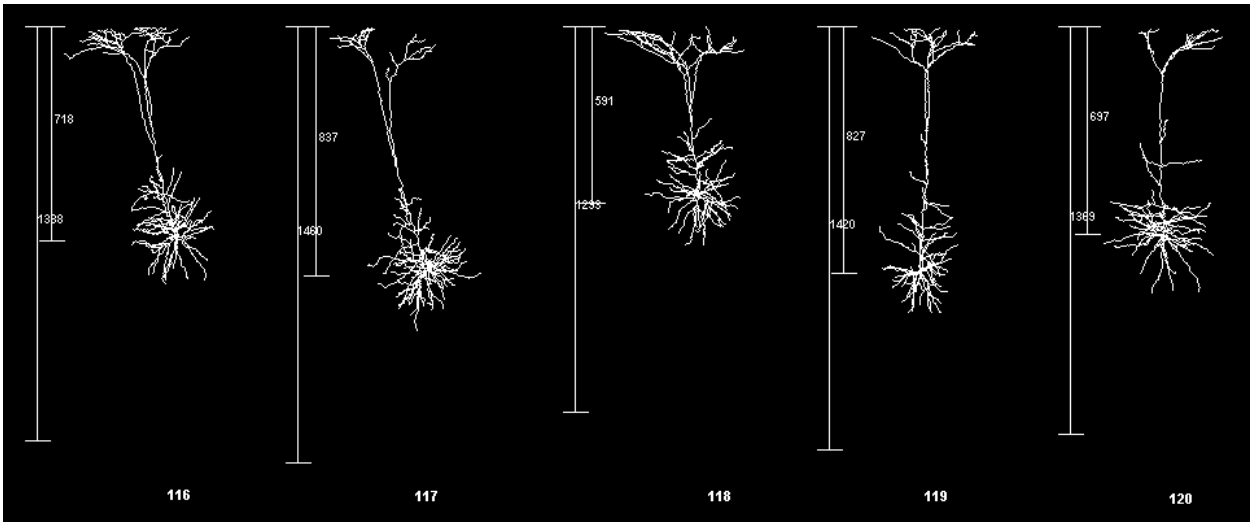
718
1388
837
1460
591
1233
827
1420
697
1389
116
117
118
119
120


622
1402
121
625
1455
122
688
1385
123
611
1452
124

Gallery 3.1.4.4: Depiction of scaled primary vibrissal motor cortex (vM1) GLT trimmed cells with the scaled distances depicted alongside.

(The linear distances are respectively, scaled pia-soma distance and scaled pia-WM distance at the far right corner. The distances and gallery were displayed using the software AMIRA)

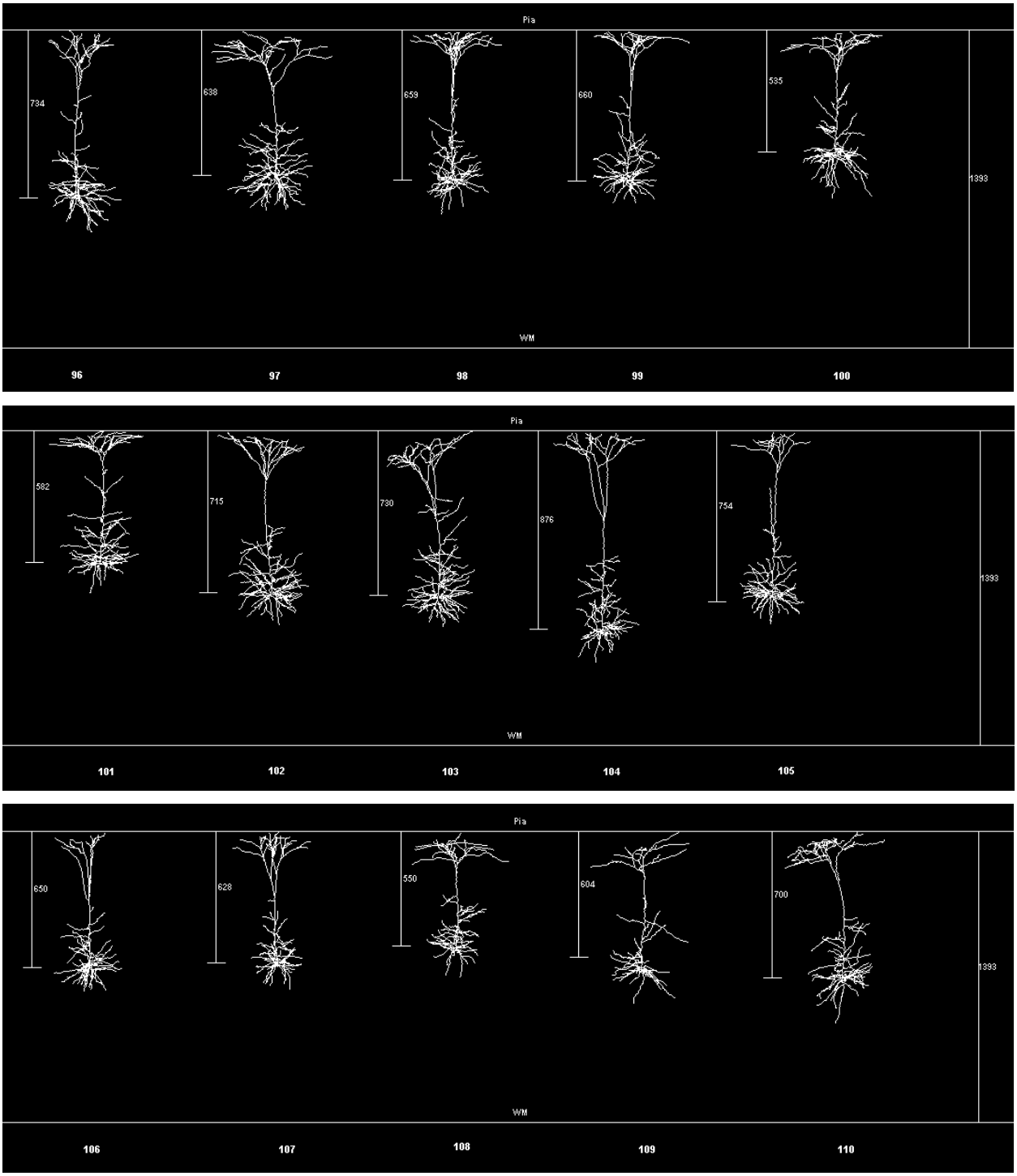

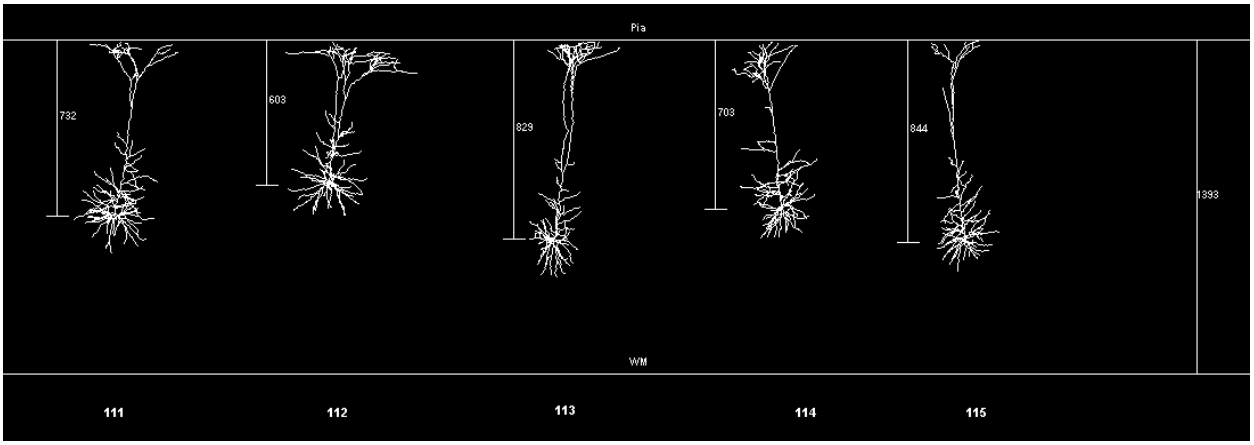
Pia
732
603
829
703
844
1393
WM
111
112
113
114
115

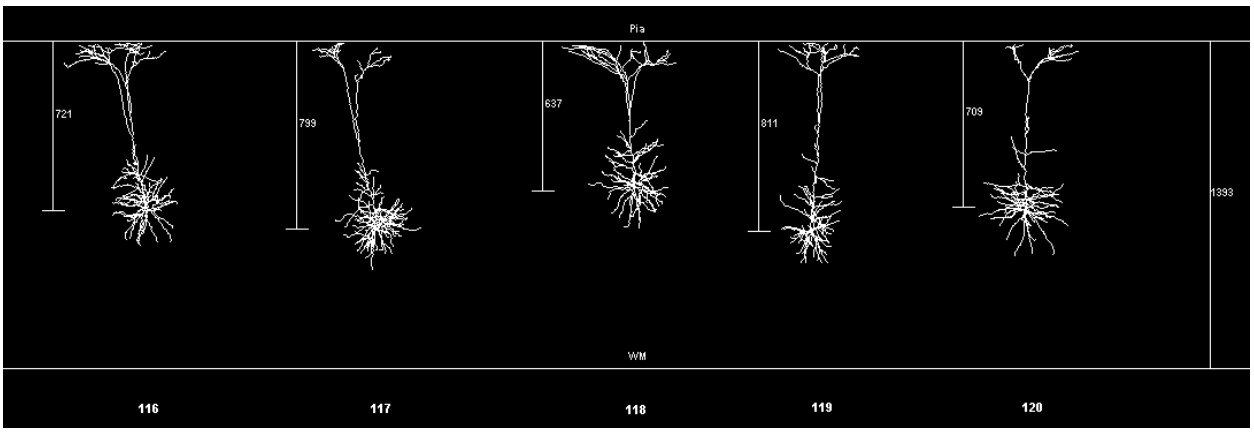
Pia
721
799
637
811
709
1393
WM
116
117
118
119
120

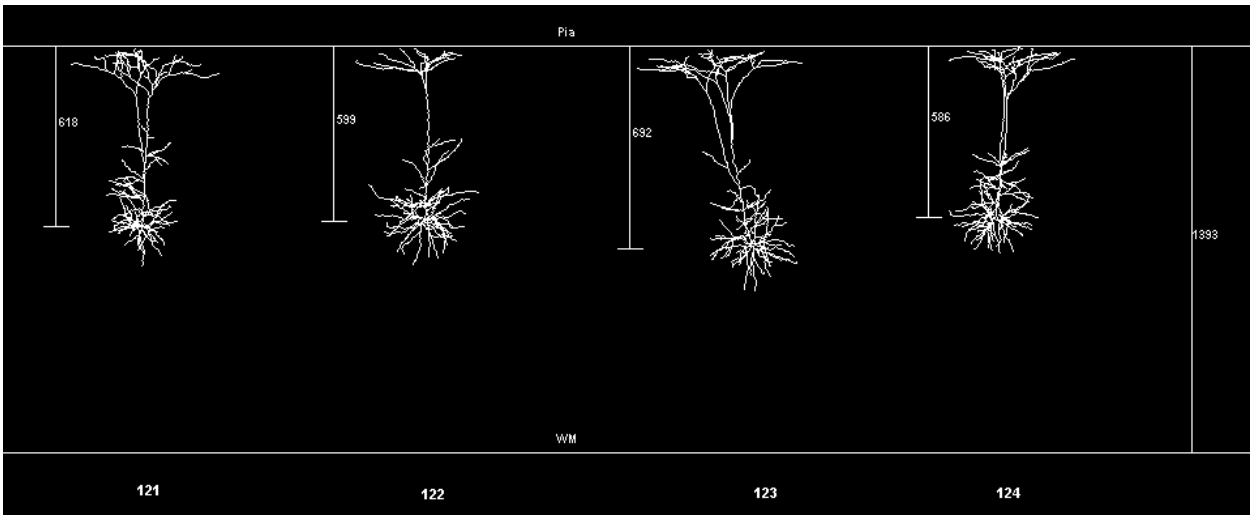
Pia
618
599
692
586
1393
WM
121
122
123
124

Gallery 3.1.4.5: Depiction of unscaled, stripped oblique dendrites of unscaled primary vibrissal motor cortex (vM1) GLT trimmed cells.

(The gallery was displayed using the software AMIRA)

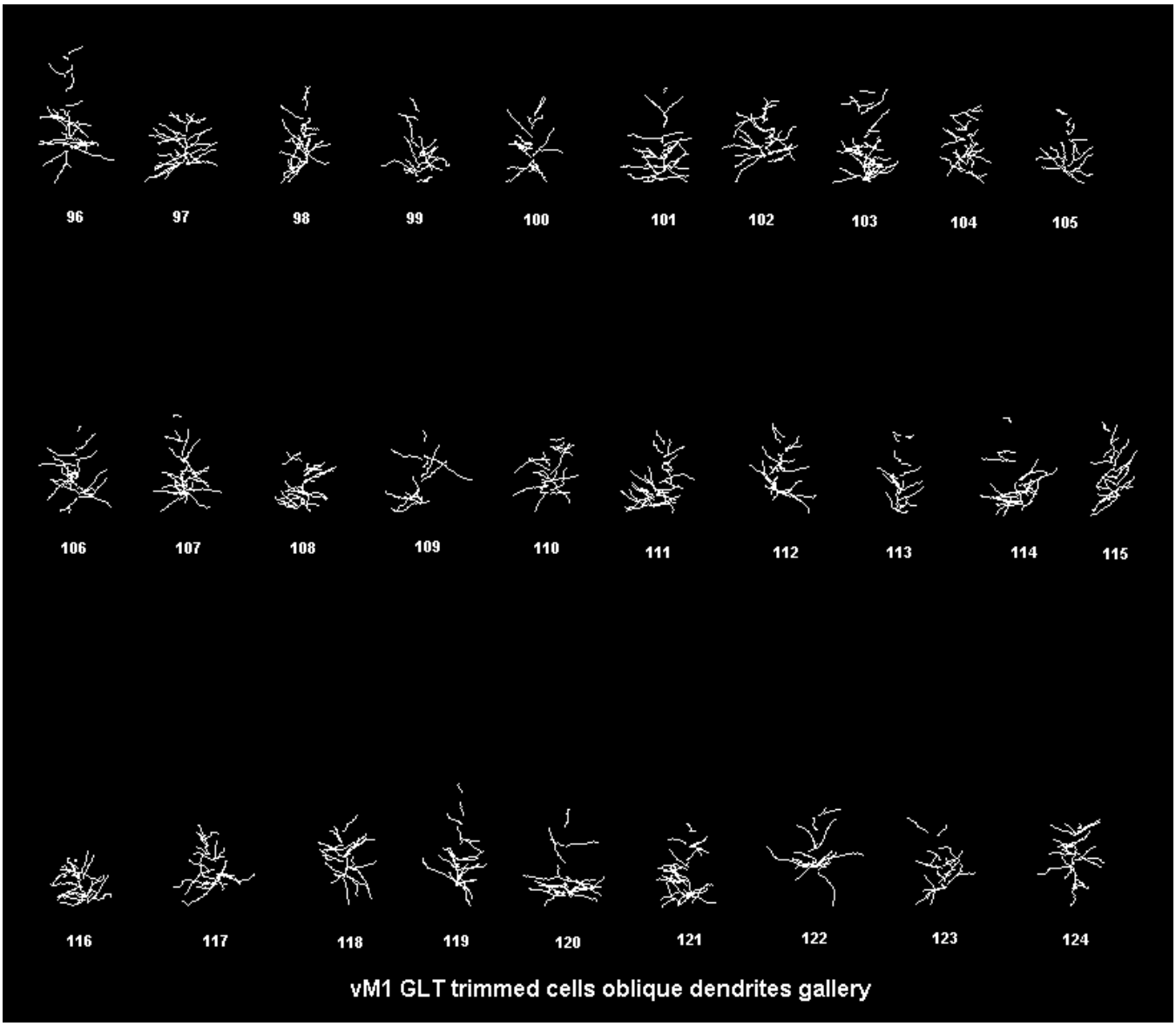

Gallery 3.1.4.6: Depiction of scaled, stripped oblique dendrites of scaled primary vibrissal motor cortex (vM1) GLT trimmed cells.

(The gallery was displayed using the software AMIRA)

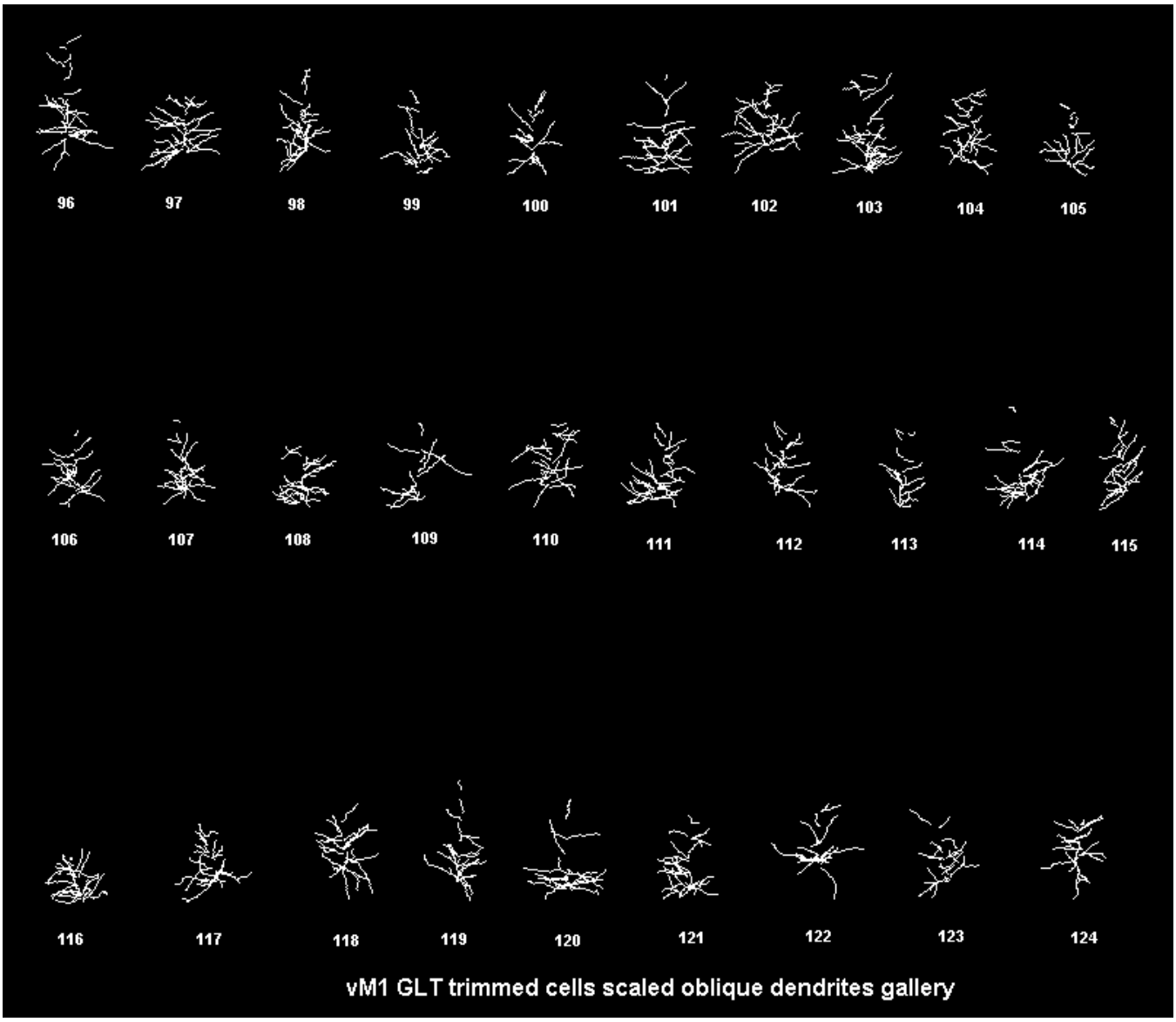

3.2 Neuroexplorer dendrite analyses of original, unscaled cells

The Neurolucida reconstructed cells in the .asc file format can be directly opened with the Neuroexplorer and can be analysed for different dendritic parameters. For example, using the "branched structure analysis" mode and selecting "neuron summary" yields the counts of nodes, endings, lengths, area, volume, etc. So both the primary somatosensory cortex cells as well as the vibrissal motor cortex cells were subjected to "branched structure analysis" to obtain a primary idea whether any structural differences existed between the control and trimmed groups.

3.2.1 Primary somatosensory cortex (S1) GLT cells

The control group of barrel cortex cells showed an average apical dendritic length of 7049 ± 1034 μm (n=31) and was highly significantly different from the mean apical dendritic length of 6074 ± 997 μm (n=36) of the trimmed group (p=<0.001). But the mean basal dendritic length of the control group (3610 ± 717 μm) was not found to be different from that of the trimmed group (3291 ± 1056 μm). In addition, the mean number of nodes in the apical tree of the control group was slightly albeit significantly higher than that in the trimmed group. A separate analysis of just the stripped oblique dendrites similarly revealed a significant difference between the control (2795 ± 717 μm) and the trimmed (2438 ± 713 μm) groups (p =0.046). All data are shown in graphs below.

However, a look at the pia-layer IV distances and the pia-soma distances also revealed significant differences between the two groups. These differences, thus, made it difficult to interpret the dendritic parameters as possible effects of the whisker trimming.

NOTE: Results of all analyses, including those to follow, are displayed in organised tables with mean values and standard deviation along with significance levels at the conclusion of parametric analysis (tables 3.8.1.1 – 3.8.2.10, pages 95-108).

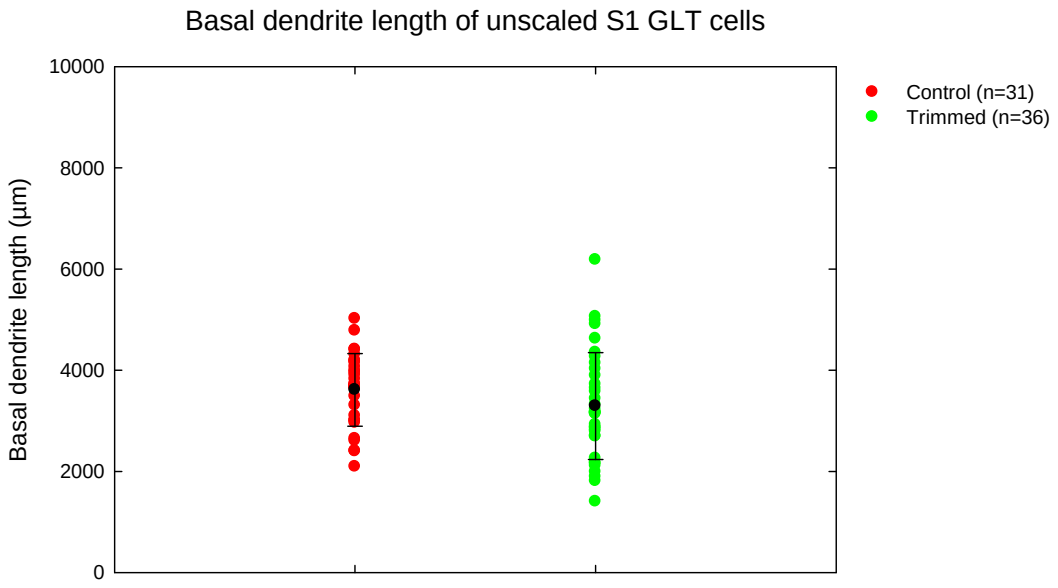

Figure 3-12: **Neuroexplorer basal dendrite of unscaled S1 GLT cells.** Comparison between control and trimmed groups did not show any significant difference (p=0.160). The means are indicated by black circles and the standard deviations are shown by the tails.

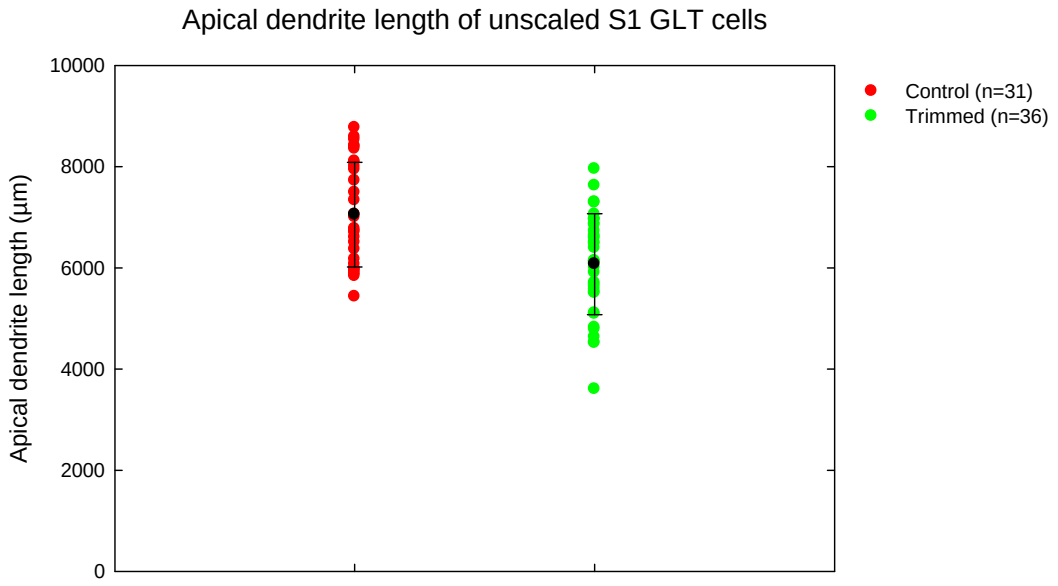

Figure 3-13: **Neuroexplorer apical dendrite of unscaled S1 GLT cells.** Comparison between control and trimmed groups revealed a significant difference (p=<0.001). The means are indicated by black circles and the standard deviations are shown by the tails.

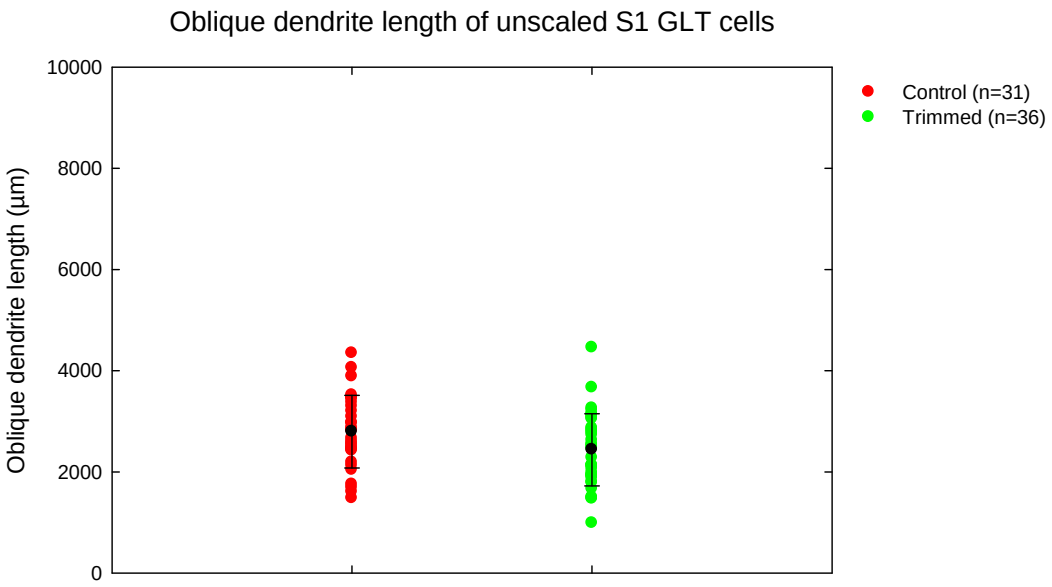

Figure 3-14: **Neuroexplorer oblique dendrite of unscaled S1 GLT cells.** Comparison between control and trimmed groups revealed that the control cells had significantly longer oblique dendrites than trimmed cells (p=0.046). The means are indicated by black circles and the standard deviations are shown by the tails.

3.2.2 Vibrissa motor cortex (vM1) GLT cells

Neuroexplorer analysis of all the apical and basal dendritic parameters of the vibrissal motor cortex GLT cells failed to reveal any differences between the control (n=28) and trimmed groups (n=29). The only exceptions were the pia-WM distance and the number of oblique dendrites. Mean control group pia-WM distance was 1501 ± 177 µm while that of the trimmed group was 1393 ± 83 µm. Mean number of oblique dendrites of the control group was 17 ± 3 while that of the trimmed group was 15 ± 3.

However, two points were noteworthy in this case. Firstly, similar to the barrel cortex cells, the significant difference in the pia-WM distance between control and trimmed vibrissal motor cortex cells made it difficult to interpret the results as a lack of a trimming effect. Secondly, the layer V band in motor cortex is rather diffuse as opposed to the compact location in other cortical areas. So the cells reconstructed had varying soma depths. Within the individual groups, cells differed in terms of their soma depths. So the vibrissal motor cortex cells were divided into two sub-groups, henceforth called upper vibrissal motor cortex cells (upper vM1 or upper vMC) and lower vibrissal motor cortex cells (lower vM1 or lower vMC) depending on whether the respective soma locations were above or below 650 µm. Despite separate analysis of upper and lower control and trimmed

vM1 cells, I failed to observe any significant differences in dendritic lengths between the control and trimmed groups. All data are shown in graphs below.

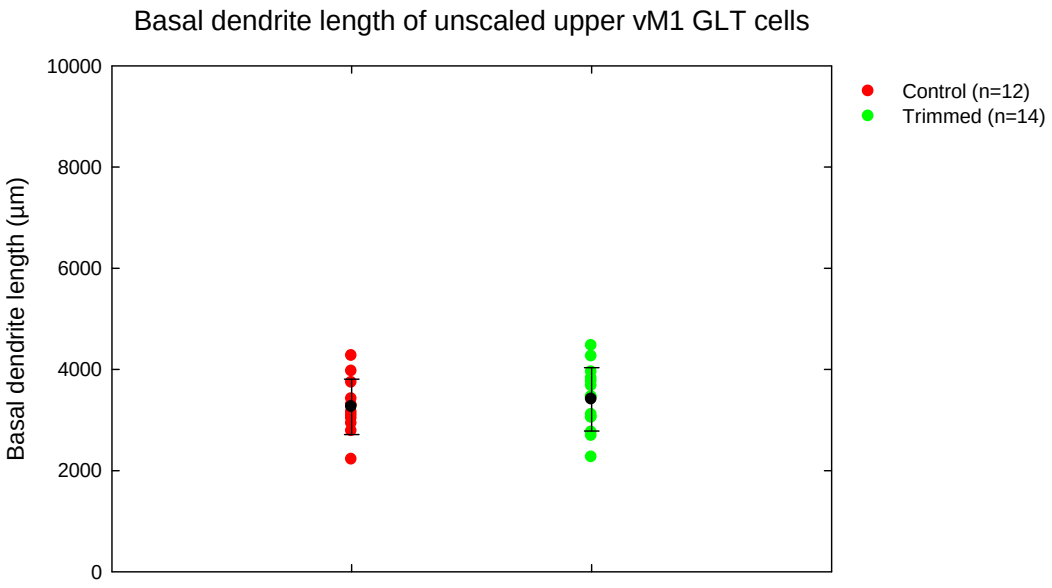

Figure 3-15: **Neuroexplorer basal dendrite of unscaled upper vM1 GLT cells.** Comparison between control and trimmed groups revealed no significant differences (p=0.534). The means are indicated by black circles and the standard deviations are shown by the tails.

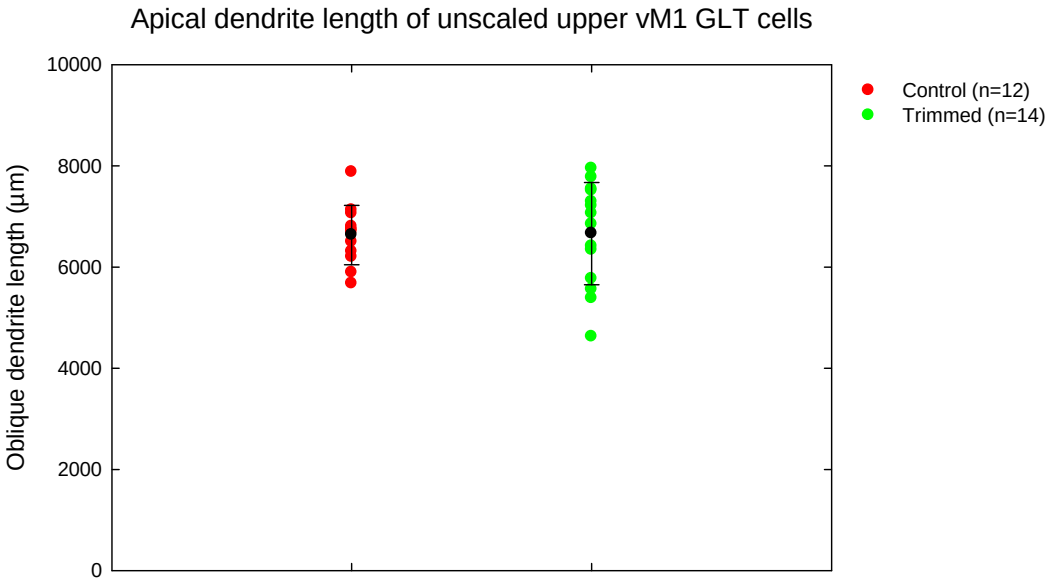

Figure 3-16: **Neuroexplorer apical dendrite of unscaled upper vM1 GLT cells.** Comparison between control and trimmed groups showed no significant differences (p=0.932). The means are indicated by black circles and the standard deviations are shown by the tails.

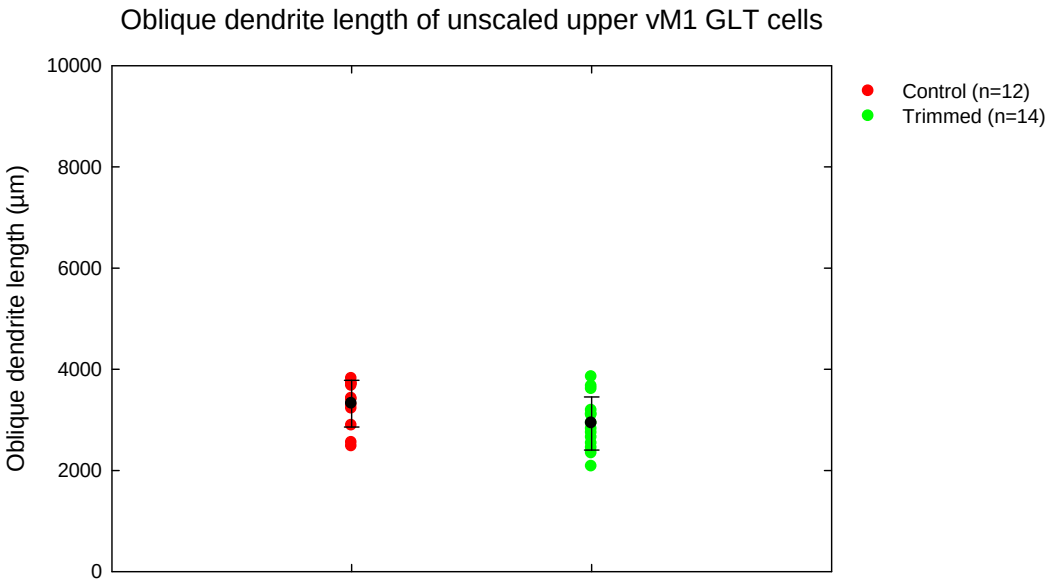

Figure 3-17: **Neuroexplorer oblique dendrite of unscaled upper vM1 GLT cells.** Comparison between control and trimmed groups indicated no significant differences (p=0.057). The means are indicated by black circles and the standard deviations are shown by the tails.

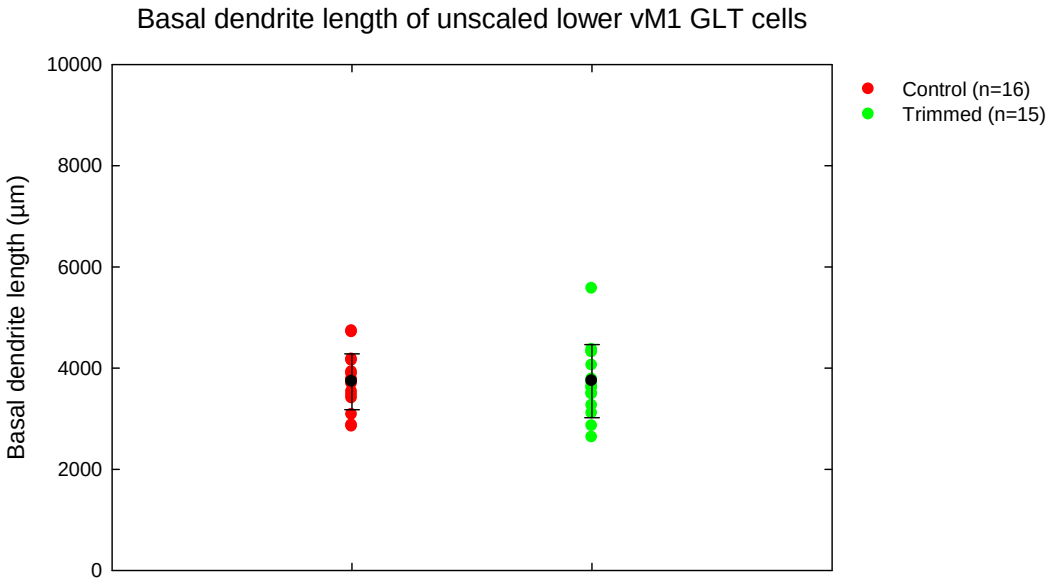

Figure 3-18: **Neuroexplorer basal dendrite of unscaled lower vM1 GLT cells.** Comparison between control and trimmed groups did not show any significant differences (p=0.956). The means are indicated by black circles and the standard deviations are shown by the tails.

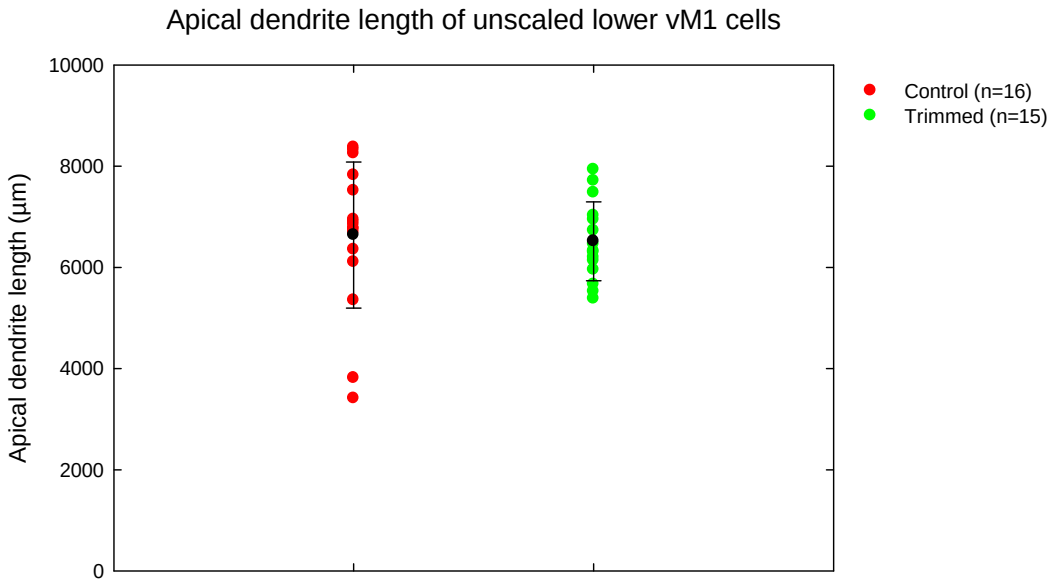

Figure 3-19: **Neuroexplorer apical dendrite of unscaled lower vM1 GLT cells.** Comparison between control and trimmed groups revealed no significant differences (p=0.771). The means are indicated by black circles and the standard deviations are shown by the tails.

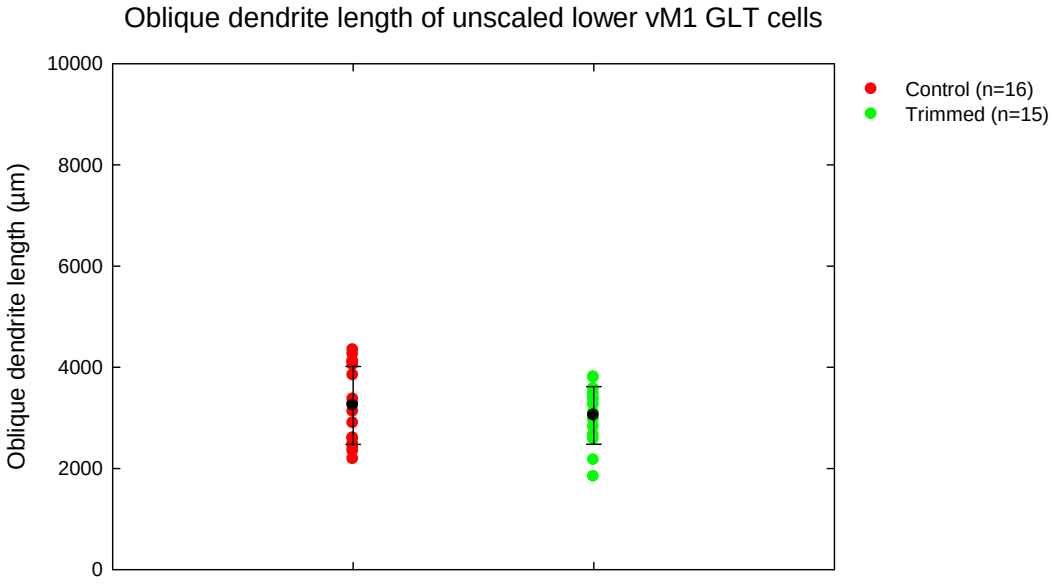

Figure 3-20: **Neuroexplorer oblique dendrite of unscaled lower vM1 GLT cells.** Comparison between control and trimmed groups indicated no significant differences (p=0.424). The means are indicated by black circles and the standard deviations are shown by the tails.

3.3 Rembrandt dendrite analyses of the original, unscaled cells

The MATLAB-based programme Rembrandt gave a bin-wise output of dendritic density per 50 μm^3 bin volume along the length of the neuron starting from piamater. Using this information, I first visually determined the length of the apical tufts of the cells. It is worthwhile to note here that the apical tuft of a cell was that part of its apical dendritic tree that is free from the proximal oblique dendrites. Usually dendritic density readout showed a feature preserved across cells: dendritic density (implicating complexity as well) was really high near the pia where these GLT cells horizontally fan out their dendrites. Moving down from the pia resulted in gradually decreasing dendritic density readouts which then abruptly decrease to stereotypically low values before increasing again in density and complexity signifying the start of the proximal oblique dendrites and the basal dendrites. I selected the topmost, high density values till the abrupt drop in values came and marked this as the apical tuft. This was done for each individual cell.

In contrast to this process, I also took the top 10, 20 and 30% of the individual pia-WM distances and called this the apical tuft as described by Groh et al (Groh et al., 2010). Usually, the visually selected apical tuft value fell between 20 and 30% apical tuft values. I then compared these different apical tufts between the control and trimmed groups.

3.3.1 Primary somatosensory cortex (S1) GLT cells

The mean length of visually selected apical tuft of the control group, 3811 ± 783 μm, was significantly higher than that of the trimmed group, namely, 3078 ± 921 μm ($p=<0.001$). Expectedly, 10, 20 and 30% apical tufts were also significantly longer in the control group than the trimmed group. The mean 10% apical tuft length of the control group was 2429 ± 745 μm whereas that of the trimmed group was 2049 ± 709 μm ($p=0.036$). 20% apical tuft length of the control and trimmed groups were 3394 ± 736 μm and 2784 ± 804 μm respectively ($p=0.002$). Mean control 30% apical tuft length was 3688 ± 729 μm in contrast to trimmed length of 3039 ± 826 μm ($p=0.001$). Lastly, mean control oblique dendrite length, 2773 ± 713 μm was also significantly higher than mean trimmed oblique dendrite length, 2422 ± 710 μm ($p=0.048$).

NOTE: Only the apical tuft and the oblique dendrites were analysed further using the Rembrandt programme to confirm or reject the differences implied by the Neuroexplorer analysis.

3.3.2 Vibrissa motor cortex (vM1) GLT cells

Supporting the data from the Neuroexplorer analyses of the unscaled, original vibrissal motor cortex cells, the Rembrandt analysis also confirmed the lack of significant differences between the control and trimmed mean dendritic lengths. Neither the visually selected apical tuft nor any of the 10, 20 or 30% apical tuft lengths was significantly different between the two groups. The oblique dendritic lengths were not an exception either.

Visually selected apical tuft had a mean length of 2569 ± 789 μm for the control group and 2909 ± 663 μm for the trimmed group. Mean control lengths of 10, 20 and 30% apical tuft were respectively, 2145 ± 725 μm, 2663 ± 736 μm, and 3212 ± 879 μm. Comparatively, the same for the trimmed group were 2253 ± 730 μm, 2882 ± 695 μm and 3351 ± 766 μm respectively. Mean control oblique dendrite length was 3259 ± 656 μm in contrast to the mean trimmed length of 2964 ± 538 μm.

Next, I separately analysed the vibrissal motor cortex cells divided into the two groups as mentioned above in the 'Neuroexplorer analyses' section, namely, upper and lower vibrissal motor cortex cells. However, there were still no significant differences between the control and the trimmed groups, thus confirming the results from the Neuroexplorer analyses.

3.4 Rembrandt dendrite analyses of scaled cells

Despite confirmation of the differences between the control and trimmed groups by the two tier analyses of original, unscaled cells with Neuroexplorer and Rembrandt, one needed an objective analytical method that could address the issues of variability in soma depth and contour distances between the two groups. This was especially imperative in order to interpret the stated differences. Hence, I scaled each cell to the group average pia-WM distance. Subsequently, I performed the Rembrandt analysis on these scaled cells to see if the differences in dendritic lengths actually hold true in a normalized scheme of things. This scaling of the cells rendered the need for visually selected apical tuft redundant and hence the data presented in the scaled analyses includes the 10, 20 and 30% apical tuft lengths as well as the oblique dendrites.

3.4.1 Primary somatosensory cortex (S1) GLT cells

Rembrandt analysis of the 10, 20 and 30% apical tuft lengths confirmed the trends that were shown in the previous analyses done on original, unscaled cells. The average 10% apical tuft length of control group of cells, 2360 ± 859 µm, was significantly higher than the average length of the trimmed group, 1825 ± 776 µm (p=0.009). The significance level even got higher with the 20% (p=0.002) and 30% (p=0.003) apical tuft lengths. The control group showed a mean 20% apical tuft length of 3505 ± 804 µm whereas the trimmed group was pegged at 2828 ± 935 µm. Similarly, in case of 30% apical tuft length, the control group's mean value was 3738 ± 799 µm while the trimmed group's mean length was 3060 ± 955 µm. The stripped oblique dendrites of the S1 GLT cells were also scaled using the same scaling factor, individual to each cell, and then subjected these scaled oblique dendrites to the Rembrandt analysis. Lastly, the oblique dendrite length mean for control group (2774 ± 656 µm) was significantly (p=0.021) higher than that of the trimmed group (2406 ± 615 µm). All data are graphically represented below.

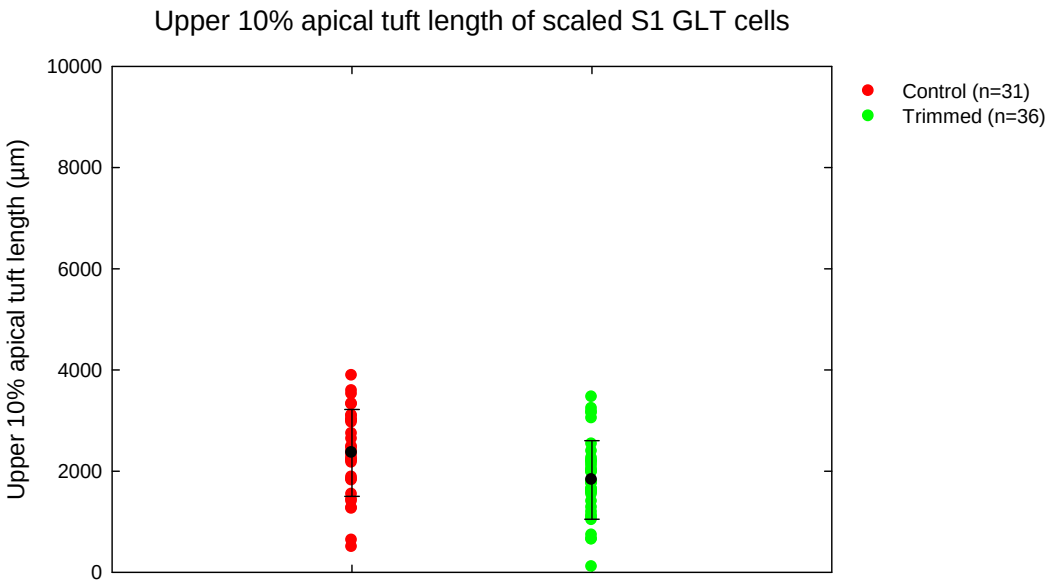

Figure 3-21: **Rembrandt 10% apical tuft of scaled S1 GLT cells**. Comparison of the 10% apical tuft length distributions in control and trimmed cells from S1. Cells from the control group had significantly longer tuft length than trimmed group (p=0.009). The means are indicated by black circles and the standard deviations are shown by the tails.

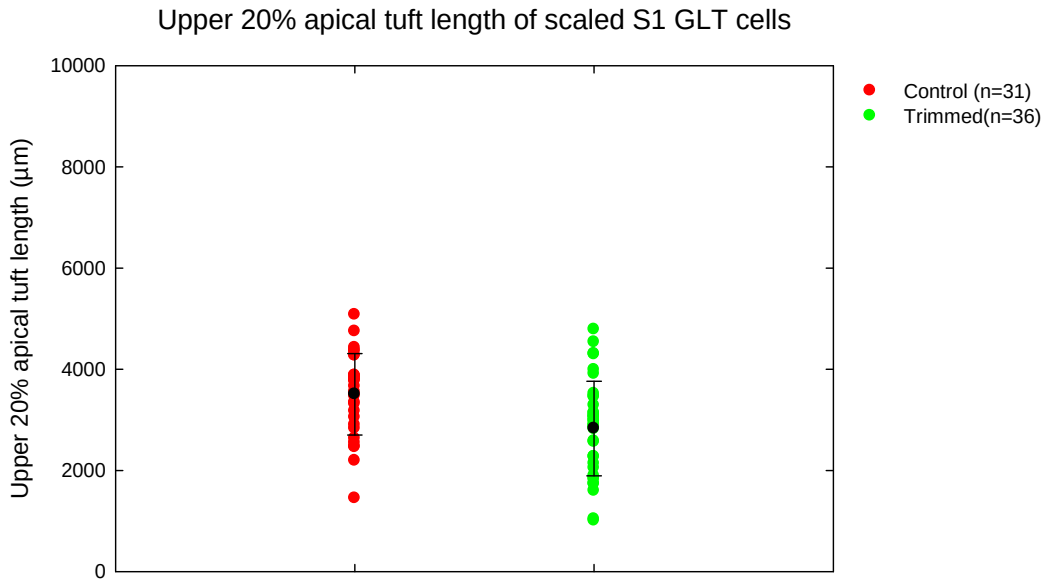

Figure 3-22: **Rembrandt 20% apical tuft of scaled S1 GLT cells.** Comparison of the 20% apical tuft length distributions in control and trimmed cells from S1. Cells from the control group had significantly longer tuft length than trimmed group (p=0.003). The means are indicated by black circles and the standard deviations are shown by the tails.

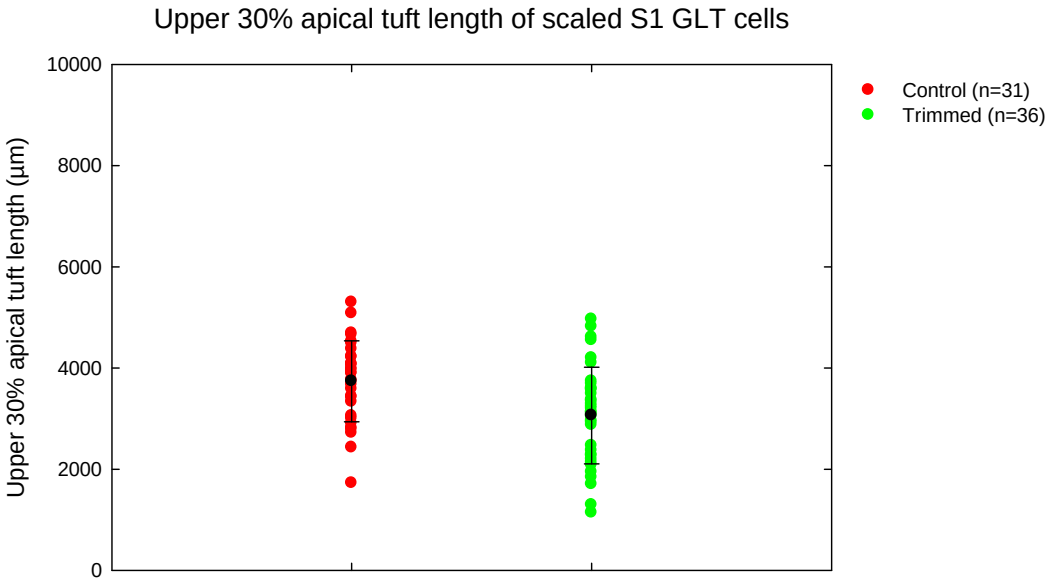

Figure 3-23: **Rembrandt 30% apical tuft of scaled S1 GLT cells.** Comparison of the 30% apical tuft length distributions in control and trimmed cells from S1. Cells from the control group had significantly longer tuft length than trimmed group (p=0.003). The means are indicated by black circles and the standard deviations are shown by the tails.

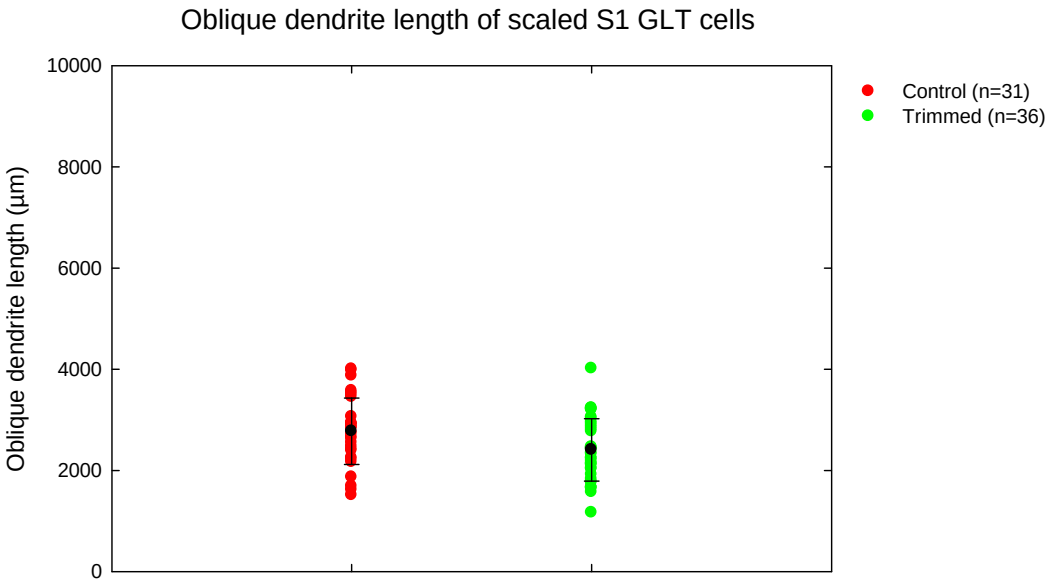

Figure 3-24: **Rembrandt oblique dendrites of scaled S1 GLT cells.** The control group had significantly longer oblique dendrites than their trimmed counterparts (p=0.021). The means are indicated by black circles and the standard deviations are shown by the tails.

3.4.2 Vibrissa motor cortex GLT cells

Not surprisingly, the trends shown by the Neurolucida and Rembrandt analyses of the unscaled cells were backed up by the Rembrandt results of the scaled vM1 cells. None of the 10, 20 or 30% apical tuft lengths showed any significant differences between control and trimmed groups. The control group had an average 10% apical tuft length of 2042 ± 736 µm while the trimmed group mean length was 2341 ± 751 µm. 20% apical tuft length of the control group was 2666 ± 783 µm on average as opposed to 2948 ± 767 µm of the trimmed cells. Similarly, 30% apical tuft length of control cells was reportedly 3180 ± 852 µm on average while mean 30% apical tuft length of the trimmed group was 3288 ± 826 µm. Lastly, the oblique dendritic length average for control cells was 3277 ± 644 µm over 2978 ± 598 µm for the trimmed cells. Also in this case, no significant differences existed. All data are shown in graphs below.

Interestingly, the trimmed group apical tuft lengths were higher than the control group but this was most probably attributable to random sampling variability. Similarly, it was difficult to interpret the comparatively higher control oblique length and random sampling variability could not be ruled out in this case either.

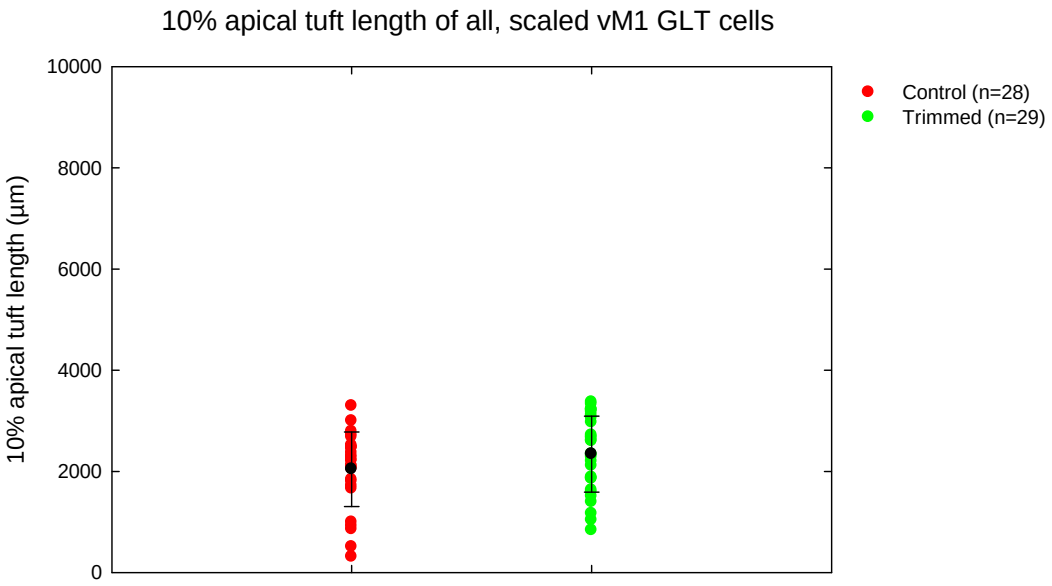

Figure 3-25: **Rembrandt 10% apical tuft of all, scaled vM1 GLT cells.** Comparison of 10% apical tuft length of control and trimmed cells from the vM1. The lengths were not significantly different (p=0.134). The means are indicated by black circles and the standard deviations are shown by the tails.

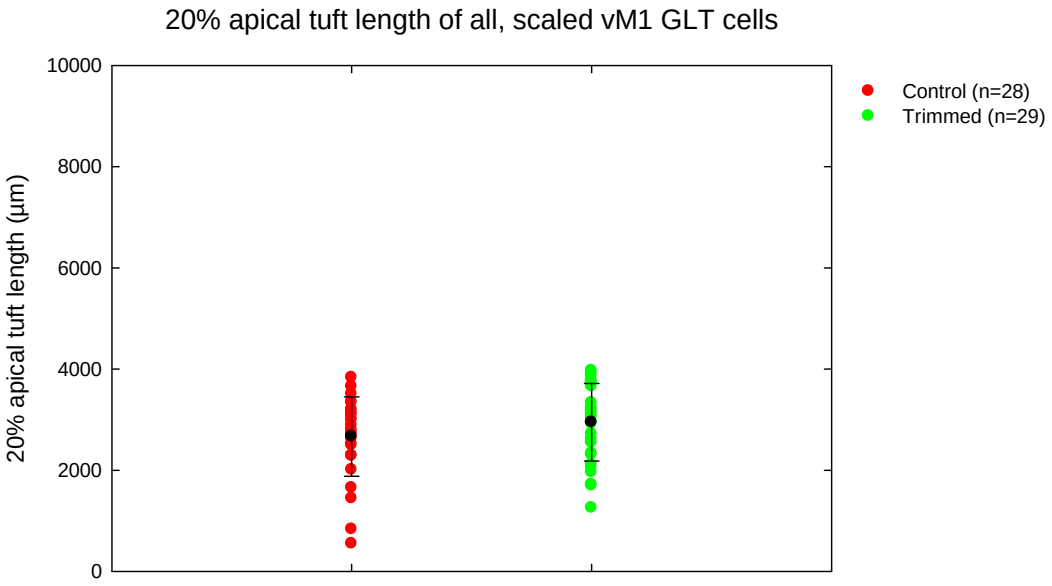

Figure 3-26: **Rembrandt 20% apical tuft of all, scaled vM1 GLT cells.** Comparison between all the cells from the control and trimmed groups of scaled vM1 cells revealed no significant difference (p=0.172). The means are indicated by black circles and the standard deviations are shown by the tails.

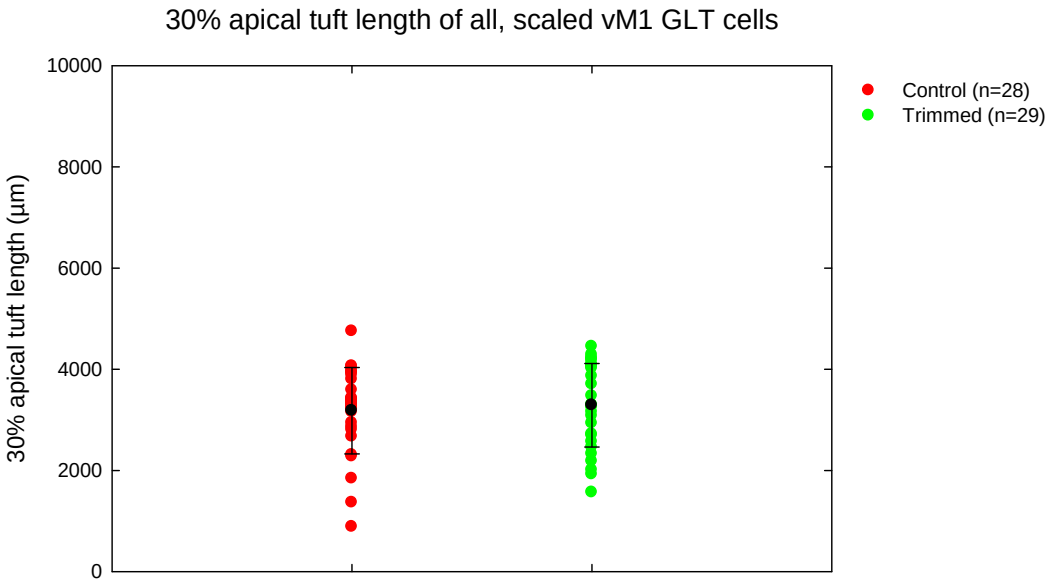

Figure 3-27: **Rembrandt 30% apical tuft of all, scaled vM1 GLT cells.** Comparison between all the cells from the control and trimmed groups of scaled vM1 cells revealed no significant difference (p=0.630). The means are indicated by black circles and the standard deviations are shown by the tails.

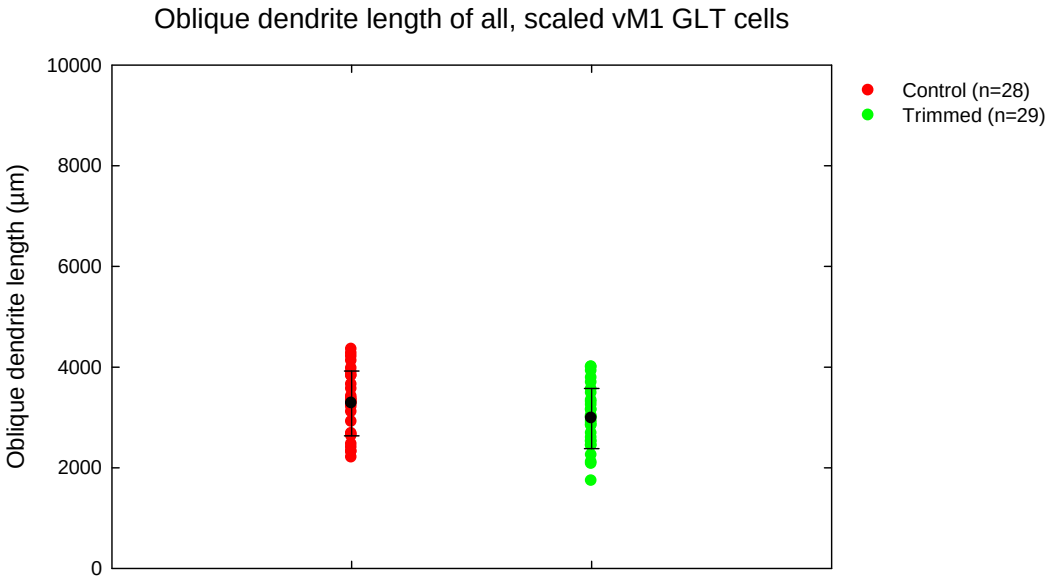

Figure 3-28: **Rembrandt oblique dendrites of all, scaled vM1 cells.** Comparison of oblique dendrite lengths of all, scaled vM1 cells from control and trimmed groups yielded no significant difference (p=0.075). The means are indicated by black circles and the standard deviations are shown by the tails.

Like earlier analyses, I also analysed the scaled vM1 cells after dividing them into upper vM1 and lower vM1 subgroups.

3.4.2.1 Upper vibrissa motor cortex (upper vM1) GLT cells

Rembrandt analysis of the scaled versions of these cells revealed that there were no significant differences between the different apical tuft lengths (10, 20 and 30%) between the control and trimmed groups. The average control group 10% apical tuft length was 2418 ± 391 µm as opposed to 2712 ±720 µm of the trimmed group. 20% apical tuft length average for the scaled control cells was pitted at 2950 ± 395 µm in contrast to the trimmed group average of 3276 ± 764 µm while 30% apical tuft length means for the control and trimmed groups were respectively, 3583 ± 541 µm and 3684 ± 794 µm.

One interesting outcome of this scaled cell analysis was that the control group average oblique length (3506 ± 588 µm) came out to be significantly (p=0.030) different from the trimmed group mean (2972 ± 592 µm). All data are represented in graphs below.

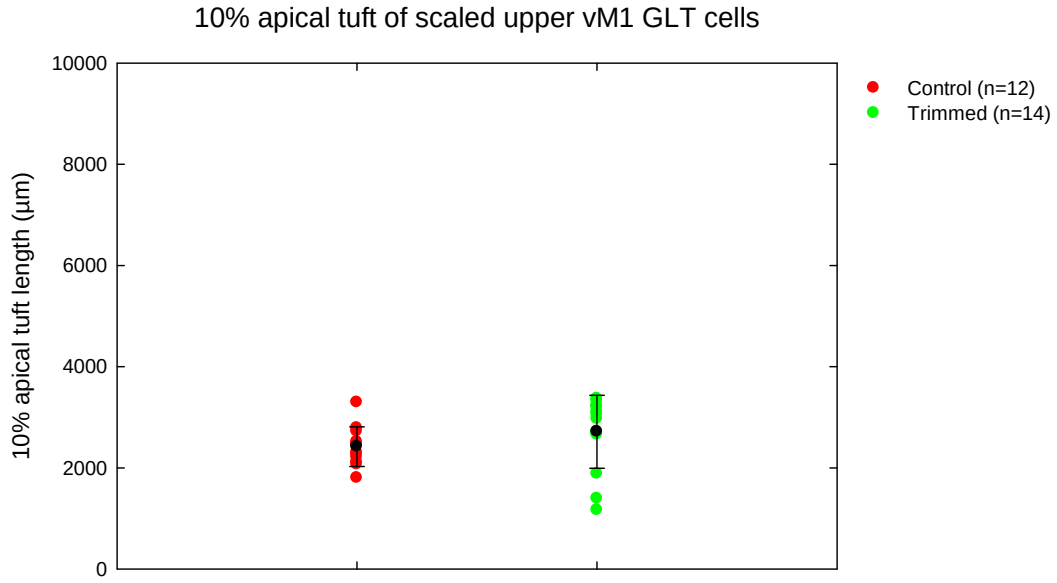

Figure 3-29: **Rembrandt 10% apical tuft of scaled upper vM1 GLT cells.** The control group did not differ significantly from the trimmed group (p=0.218). The means are indicated by black circles and the standard deviations are shown by the tails.

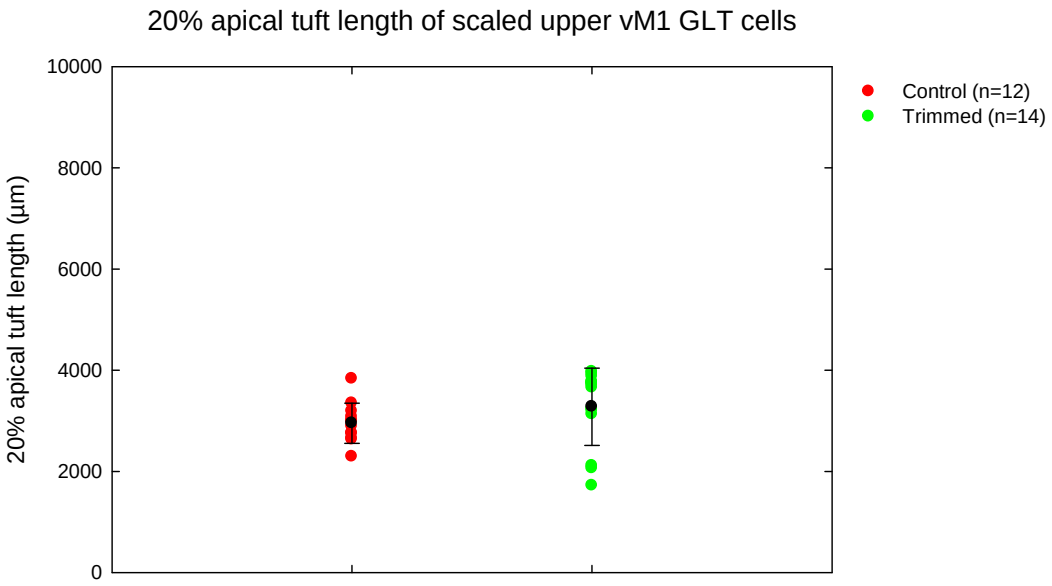

Figure 3-30: **Rembrandt 20% apical tuft of scaled upper vM1 GLT cells.** Comparison of the control and the trimmed group did not show any significant difference (p=0.196). The means are indicated by black circles and the standard deviations are shown by the tails.

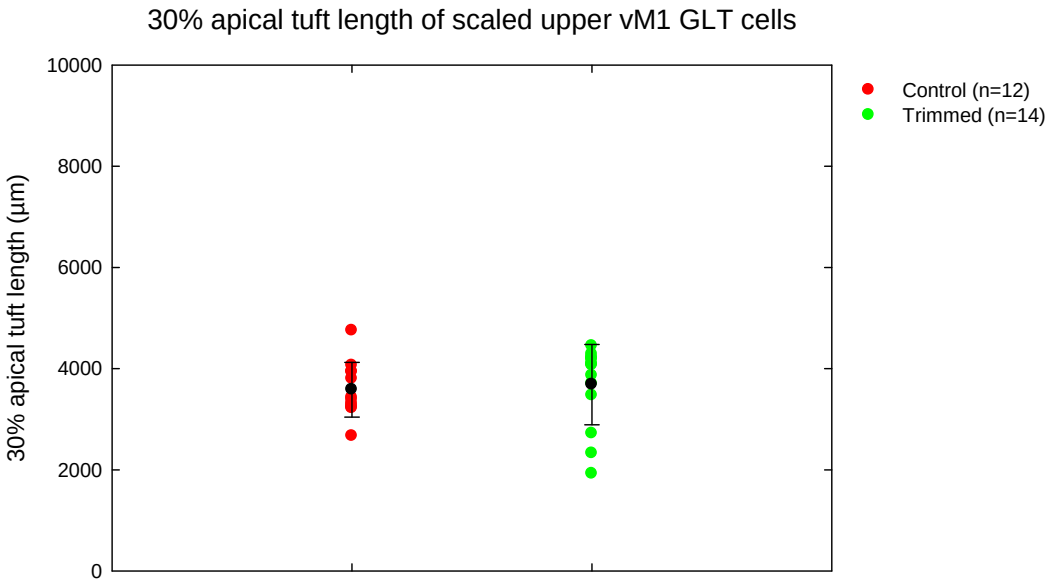

Figure 3-31: **Rembrandt 30% apical tuft of scaled upper vM1 GLT cells.** Comparison between control and trimmed groups did not reveal any significant difference (p=0.714). The means are indicated by black circles and the standard deviations are shown by the tails.

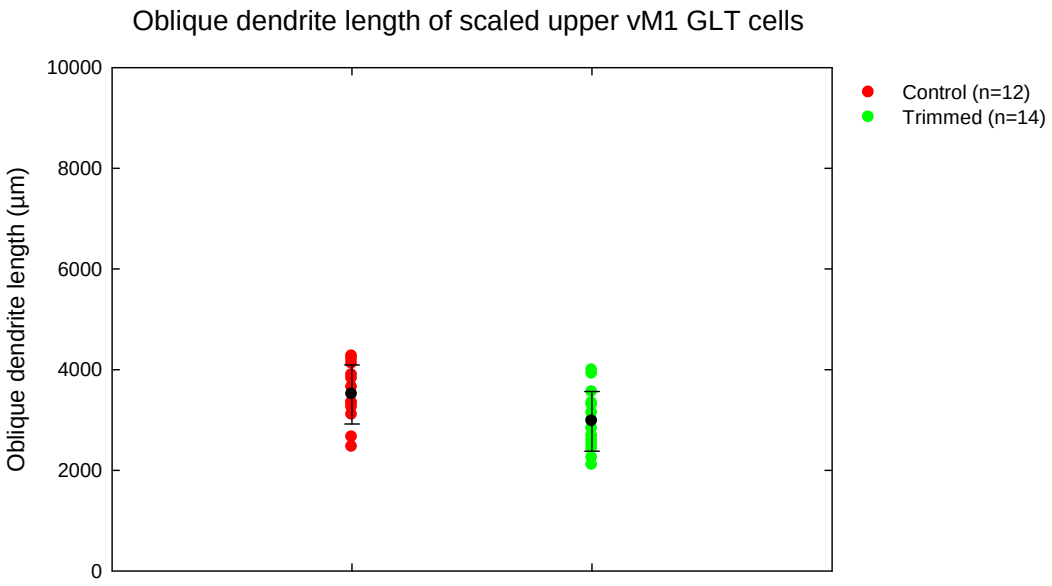

Figure 3-32: **Rembrandt oblique dendrites of scaled upper vM1 GLT cells.** The control group had significantly longer oblique dendrites than their trimmed counterparts (p=0.030). The means are indicated by black circles and the standard deviations are shown by the tails.

3.4.2.2 Lower vibrissa motor cortex (lower vM1) GLT cells

Even in the case of scaled lower vM1 cells, the Rembrandt analysis supported the previous analyses. No significant differences were found to exist between the control and trimmed groups in either the different apical tuft lengths or the oblique dendrite lengths. 10% apical tuft length average for control cells was 1760 ± 816 µm against 1995 ±617 µm for the trimmed group. Similarly, 20% apical tuft length of control group was 2453 ± 936 µm on average while the trimmed group average was 2641 ± 651 µm. Finally, the 30% tuft length was 2878 ± 930 µm on average in case of control group as opposed to 2918 ±690 µm on average in case of the trimmed cells.

However, as stated above, unlike the upper vM1 cells, the control average oblique length (3104 ± 647 µm) was not significantly different from the trimmed average (2983 ± 624 µm).

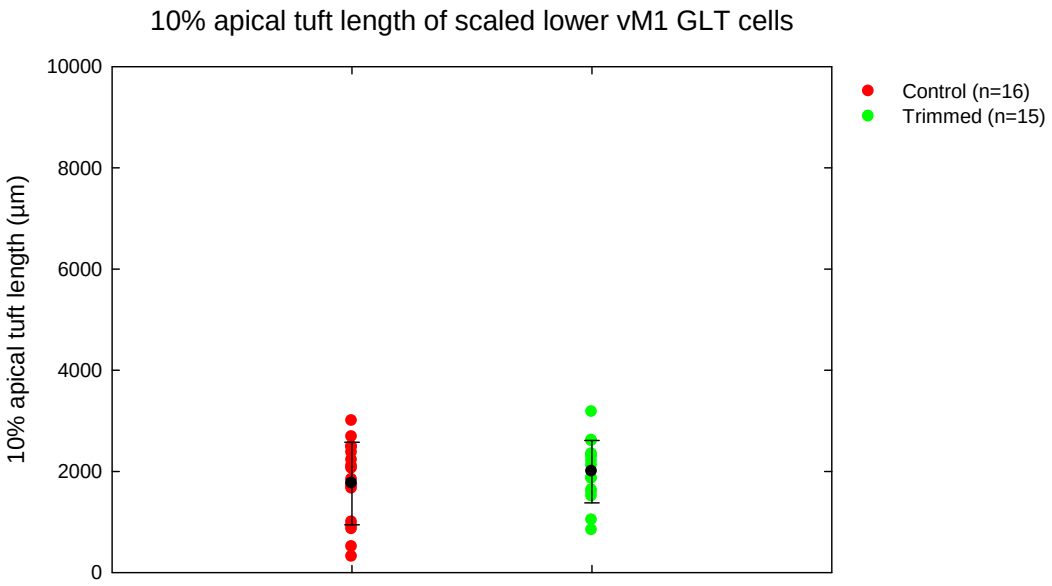

Figure 3-33: **10% apical tuft length of scaled lower vM1 GLT cells.** Comparison between the control and trimmed groups showed no significant difference (p=0.375). The means are indicated by black circles and the standard deviations are shown by the tails.

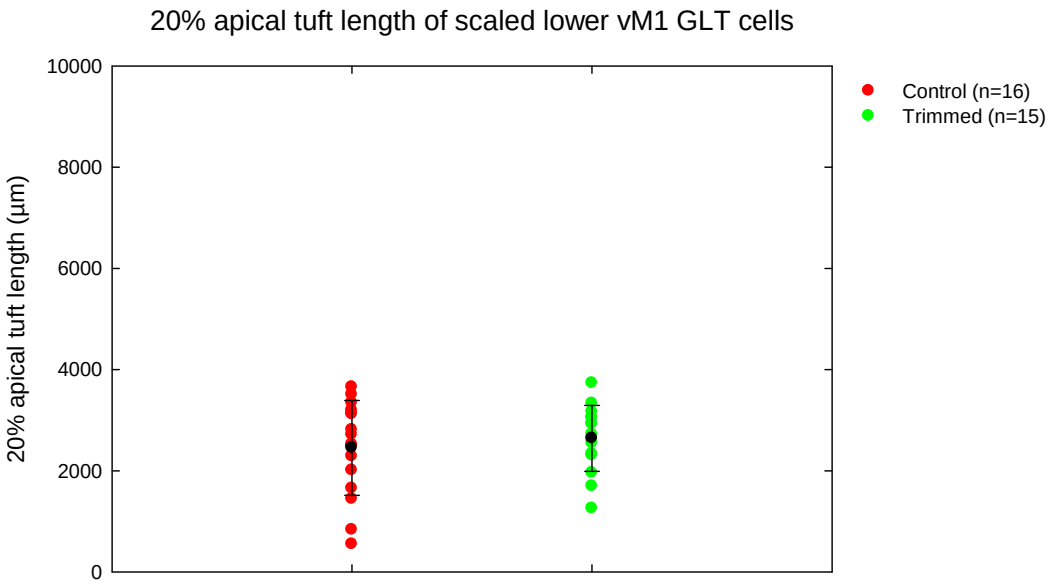

Figure 3-34: **20% apical tuft length of scaled lower vM1 GLT cells.** There were no significant differences between control and trimmed group lengths (p=0.523). The means are indicated by black circles and the standard deviations are shown by the tails.

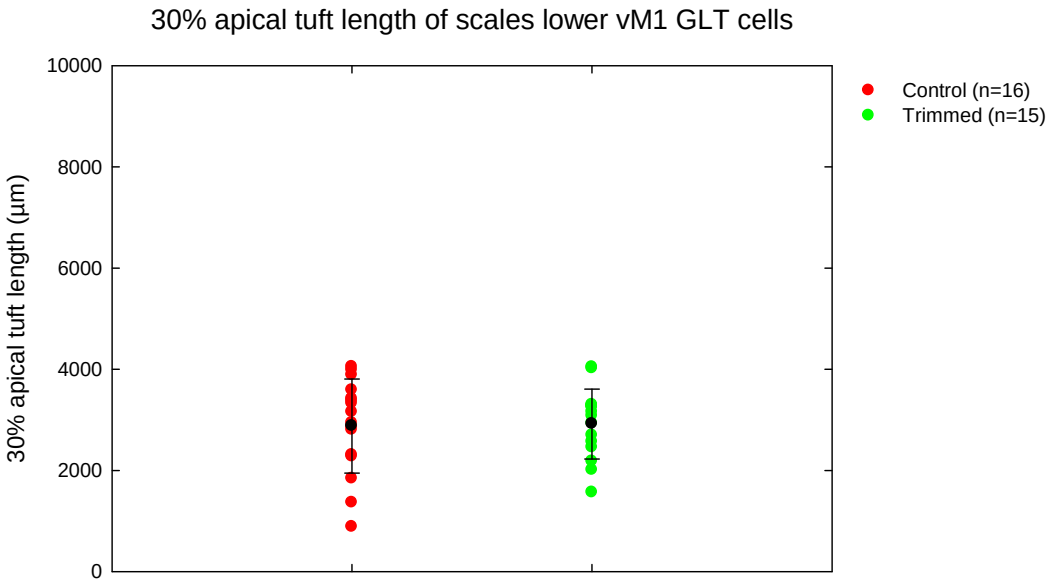

Figure 3-35: **30% apical tuft length of scaled lower vM1 GLT cells.** Comparison between the control and trimmed groups did not reveal a significant difference (p=0.892). The means are indicated by black circles and the standard deviations are shown by the tails.

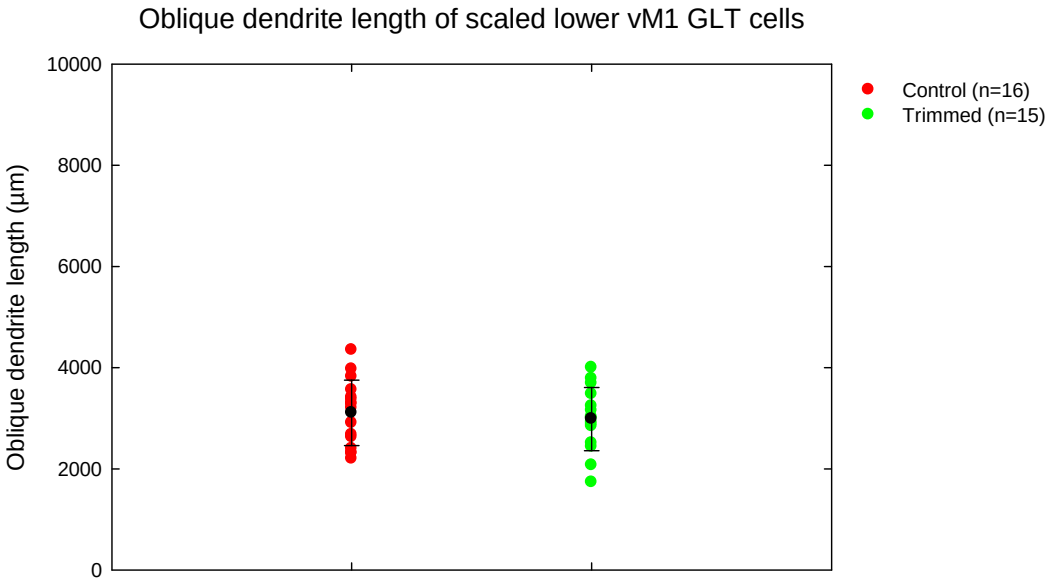

Figure 3-36: **Oblique dendrites of scaled lower vM1 GLT cells.** Comparison of the oblique dendrites of control and trimmed GLT cells. The control group did not differ in their oblique dendritic length significantly from those from trimmed group (p=0.601). The means are indicated by black circles and the standard deviations are shown by the tails.

3.5 Summary of Neuroexplorer and Rembrandt analysis

Although the Neuroexplorer analysis of the original, unscaled cells indicated the existing differences between the control and trimmed groups exhaustively, a method was needed to validate these differences in the light of the existing differences in the soma depth, pia-WM distance, pia-layer 4 distances between the groups. Only then could these differences be established conclusively as valid effects of the sensory deprivation paradigm (whisker trimming in this case). Hence, I investigated the stated differences first in the original, unscaled cells using Rembrandt, a custom-written programme that takes care of registering and normalizing the cells to standard contour distances chosen by the user.

The parameters in contention, where a possible trimming effect was thought to exist, were the apical tuft lengths and the oblique dendrite lengths. The definition of the apical tuft in case of Rembrandt analysis was stricter than Neuroexplorer analysis in order to exclude the proximal oblique dendrites (which constituted a separate quantity for analysis) completely from the apical tuft. In addition to visually selecting and defining the apical tuft for each cell individually, 10, 20, 30% of the respective pia-WM distances were assigned to be the length of the apical tuft along the lines of a study by Groh et al (Groh et al., 2010). Typically, the visually selected apical tuft length lay in between the 20 and 30% categories. However, the point of using the Rembrandt programme first on the original cells was to see whether the differences shown by Neuroexplorer analysis still held ground. I confirmed previously that this was indeed the case and that the stated differences between the groups were also present in the Rembrandt results from original cells. While the S1 GLT cells from control group showed significant differences in their apical tuft and oblique dendrites (basal dendrites showing no significant differences) in comparison to those from the trimmed group, the cells from the vM1 showed no differences between control and trimmed groups. Even a division of vM1 cells into subgroups (to reduce intra-group variability) supported the previous results from Neuroexplorer analysis.

However, in order to be more accurate, I also then scaled the original cells to conform to their group's average pia-WM distance to remove any false-positive differences that could be due to the contour differences. In this case 10, 20 and 30% of pia-WM distance were the same for the cells of a particular group. Thus, the definition of apical tuft became even stricter than the last analysis and at the same time more standardized and objective. The scaled Rembrandt analyses fully supported the previously confirmed results and showed significant differences in the apical tuft and oblique dendrites of S1 GLT cells while confirming once again the lack of differences in the apical tuft of the

vM1 cells. However, surprisingly, this analysis showed a significant difference between the control and trimmed oblique dendrites of the upper vM1 cells, which had, thus far, failed to turn up in the analyses of original, unscaled cells.

Taken together, my results show that the apical tufts and oblique dendrites of the control group of cells are significantly longer than those from the trimmed group of cells in case of S1 GLT cells (at all levels of analysis) while only the upper vM1 cells from the control group exhibited significantly longer oblique dendrites than those from the trimmed group (but only in the scaled cells). That aside, the vM1 cells in general were not different in the control and the trimmed groups.

3.6 Tabled results

Table 3.8.1.1: Neuroexplorer summary of apical and basal dendrite parameters of all unscaled S1 GLT cells

Cell and group type	Pia-WM (µm)	Pia-lower L4(µm)	Pia-soma (µm)	Pia-upper L4(µm)	Apical dendritic length (µm)	Nodes in apical tree	Endings in apical tree	Basal dendritic length (µm)	Nodes in basal tree	Endings in basal tree	Number of 1° basal dendrites
BC GLT control	1174 ± 124	623 ± 45	741 ± 58	431 ± 60	7049 ± 1034	46 ± 7	47 ± 7	3610 ± 717	25 ± 8	33 ± 8	8 ± 2
BC GLT trimmed	1228 ± 116	663 ± 42	784 ± 72	472 ± 46	6074 ± 997	42 ± 8	43 ± 8	3291 ± 1056	24 ± 8	31 ± 9	7 ± 2

Comparison between the two groups

p=0.072	p=<0.001	p=0.009	p=<0.001	p=<0.001	p=0.043	p=0.052	p=0.160	p=0.426	p=0.352	p=0.561

1. This table shows apical and basal dendrite parameters of all raw, unscaled S1 GLT cells as measured with Neuroexplorer.
2. Dark squares indicate significant differences between the groups while white squares indicate insignificant differences
p value of p=<0.05 was considered significant. The programme Sigmaplot was used for statistical analysis.
3. Statistical tests performed include Student's T-test in cases of normal, equally-varying data distribution and Mann-Whitney rank sum test in cases of non-normal distributions. Only the distribution of number of basal dendrites was found to be non-normal.

Table 3.8.1.2: Neuroexplorer summary of oblique dendrite parameters of all unscaled S1 GLT cells

Cell and group type	Number of oblique dendrites	Oblique dendrite length (µm)	Rembrandt scaled oblique dendrite length (µm)
BC GLT control	11 ± 3	2795 ± 717	2774 ± 656
BC GLT trimmed	11 ± 3	2438 ± 713	2406 ± 615

Comparison between the two groups

p=0.176	p=0.046

1. This table shows oblique dendrite parameters of all raw, unscaled S1 GLT cells as measured with Neuroexplorer.
2. Dark squares indicate significant differences between the groups while white squares indicate insignificant differences
p value of p=<0.05 was considered significant. The programme Sigmaplot was used for statistical analysis.
3. Statistical tests performed include Student's T-test in cases of normal, equally-varying data distribution and Mann-Whitney rank sum test in cases of non-normal distributions. Only the distribution of number of oblique dendrites was found to be non-normal.

Table 3.8.1.3: Rembrandt summary of apical tuft and oblique dendrites of all unscaled S1 GLT cells

Cell and group type	Rembrandt visually selected apical tuft length (µm)	Rembrandt 10% apical tuft length (µm)	Rembrandt 20% apical tuft length (µm)	Rembrandt 30% apical tuft length (µm)	Oblique dendrite length (µm)
BC GLT control	3811 ± 783	2429 ± 745	3394 ± 736	3688 ± 729	2773 ± 713
BC GLT trimmed	3078 ± 921	2049 ± 709	2784 ± 804	3039 ± 826	2422 ± 710

Comparison between control and trimmed groups

p=<0.001	p=0.036	p=0.002	p=0.001	p=0.048

1. This table shows apical tuft and oblique dendrite lengths of all raw, unscaled S1 GLT cells as measured with Rembrandt.
2. Dark squares indicate significant differences between the groups while white squares indicate insignificant differences p value of p=<0.05 was considered significant. The programme Sigmaplot was used for statistical analysis.
3. Statistical tests performed include Student's T-test in cases of normal, equally-varying data distribution and Mann-Whitney rank sum test in cases of non-normal distributions. Only the distribution of number of oblique dendrites was non-normal.
4. Manual determination of apical tuft length: when the Rembrandt dendritic density/50 µm bins reached stereotypical low values in comparison to the heavily dense topmost tuft readouts, the apical tuft was taken to have ended. It was on average 7.6 bins for the control group and 7.1 bins for the trimmed group.

Table 3.8.1.4: Rembrandt summary of apical tuft and oblique dendrites of all scaled S1 GLT cells
(scaled to mean pia-WM distances of 1174 µm and 1228 µm for control and trimmed cells respectively)

Cell and group type	Rembrandt 10% apical tuft length (µm)	Rembrandt 20% apical tuft length (µm)	Rembrandt 30% apical tuft length (µm)	Oblique dendrite length (µm)
BC GLT control	2360 ± 859	3505 ± 804	3738 ± 799	2774 ± 656
BC GLT trimmed	1825 ± 776	2828 ± 935	3060 ± 955	2406 ± 615

Comparison between control and trimmed groups

p=0.009	p=0.002	p=0.003	p=0.021

1. This table shows apical tuft and oblique dendrite lengths of all scaled S1 GLT cells as measured with Rembrandt.
2. Dark squares indicate significant differences between the groups while white squares indicate insignificant differences p value of p=<0.05 was considered significant. The programme Sigmaplot was used for statistical analysis.
3. Statistical tests performed include Student's T-test in cases of normal, equally-varying data distribution.

Table 3.8.2.1: Neuroexplorer summary of apical and basal dendrite parameters of all unscaled vMC GLT cells

Cell and group type	Pia-WM (µm)	Pia-lower L4 (µm)	Pia-soma (µm)	Pia-upper L4 (µm)	Apical dendritic length (µm)	Nodes in apical tree	Endings in apical tree	Basal dendritic length (µm)	Nodes in basal tree	Endings in basal tree	Number of 1° basal dendrites
vMC GLT control	1501 ± 177		733 ± 104		6635 ± 1140	45 ± 9	47 ± 9	3528 ± 588	22 ± 5	30 ± 5	9 ± 2
vMC GLT trimmed	1393 ± 83		686 ± 95		6585 ± 885	44 ± 8	46 ± 8	3580 ± 687	23 ± 6	32 ± 6	9 ± 2

Comparison between the two groups

p=0.005		p=0.098		p=0.852	p=0.660	p=0.701	p=0.761	p=0.077	p=0.076	p=0.401

1. This table shows apical and basal dendrite parameters of all raw, unscaled vMC GLT cells as measured with Neuroexplorer.
2. Dark squares indicate significant differences between the groups while white squares indicate insignificant differences.
p value of p=<0.05 was considered significant. Sigmaplot was used for statistical analysis.
3. Statistical tests performed include Student's T-test in cases of normal, equally-varying data distribution and Mann-Whitney rank sum test in cases of non-normal distributions. The distributions of numbers of basal and apical dendrites, number of endings in basal and apical dendrites, pia soma distances and pia WM distances were found to be non-normal.

Table 3.8.2.2: Neuroexplorer summary of oblique dendrite parameters of all unscaled vMC GLT cells

Cell and group type	Number of oblique dendrites	Oblique dendrite length (µm)
vMC GLT control	17 ± 3	3277 ± 647
vMC GLT trimmed	15 ± 3	2990 ± 541

Comparison between the two groups

p=<0.001	p=0.074

1. This table shows oblique dendrite parameters of all raw, unscaled vMC GLT cells as measured with Neuroexplorer.
2. Dark squares indicate significant differences between the groups while white squares indicate insignificant differences.
p value of p=<0.05 was considered significant. The programme Sigmaplot was used for statistical analysis.
3. Statistical tests performed include Student's T-test in cases of normal, equally-varying data distribution and Mann-Whitney rank sum test in cases of non-normal distributions. Only the distribution of number of oblique dendrites was found to be non-normal.

Table 3.8.2.3: Neuroexplorer summary of dendrite parameters of unscaled upper vMC GLT cells

Cell and group type	Basal dendritic length (µm)	Apical dendritic length (µm)	Oblique dendrite length (µm)
Upper vMC GLT control	3260 ± 546	6632 ± 588	3320 ± 462
Upper vMC GLT trimmed	3406 ± 626	6660 ± 1010	2929 ± 523

Comparison between the control and trimmed groups

p=0.534	p=0.932	p=0.057

1. This table shows dendrite parameters of raw, unscaled upper vMC GLT cells as measured with Neuroexplorer.
2. Dark squares indicate significant differences between the groups while white squares indicate insignificant differences p value of p=<0.05 was considered significant. Sigmaplot was used for statistical analysis.
3. Statistical tests performed include Student's T-test in cases of normal, equally-varying data distribution.

Table 3.8.2.4: Neuroexplorer summary of dendrite parameters of unscaled lower vMC GLT cells

Cell and group type	Basal dendritic length (µm)	Apical dendritic length (µm)	Oblique dendrite length (µm)
Lower vMC GLT control	3729 ± 551	6638 ±1444	3246 ± 771
Lower vMC GLT trimmed	3742 ± 723	6515 ± 779	3047 ± 569

Comparison between the control and trimmed groups

p=0.956	p=0.771	p=0.424

1. This table shows dendrite parameters of raw, unscaled lower vMC GLT cells as measured with Neuroexplorer.
2. Dark squares indicate significant differences between the groups while white squares indicate insignificant differences p value of p=<0.05 was considered significant. The programme Sigmaplot was used for statistical analysis.
3. Statistical tests performed include Student's T-test in cases of normal, equally-varying data distribution.

Table 3.8.2.5: Rembrandt summary of apical tuft and oblique dendrites of all unscaled vMC GLT cells

Cell and group type	Rembrandt visually selected apical tuft length (µm)	Rembrandt 10% apical tuft length (µm)	Rembrandt 20% apical tuft length (µm)	Rembrandt 30% apical tuft length (µm)	Oblique dendrite length (µm)
vMC GLT control	2569 ± 789	2145 ± 725	2663 ± 736	3212 ± 879	3259 ± 656
vMC GLT trimmed	2909 ± 663	2253 ± 730	2882 ± 695	3351 ± 766	2964 ±538

Comparison between the control and trimmed groups

p=0.105	p=0.579	p=0.250	p=0.526	p=0.067

1. This table shows apical tuft and oblique dendrite lengths of all raw, unscaled vMC GLT cells as measured with Rembrandt.
2. Dark squares indicate significant differences between the groups while white squares indicate insignificant differences p value of p=<0.05 was considered significant. The programme Sigmaplot was used for statistical analysis.
3. Statistical tests performed include Student's T-test in cases of normal, equally-varying data distribution and Mann-Whitney rank sum test in cases of non-normal distributions. Only the distributions of number of oblique dendrites and manually selected apical tuft lengths were non-normal.
4. Manual determination of apical tuft length: when the Rembrandt dendritic density/50 µm bins reached stereotypical low values in comparison to the heavily dense topmost tuft readouts, the apical tuft was taken to have ended. It was on average 4.9 bins for the control group and 5.6 bins for the trimmed group. When classified into upper and lower vMC cells, upper and lower vMC control cells had respectively 4.6 and 5.3 bins of apical tuft while upper and lower vMC trimmed cells had respectively 4.9 and 6.1 bins of apical tuft respectively.

Table 3.8.2.6: Rembrandt summary of apical tuft and oblique dendrite length of all scaled vMC GLT cells (scaled to mean pia-WM distances of 1501 µm and 1393 µm for control and trimmed cells respectively)

Cell and group type	Rembrandt 10% apical tuft length (µm)	Rembrandt 20% apical tuft length (µm)	Rembrandt 30% apical tuft length (µm)	Oblique dendrite length (µm)
vMC GLT control	2042 ± 736	2666 ± 783	3180 ± 852	3277 ± 644
vMC GLT trimmed	2341 ± 751	2948 ± 767	3288 ± 826	2978 ± 598

Comparison between the control and trimmed groups

p=0.134	p=0.172	p=0.630	p=0.075

1. This table shows apical tuft and oblique dendrite lengths of all scaled vMC GLT cells as measured with Rembrandt.
2. Dark squares indicate significant differences between the groups while white squares indicate insignificant differences p value of p=<0.05 was considered significant. The programme Sigmaplot was used for statistical analysis.
3. Statistical tests performed include Student's T-test in cases of normal, equally-varying data distribution and Mann-Whitney rank sum test in cases of non-normal distributions. Only the distribution of 20% apical tuft length was found to be non-normal.

Table 3.8.2.7: Rembrandt summary of apical tuft and oblique dendrite length of unscaled upper vMC GLT cells

Cell and group type	Rembrandt 10% apical tuft length (µm)	Rembrandt 20% apical tuft length (µm)	Rembrandt 30% apical tuft length (µm)	Oblique dendrite length (µm)
Upper vMC GLT control	2370 ± 391	2797 ± 396	3437 ± 616	3294 ± 463
Upper vMC GLT trimmed	2493 ± 779	3138 ± 701	3686 ± 734	2903 ± 521

Comparison between the control and trimmed groups

p=0.623	p=0.148	p=0.363	p=0.056

1. This table shows apical tuft and oblique dendrite lengths of raw, unscaled upper vMC GLT cells as measured with Rembrandt.
2. Dark squares indicate significant differences between the groups while white squares indicate insignificant differences
p value of p=<0.05 was considered significant. The programme Sigmaplot was used for statistical analysis.
3. Statistical tests performed include Student's T-test in cases of normal, equally-varying data distribution.

Table 3.8.2.8: Rembrandt summary of apical tuft and oblique dendrite length of unscaled lower vMC GLT cells

Cell and group type	Rembrandt 10% apical tuft length (µm)	Rembrandt 20% apical tuft length (µm)	Rembrandt 30% apical tuft length (µm)	Oblique dendrite length (µm)
Lower vMC GLT control	1977 ± 874	2563 ± 914	3044 ± 1021	3233 ± 785
Lower vMC GLT trimmed	2029 ± 626	2643 ± 619	3039 ± 675	3020 ± 565

Comparison between the control and trimmed groups

p=0.852	p=0.779	p=0.998	p=0.394

1. This table shows apical tuft and oblique dendrite lengths of raw, unscaled lower vMC GLT cells as measured with Rembrandt.
2. Dark squares indicate significant differences between the groups while white squares indicate insignificant differences
p value of p=<0.05 was considered significant. The programme Sigmaplot was used for statistical analysis.
3. Statistical tests performed include Student's T-test in cases of normal, equally-varying data distribution and Mann-Whitney rank sum test in cases of non-normal distributions. Only the distribution of number of oblique dendrites was non-normal.

Table 3.8.2.9: Rembrandt summary of apical tuft and oblique dendrites of scaled upper vMC GLT cells
(scaled to mean pia-WM distances of 1501 µm and 1393 µm for control and trimmed cells respectively)

Cell and group type	Rembrandt 10% apical tuft length (µm)	Rembrandt 20% apical tuft length (µm)	Rembrandt 30% apical tuft length (µm)	Oblique dendrite length (µm)
Upper vMC GLT control	2418 ± 391	2950 ± 395	3583 ± 541	3506 ± 588
Upper vMC GLT trimmed	2712 ±720	3276 ± 764	3684 ± 794	2972 ± 592

Comparison between the control and trimmed groups

p=0.218	p=0.196	p=0.714	p=0.030

1. This table shows apical tuft and oblique dendrite lengths of scaled upper vMC GLT cells as measured with Rembrandt.
2. Dark squares indicate significant differences between the groups while white squares indicate insignificant differences p value of p=<0.05 was considered significant. The programme Sigmaplot was used for statistical analysis.
3. Statistical tests performed include Student's T-test in cases of normal, equally-varying data distribution.

Table 3.8.2.10: Rembrandt summary of apical tuft and oblique dendrites of scaled lower vMC GLT cells
(scaled to mean pia-WM distances of 1501 µm and 1393 µm for control and trimmed cells respectively)

Cell and group type	Rembrandt 10% apical tuft length (µm)	Rembrandt 20% apical tuft length (µm)	Rembrandt 30% apical tuft length (µm)	Oblique dendrite length (µm)
Lower vMC GLT control	1760 ± 816	2453 ± 936	2878 ± 930	3104 ± 647
Lower vMC GLT trimmed	1995 ±617	2641 ± 651	2918 ±690	2983 ± 624

Comparison between the control and trimmed groups

p=0.375	p=0.523	p=0.892	p=0.601

1. This table shows apical tuft and oblique dendrite lengths of scaled lower vMC GLT cells as measured with Rembrandt.
2. Dark squares indicate significant differences between the groups while white squares indicate insignificant differences p value of p=<0.05 was considered significant. The programme Sigmaplot was used for statistical analysis.
3. Statistical tests performed include Student's T-test in cases of normal, equally-varying data distribution.

3.7 Rothko two-dimensional plots of dendritic distribution

Having established the existence of the inter-group differences, I was interested in finding out, exactly where along the vertical span of the apical tuft the changes existed. This was interesting, given that the thalamic innervation from VPM and/or POm were hypothesized to influence any changes in S1 dendrite complexity due to the trimming protocol. In order to investigate the spatial location of the inter-group differences, I used another custom-written programme called Rothko v041 that used the dendritic density patterns for cells obtained from the Rembrandt programme and plotted them on a two-dimensional scale. So, using this programme, one could see the quantitative pattern of dendritic length/complexity of cells starting from the pia to the entire vertical span of the cell. However, because the oblique dendrites are by and large concentrated in a small volume near the soma, this analysis was not of paramount interest in the case of the oblique dendrites. In any case, the programme Rothko was not sensitive enough to separately pick up differences between oblique and basal dendrites.

As the VPM and POm innervation is strictly dependent on the contour positions and relatively indifferent to the soma location, I re-registered and scaled the cells from a pia-centred perspective, that is, the pia was taken to the reference point. This made sure that the cells were scaled starting right below the pia in order to obtain an optimized overlap with the VPM and/or POm innervation patterns to be able to infer their possible influences on dendritic complexity.

Hence using this pia centred Rothko displays of dendritic distribution, I generated overlaps of the dendritic profiles of the cells of the control and trimmed groups. This gave me direct evidence of the exact spatial locations of any inter-group differences. Additionally, I also generated Rothko two-dimensional distribution of the absolute differences in dendritic distributions of control and trimmed cells using the Rembrandt binned values.

The following two-dimensional profiles (profiles 3.6.1-3.6.2.2.1, pages 92-97) illustrate the results of Rothko analysis.

Profile 3.6.1: Dendritic density distribution of pia-centred primary barrel cortex (S1) control and trimmed GLT cells.

(The plots were generated using custom-made programme Rothko and merged using CorelDRAW; control in blue, n=31 and trimmed in yellow, n=36; the bold lines show the mean and the dotted lines indicate standard deviation. The asterisk(s) and adjacent bar(s) show the bin(s) of significant difference.)

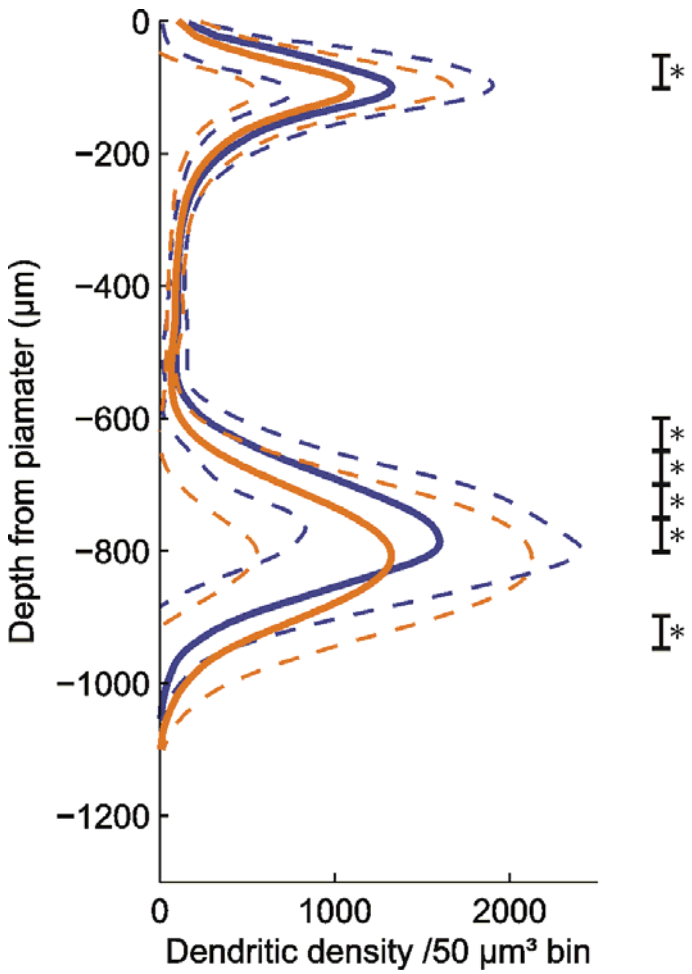

Profile 3.6.1.1: Absolute difference in the dendritic density distributions of pia-centred primary barrel cortex (S1) control and trimmed GLT cells shown as area under the curve.
(The plots were generated using custom-made programme Rothko; control n=31, trimmed n=36.The asterisk(s) and adjacent bar(s) show the bin(s) of significant difference.)

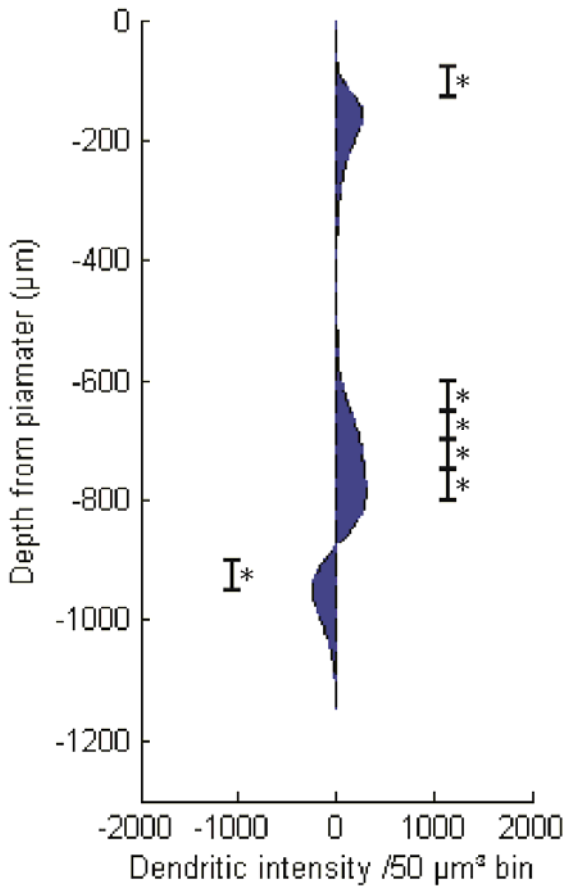

Profile 3.6.2.1: Dendritic density distribution of pia-centred upper primary vibrissa motor cortex (vM1) control and trimmed GLT cells.

(The plots were generated using custom-made programme Rothko and merged using CorelDRAW; control in blue, n=12 and trimmed in yellow, n=14; the bold lines show the mean and the dotted lines indicate standard deviation. The asterisk(s) and adjacent bar(s) show the bin(s) of significant difference.)

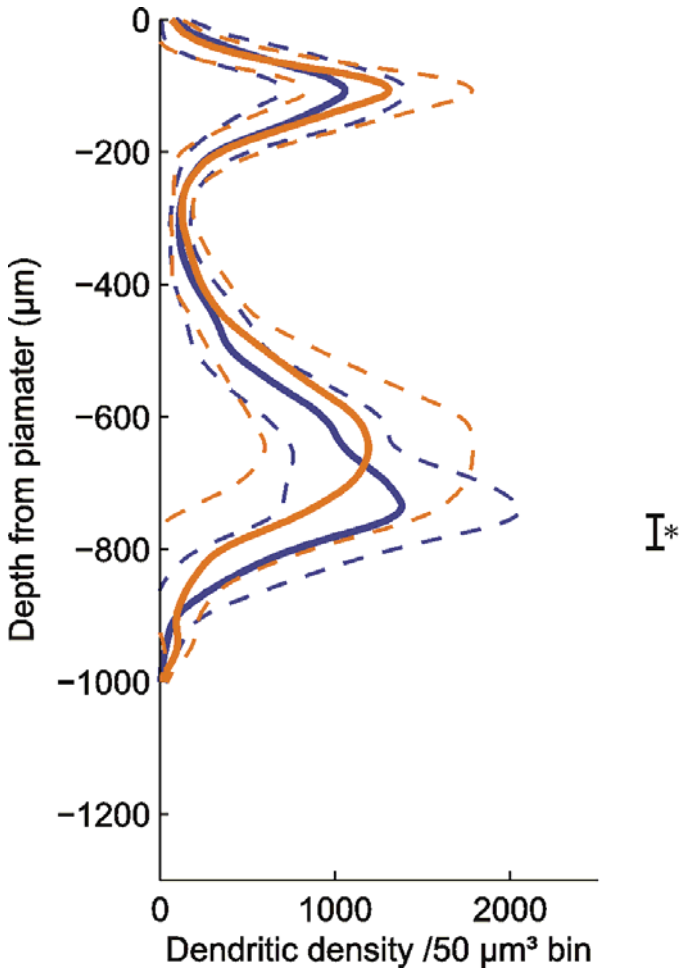

Profile 3.6.2.1.1: Absolute difference in the dendritic density distributions of pia-centred upper primary vibrissa motor cortex (vM1) control and trimmed GLT cells shown as area under the curve.

(The plots were generated using custom-made programme Rothko; control n=12, trimmed n=14. The asterisk(s) and adjacent bar(s) show the bin(s) of significant difference.)

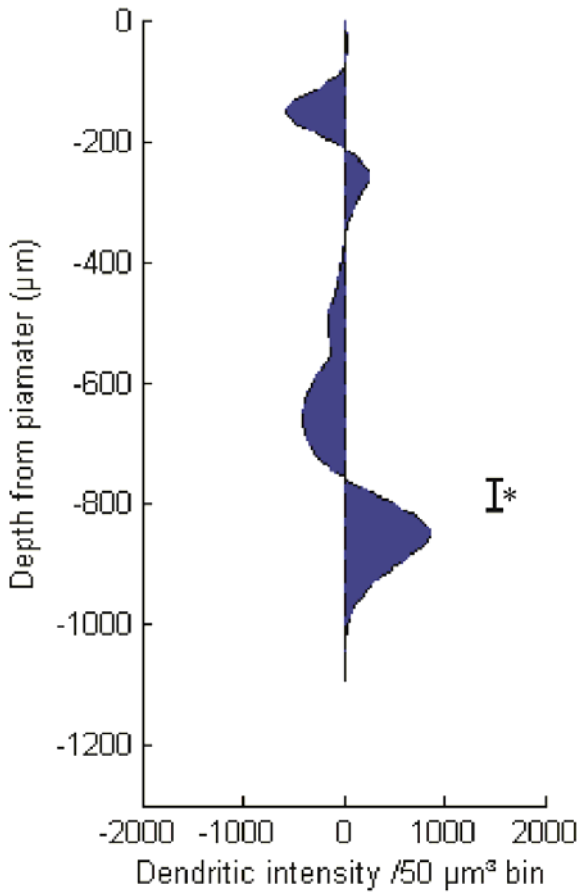

Profile 3.6.2.2: Dendritic density distribution of pia-centred lower primary vibrissa motor cortex (vM1) control and trimmed GLT cells.

(The plots were generated using custom-made programme Rothko and merged using CorelDRAW; control in blue, n=16 and trimmed in yellow, n=15; the bold lines show the mean and the dotted lines indicate standard deviation. The asterisk(s) and adjacent bar(s) show the bin(s) of significant difference.)

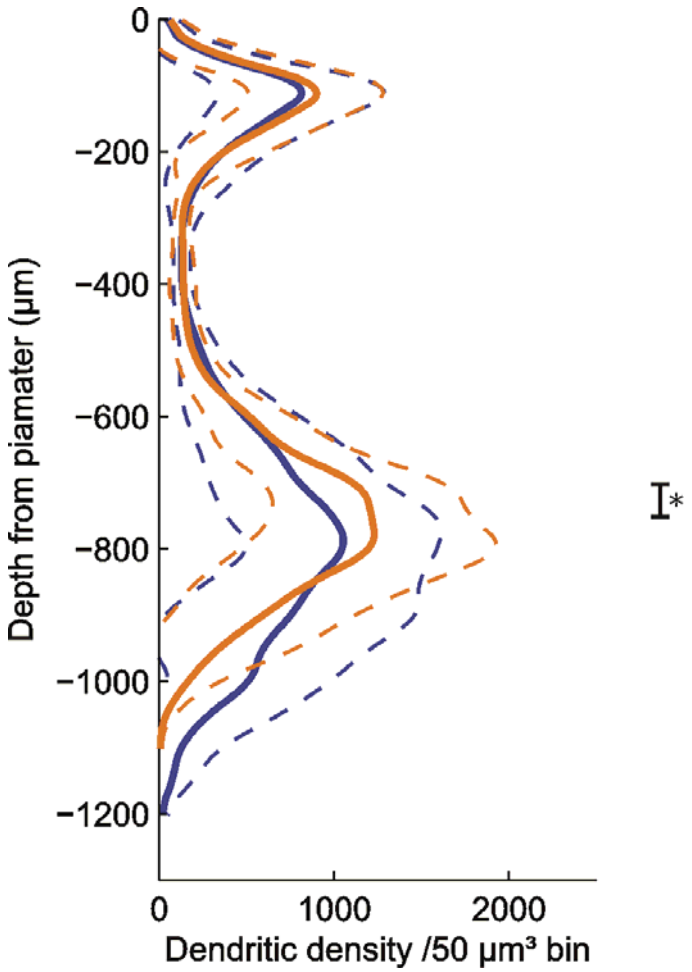

Profile 3.6.2.2.1: Absolute difference in the dendritic density distributions of pia-centred lower primary vibrissa motor cortex (vM1) control and trimmed GLT cells shown as area under the curve.

(The plots were generated using custom-made programme Rothko; control n=16, trimmed n=15. The asterisk(s) and adjacent bar(s) show the bin(s) of significant difference.)

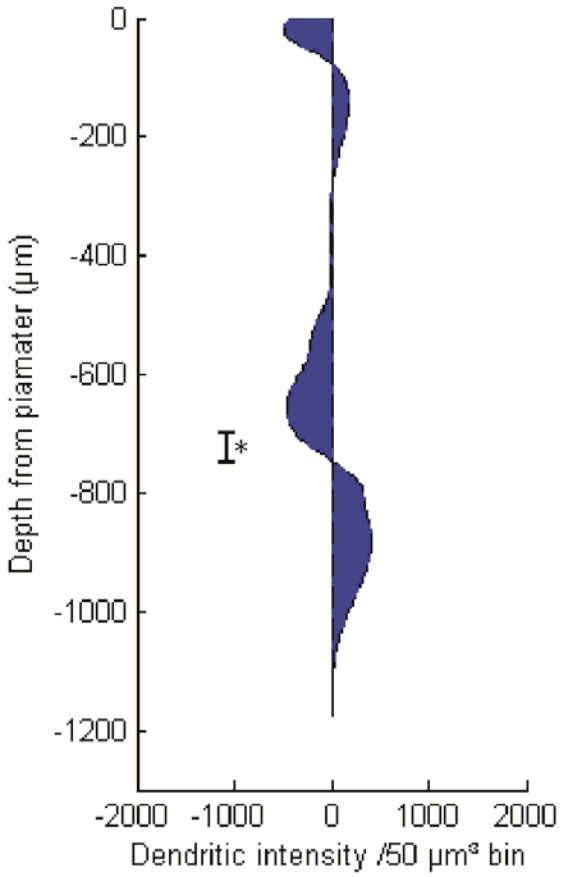

3.8 Overlaps of GLT dendrites with VPM and POm innervation

Several tracing studies had already established the pattern of VPM and POm innervation of the primary barrel cortex in mice. Given that the thalamic nuclei is the direct source of barrel- and septae-related information in S1, I was motivated to look into how the innervation pattern of the thalamic nuclei would overlap with the dendritic profiles of the S1 GLT cells. The figure below shows the overlap of the S1 GLT control and trimmed profiles with the VPM and POm innervation in S1 (VPM and POm innervation data kindly provided by Dr. Alexander Groh, AG Sakmann, Institute of Neuroscience, Technical University Munich).

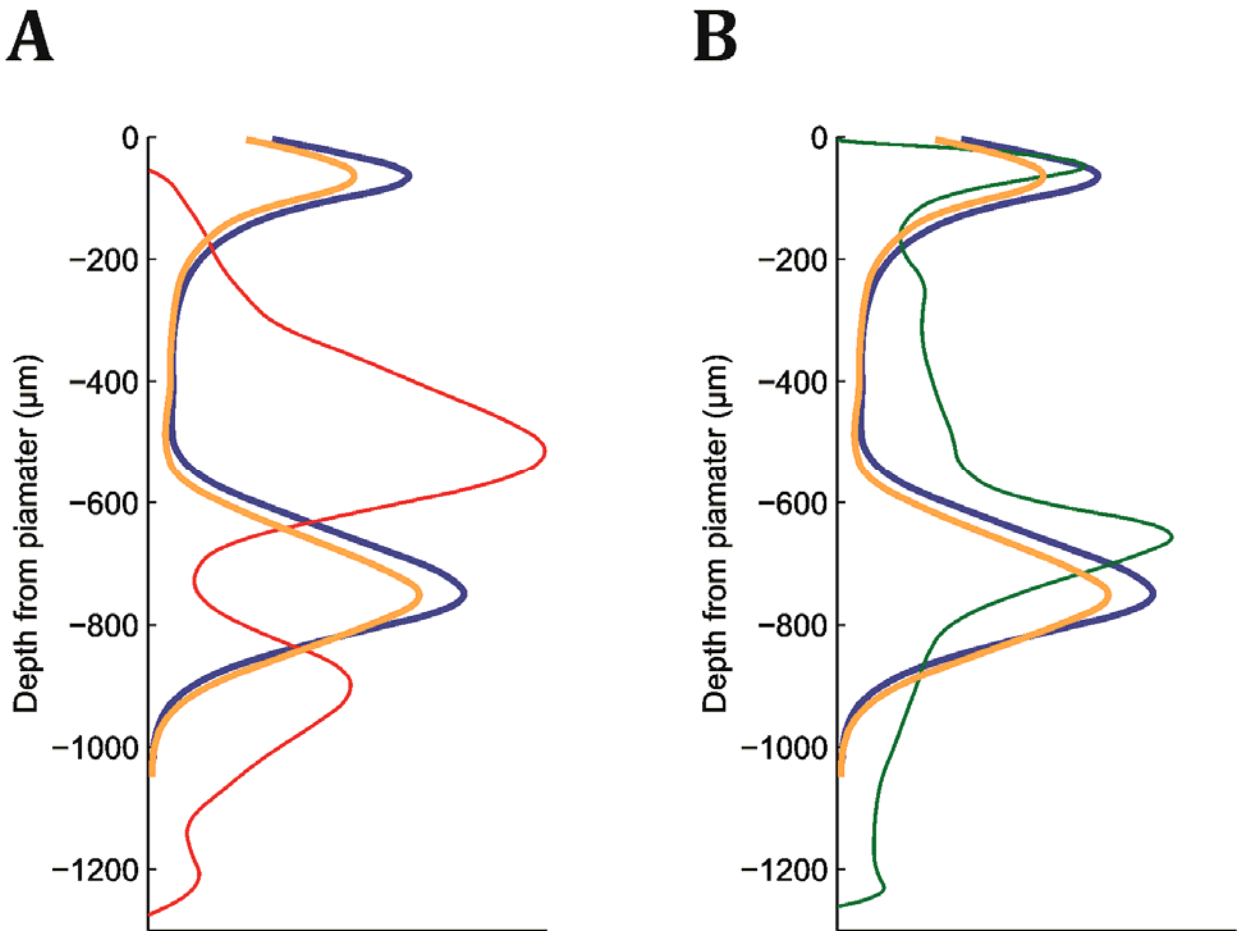

Figure 3-37: **VPM and POm innervation in S1.** The thalamic innervation pattern is overlaid on the dendritic profiles of S1 GLT cells. S1 control cells are represented in blue, S1 trimmed in yellow, VPM in red (**A**) and POm in green (**B**).

4 Discussion

In this thesis, I have investigated an enduring question of systems neuroscience, namely, whether a mature neocortex can be malleable enough in the face of incoming sensory information. Otherwise stated, can experience alter the structural organisation of an adult neuronal network?
To investigate this, I looked into the effect of sensory experience on the structure of genetically defined layer Vb thick-tufted cells, that expressed EGFP under the control of the promoter for the enzyme glycosyltransferase 25 domain containing 2 (GLT or glt25d2), characteristically found in a subpopulation of layer Vb pyramidal cells. The afferent innervations, as well as, the efferent projections from these cells are well known. The work presented in this thesis is the first known attempt to study structural plasticity in genetically identified layer Vb cells in mature neocortical areas.

A three-tier analysis of the dendritic complexity of these neurons threw up interesting changes in various parameters. The main findings of this study were that although the lack of sensory input resulted in no significant changes in the branchiness of the dendrites in the deprived animals as compared to the controls, there were significant differences in dendritic lengths between the groups. The apical tufts of the barrel cortex layer Vb thick-tufted (GLT) cells were significantly shorter in the deprived group than in the control group. On the contrary, however, the basilar dendrites of the same cells did not significantly differ in length in the two groups. Moreover, another parameter, namely, oblique dendrites, also exhibited significantly longer lengths in the control group when compared to those of the deprived groups. Further, these changes were compartmentalised in certain specific regions along the vertical span of the cells. Interestingly, the loci of changes reported here overlap rather well with the innervation maxima of the POm axons and to a minor extent with the VPM axons. The shortening of dendrites in the deprived barrel cortex cells took place at the apical tufts as well as the proximal oblique dendrites (innervated by POm axons) while showing no changes of basal dendrites and distal oblique dendrites where the VPM axons project. In surprising contrast however, the vibrissa motor cortex cells showed no significant differences between the control and deprived groups. Nonetheless, even these cells showed compartmentalised changes in their dendritic pattern when the control group was compared to the deprived group; these differences, as pointed out, were not significant.

4.1 Studies on adult cortical plasticity

Although a number of studies show various plastic mechanisms in adult animals, a heavy majority of these studies have concentrated on spine dynamics and synaptic changes (Buonomano and Merzenich, 1998, Grutzendler et al., 2002, Trachtenberg et al., 2002). Relatively lesser number of studies, however, has focussed on dendritic complexity and length in adult animals (Hickmott and Ethell, 2006). It is generally believed that the geometry of a neuron, apart from the orientation of its dendritic arborisation, remains true to the intrinsic programme followed during development and does not change much during adulthood (Harris and Woolsey, 1981, Tailby et al., 2005). In all these studies however, effects of sensory deprivation or enrichment have been carried out without previous knowledge of the genetic identity of the cells and consequently, without prior knowledge of their afferent innervations.

4.1.1 Earlier investigations

That adult neocortex could be pliable was reported by, among others, Volkmar and Greenough as early as 1972 (Volkmar and Greenough, 1972), when they observed increased branchiness in higher order dendrites in adult rat visual cortex when raised in social- and tactile-enriched environs. When compared to the rats raised individually or in pairs, in standard laboratory cages, rats that were raised in groups in much larger cages with environmental enrichment (sets of wood, metal and plastic toys) showed more branchiness in higher order dendrites. Additionally higher- order dendrites had more branches in the paired housing animals than the isolated ones. The authors attributed this difference to the effect of differential environmental stimulation during rearing. An extension of this study by the same group using the same experimental protocol confirmed the earlier results and further looked at the domains of such changes (Greenough and Volkmar, 1973). They reported increased branches in the proximally located dendrites of visual cortex pyramids of rats from the environmental-enrichment group in comparison to the isolated or pair-raised rats. However, they failed to see any changes in dendritic lengths in between the groups, although, they did report on a tendency of longer apical shafts in rats raised in complex environments. This was probably due to limited preservation of the arborisations of apical dendrites in the 100 μm slices used in the study. In 1978, Uylings and colleagues, also using similar protocol of enriched environment and standard laboratory caging, found increased branchiness and length of terminal basal dendritic segments in pyramidal cells of adult rat visual cortex (Uylings et al., 1978) raised in enriched conditions.

Greenough and colleagues reported an increase in the number of branches in the distal regions (more than 250 μm away from soma) of visual cortex layer IV and V pyramidal cell apical dendrites in adult rats that were subjected to the Hebb-Williams maze training (Greenough et al., 1979). In stark contrast to the studies mentioned above however, they could not find any significant differences in the basal dendrites or the proximal apical dendrites of the pyramids. Even here, the limited preservation of dendritic arborisations was an issue in the 100 μm thick slices used. Subsequently, Chang and Greenough, by training split-brained rats in a visually-guided maze task with one eye occluded, showed that the dendritic complexity of layer V neurons in the visual cortex was higher in the trained hemisphere than in the untrained (Chang and Greenough, 1982). Using two paradigms of occlusion, one unilateral fixed on one eye, and the other alternating on both eyes, the authors observed that the rats trained in the Hebb-Williams maze task had longer distal apical oblique dendrites in their visual cortex layer V pyramids (in the contralateral cortex of the unilaterally occluded eye). This study showed for the first time that effects of training were localised in the sensory areas related to the training-experience (Chang and Greenough, 1982). Training related changes were also reported in the forepaw-representative motor-sensory frontal cortex dendrites of rats trained in a food-reaching task (Greenough et al., 1985). By training adult rats to either use their preferred forepaw or the non-preferred one or both to reach for food rewards, the group showed that the apical dendrites of layer V pyramids had larger apical dendritic fields, longer lengths, more apical oblique dendrites and longer terminal branches in the trained groups as compared to untrained ones. The effects were strongest in the contralateral hemisphere of the preferred paw, and weaker but consistent trends were also observed in the other two trained groups. One important belief that has been underlined in these studies is that enrichment-related structural changes were concentrated in the basilar dendrites while training-related changes in the apical and oblique dendritic domains (Greenough et al., 1979).

Moreover, Rutledge and colleagues observed increased dendritic length and branchiness in apical dendrites of pyramidal cells in layers II and III of cats (Rutledge et al., 1974) after electrical brain stimulation. They coupled the stimulation protocol with a foreleg shock (trained) in one group and left the other group without shock (untrained). In the hemisphere contralateral to the stimulated side, apart from the length and branchiness changes, they also found increased dendritic density near the pia and higher spine counts on apical and oblique dendrites; the higher spine counts more related to training than just brain stimulation (Rutledge et al., 1974).

Interestingly enough, extending the knowledge from animal studies to humans, Jacobs and Scheibel reported a positive correlation between the complexity of neurons in the cortical area for

language, Wernicke's area, and the level of education in human samples obtained post-mortem (Jacobs et al., 1993). Subjects with a university education reportedly had longer dendrites than subjects with a high school background, who, in turn, had longer dendrites than those with even lesser education. The effects were more pronounced in distal dendritic segments than in the proximal. To test the hypothesis that dendritic complexity in the brain was dependent on the computational complexities of the tasks performed by the area, Scheibel and colleagues looked at and reported increased dendritic complexity in the digit region of human somatosensory cortical area, related to more complex and finer movements, than in the regions associated with the trunk (Scheibel et al., 1990). Additionally, inter-individual complexity of dendrites in the trunk and digit regions was positively correlated with the manual dexterity required in the profession of the subject (for example, a typist having longer dendrites as against a civil servant). This indicated that the dendritic complexities are subject to experience-related changes (Kolb and Whishaw, 1998).

4.1.2 Recent studies

With the advent of the new millennium, there was an explosion in the use of two-photon microscopy (Denk et al., 1990) to study structural plasticity dynamically over time both *in vitro* and *in vivo* (Fu and Zuo, 2011). This technique afforded the benefits of non-invasive imaging over long periods of time so that neuronal structures can be followed continuously over a period of time and hence structural alterations could be dynamically tracked. However, most of these studies looked at spine dynamics rather than gross dendritic rearrangements (Lee et al., 2006).

Trachtenberg and colleagues studied anatomical plasticity of dendrites and dendritic spines of layer V pyramids in primary somatosensory (barrel) cortex of adult mice (Trachtenberg et al., 2002). After chessboard whisker deprivation (trimming every other whisker), they reported an increase in spine turnover (more transient spines) at the cost of stable spines albeit leaving spine density unaltered. About 60% of all spines were reportedly stable, of which, 50% were really stable over long time periods (>30 days). They also looked at structural stability of dendrites over time and found no length changes, although they did not compare with that in deprived animals.

Mizrahi and Katz looked at the stability of mitral and tufted cell apical dendrite stability in the olfactory bulb of adult mice expressing yellow flouorescent protein (YFP) (Mizrahi and Katz, 2003). In addition to imaging dendritic stability over time in natural conditions, they also looked at dendritic stability in the face of altered neuronal activation either induced pharmacologically or by a physiologically more relevant olfactory learning task. They found that the gross dendritic structure remained stable in all conditions while finer structures were either sprouting or being

pruned in the pharmacologically manipulated animals. It is relevant to note here that this study did not look at whole dendritic trees, focussing instead on randomly chosen dendritic fields.

Another study imaged the stability of spines over time in stretches of layer V pyramidal neurons in visual cortex of adult mice expressing yellow flouorescent protein and came to conclude that about 96% of all spines were stable. This fraction of stable spines did go down with increases in imaging intervals but remained consistently higher than in young animals (Grutzendler et al., 2002).

Tailby and colleagues also studied experience-dependent dendritic structural plasticity in adult barrel cortex of whisker-deafferented rats. Using acute barrel cortex slices (150 μm thick), they investigated whether vibrissectomy of all the major posterior snout vibrissae and follicles and some of those on the mystacial pad had an impact on the dendritic length, orientation, and spine density of immunohistochemically stained, dye-filled layer III/IV pyramidal neurons. They found that although the dendrites lost their orientation bias towards their home-barrel centre, dendritic length and spine density remained unchanged (Tailby et al., 2005).

Interestingly, Lee and colleagues (Lee et al., 2006) imaged dendritic stability in layer II/III pyramidal and interneurons of adult mice visual cortex expressing GFP under *thy*-1 promoter. They found that pyramidal neurons had stable dendrites, while the interneurons exhibited considerable dendritic structural alterations. However, they could only track 42% of pyramidal cell dendrites and also did not rule out remodelling of dendritic arbours in pyramidal neurons following peripheral sensory manipulations (Lee et al., 2006).

Cheetham and co-workers, on bilateral whisker trimming of rats, reported considerable axonal remodelling in the vicinity of synaptically coupled layer II/III pyramids in rat barrel cortex but only minor alterations in dendritic structure (Cheetham et al., 2008). Although, total dendritic length and path length remained constant, they looked closely at the basal dendrites and found a slight reduction in trimmed animals. However, since they started the deprivation protocol relatively early (post-natal day 19), they speculated that this alteration of basal dendrites set in before, and persisted through adulthood (Cheetham et al., 2008).

A host of other studies have similarly looked at experience-dependent spine dynamics in visual (Keck et al., 2008, Hofer et al., 2009), barrel (Zuo et al., 2005, Holtmaat et al., 2006, Yang et al., 2009, Wilbrecht et al., 2010) and motor (Xu et al., 2009, Yang et al., 2009) cortices of adult mice; a detailed look at each of which is beyond the scope of this thesis.

However, all the *in vivo* studies did not look at cell types in deeper layers because current imaging techniques are limited to superficial layers; they also did not look at full dendritic

arborisations, choosing instead to look at small stretches of dendrites at a time. Moreover, in all of these studies effects of sensory deprivation or enrichment have been looked at without previous knowledge of the genetic identity of the cells and consequently, without prior knowledge of their afferent innervations.

4.2 Implications of dendritic remodelling on spine loss

In light of the dendritic remodelling reported in this thesis, one can provide an estimate of the amount of changes at the level of spines owing to the reduction in lengths. Spines form the post-synaptic compartment of the functional connections (mostly excitatory) called synapses. So, a reduction in the number of spines could also be translated to a loss of potential synapses. This, coupled with the simultaneous reduction in presynaptic boutons and lengths of thalamocortical axons, in line with several studies (Wimmer et al., 2010, Oberlaender et al., 2012), could result in a substantial alteration of possible connections in the deprived animals.

Larkman in 1991 provided a good absolute estimate of the distribution of spines in thick-tufted neurons from layer V (Larkman, 1991). In rat visual cortex layer V thick-tufted neurons, which were intracellularly labelled with *horseradish peroxidase*, he reported the maximum spine density of 5-8 spines/µm on the apical trunk, which were in good agreement with contemporary studies (Feldman and Peters, 1979). For thick-tufted layer V neurons, Larkman observed an overall spine density of about 1.65 spines/µm of dendrite. However, spine distribution was very compartment specific. Among a total of ≈15000 spines per thick-tufted neuron, apical trunk contained ≈20% (≈3100 spines, 6.3 spines/µm), terminal apical arbours ≈11% (≈1700 spines, 0.91 spines/µm) and oblique dendrites ≈27% (≈4100 spines, 1.50 spines/µm).

If one was to extrapolate these findings in the visual cortex of the rat to the somatosensory cortex in context of the dendritic restructuring presented in this thesis, one could provide an estimate of the number of spines lost due to the dendritic shrinkage. Since, the dendritic shrinkage in apical dendrites observed in the study presented in this thesis are concentrated specific dendritic compartments, namely terminal apical arbours and oblique dendrites, I will base my calculations on the terminal arbour spine density, i.e. 0.91 spines/µm and oblique dendrite spine density, i.e. 1.50 spines/µm. Hence, a dendritic shrinkage of 535 µm (≈23%), 677 µm (≈19%) and 678 µm (≈18%), as is the case in 10%, 20% and 30% apical tuft lengths of the scaled barrel cortex layer V thick-tufted cells, translate to a loss of about 487 (≈29%), 616 (≈36%), and 617 (≈36%) spines respectively from the apical tuft spine pool. If one takes the shrinkage of apical oblique dendrites (368 µm; ≈13%) into consideration, given a spine density of 1.50 spines/µm, this leads to an

additional loss of 552 (≈14%) spines from the oblique dendrite spine pool in the deprived animals. Taken together, spine loss reported, when 30% apical tuft length and oblique dendrites are considered, the deprived group had a shortfall of 1169 spines compared to the control group. Larkman's estimate predicted a total of about 15000 spines for each thick-tufted layer V neuron, of which about 5774 spines (≈39%) were located on the apical dendrite terminal arbour and oblique dendrites combined. This means, the deprived animals in this study had, in all, ≈20% lesser spines in the apical and oblique dendrites combined spine pool, and ≈8% fewer spines in their total spine pool in thick-tufted layer V cells than the control animals. Considering that the animals were whisker-deprived for 8 days on average, average daily loss of spines amounts to 146 (≈1% of the total spine pool). Breaking the numbers further down to hours and minutes amounts to a spine loss of ≈6 spines/hour and ≈0.1 spine/minute respectively.

A morphological-physiological investigation showed that the preferred synaptic contacts of the layer V thick-tufted neurons were located preferentially on the basal and apical oblique dendrites (Markram et al., 1997). Although, the particular types of spines among the missing pool cannot be determined, it is perceivable, that there were stable spines among 8% of the total spine pool, and hence, their loss could possibly have a significant effect on plasticity, and thereby, learning and memory, of the animal.

Although spine densities, distribution bias, dendritic lengths and extent of plasticity in cortical cells is cell-type and layer specific, these extrapolations per cell shown above could be extended to all the excitatory neurons in a column, totalling 16189 cells (Meyer et al., 2010), and the macrovibrissae representation of all columns (an average of 32 columns). One could then get to an estimate of the maximum extent of plasticity conceivable in the given setting. These computations are tabulated below.

Table 4.1: Tabulation of extrapolated values of maximum spine loss resulting from deprivation

	Number of spines lost in deprived animals due to dendritic shrinkage			
	in total over 8 days	per day	per hour	per minute
in 30% apical tuft	617	77	3.2	0.05
in oblique dendrites	552	69	2.9	0.05
per GLT cell*	1169	146	6	0.1
per column	18924941	2365618	98567	1643
vibrissal field	605598112	75699764	3154157	52569

*cell here stands for the 30% apical tuft length and oblique dendrite length taken together

4.3 Implications of dendritic remodelling on spine turnover

As outlined by numerous studies discussed before, dendritic circuitry is in constant flux, both in development as well as adulthood. Like in development, experience-dependent structural plasticity is also actualised, apart from other mechanisms, through simultaneous spine loss and spine gain, collectively called spine turnover, in all areas of the neocortex (Grutzendler et al., 2002, Trachtenberg et al., 2002, Holtmaat et al., 2005, Zuo et al., 2005, Holtmaat et al., 2006, Keck et al., 2008, Hofer et al., 2009, Xu et al., 2009). However, the extent of turnover decreases in animals with age and the fraction of stable structures increase (Holtmaat et al., 2005).

However, one issue of contention in this field is that of the reported values of spine turnover (Xu et al., 2007); depending on two methods of imaging, one using a thinned skull (Grutzendler et al., 2002) and the other involving craniotomy to create a glass window (Holtmaat et al., 2009), various studies have come up with highly varying spine turnover values. Trachtenberg and colleagues (Trachtenberg et al., 2002) observed using a cranial window in adult mouse barrel cortex that barring ≈50% of the total spine pool, which was stable, or persistent for the imaged period of 8 days, other spines were fleeting structures. Some disappeared within a day and were termed transient spines (≈17%) while others persisted for 2-3 days and were called semi-stable spines (≈23%). At this juncture, chessboard deprivation increased the pool of transient spines at the cost of stable spines.

Simultaneously, Grutzendler and his colleagues employed an alternative technique using a thinned skull (minimally invasive) to study spine turnover in visual cortex of young and adult mice raised in normal environments (Grutzendler et al., 2002). Interestingly, they came up with much lower values of spine turnover than the studies using cranial window (involving invasive skull opening). In animals of age comparable to the ones used in the study presented in this thesis (which the authors defined as young instead of adult), they observed that ≈73% of the spine pool remains stable over a period of 1 month and 27% comprise the turnover pool. In older animals (≈4 months), ≈96% of the spines remains stable over the same time period. The same group used both the methods simultaneously in a separate study to qualitatively compare and find possible explanations for the vastly differential values (Xu et al., 2007) and found that in a more invasive paradigm like cranial window, there is massive activation of microglia and astrocytes around the site of skull opening (for up to 2 months after surgery) and this probably leads to altered spine dynamics in this set-up (more spine loss). Considering that glial cells have been shown to influence structural

plasticity (Allen and Barres, 2005), and hence, could alter observed spine turnover in cranial window models, the thinned skull model might provide a more realistic estimate of spine turnover.

If one takes the spine turnover literature in context of the results of this thesis, then it is conceivable, assuming a homogenous distribution of *stable*, *semi-stable* and *transient* spines all over the dendritic tree, that the dendritic shrinkage observed in the whisker-deprived animals would lead to a loss of stable spines on the one hand, as well as loss of the turnover-ready spine pool on the other. If the results from the study by Grutzendler and colleagues (Grutzendler et al., 2002) are extended to the barrel cortex, ≈73% of the spines lost due to deprivation-related dendritic shortage were likely to be stable spines and the other ≈27% constituting the turnover pool. Similar to the spine loss estimates in last section, this loss of specific spine types could be extended to the column, vibrissal area as well as its dynamics over days, hours and months could be approximated as tabulated below.

Table 4.2: Tabulation of extrapolated values of loss of spine types resulting from deprivation

	Types of spines lost in deprived animals due to dendritic shrinkage shown as **stable + turnover ready**			
	in total over 8 days	per day	per hour	per minute
in 30% apical tuft	450 + 167	56 + 21	2.3 + 0.9	0.03 + 0.02
in oblique dendrites	403 + 149	50 + 19	2.1 + 0.8	0.03 + 0.01
per GLT cell*	853 + 316	107 + 40	4.5 + 1.7	0.08 + 0.03
per column	13809217 + 5115724	1726152 + 639466	71923 + 26644	1199 + 444
vibrissal field	441894944 + 163703168	55236868 + 20462896	2301536 + 852621	38359 + 14210

*cell here stands for the 30% apical tuft length and oblique dendrite length taken together

Spine remodelling and turnover have been shown to correlate positively with learning-induced behavioural improvements (Yang et al., 2009). Especially, stable spines from the existing pool as well as learning-induced newly formed spines that would go on to become stable, provide a structural scaffold for memory consolidation in the animal (Yang et al., 2009). In light of this, the loss of *stable* and *transient* (that could go on to become stable) spines in animals deprived of sensory input shown above in table 4.2 could have implications in the learning-induced behaviour of the animal. Lost spines, for example, cannot be re-employed for subsequent learning or consolidation of already acquired memory and thus reduces the potential plasticity repertoire of the animal.

4.4 Dendritic remodelling alters electrical properties

Layer V pyramidal neurons are known to exhibit back-propagating action potentials (Stuart and Sakmann, 1994), that travel back to the distal dendrites from the soma. In addition, they also exhibit distal-synaptic input evoked Ca^{2+} depolarisations that originate in distal apical dendrites (Schiller et al., 1995, Schiller et al., 1997, Helmchen et al., 1999). These back propagating action potentials have been shown to be able to lower the threshold for the Ca^{2+} induced depolarisations and action potentials mentioned above (Larkum et al., 1999a, Larkum et al., 1999b, 2001). Moreover, in these neurons, the exact spatial location of the oblique dendrites in relation to the soma have been shown to influence *coupling*, the reduction in threshold for initiation of a dendritic Ca^{2+} action potential due to a coincident somatic back propagating action potential, between somatic and dendritic action potential initiation sites. Proximity of oblique dendrites to the soma increases coupling while increase in amount of distal oblique dendrites reduces coupling (Schaefer et al., 2003). In a way, the oblique dendrites act as a kind of communication gateway between the somatic and the apical dendritic compartments of the cell. Moreover, layer I input to the apical tufts of these layer V pyramidal cells appear to be more important than thought, and is more likely to trigger cell firing than an equal input to the proximal compartments (Rhodes and Llinas, 2001, Komendantov and Ascoli, 2009). Thus, in case of these cells, structural plasticity of dendrites could be a significant factor in regulating the responses to incoming (coincident) laminar synaptic inputs (Mainen and Sejnowski, 1996, Poirazi and Mel, 2001, van Ooyen et al., 2002, Schaefer et al., 2003).

Taking this into consideration, the findings of this thesis become all the more relevant, since the deprived animals show their maximum dendritic shrinkage in the apical tuft of layers I and II/III as well as in the proximal apical oblique dendrites in layer V and partly in layer IV, the sites of maximum plastic potential through various mechanisms, possibly indicating that sensory input can indeed restructure dendritic branching patterns, to unleash the plastic potential of the neuronal circuitry and accommodate new experiences.

4.5 Sparing of vibrissa motor cortex cells

A comparison between the dendritic lengths of the vibrissa motor cortex (vM1) cells from control and deprived groups showed no significant differences. Even after dividing the cells into the two classes, namely upper and lower vibrissa motor cortex cells to reduce intra-group variation, I found no significant differences. This was surprising given the knowledge of the projections to and from vibrissa motor cortex and makes the observations comparatively more difficult to interpret.

From a number of studies in the rat, it is known that the vibrissae representation in the primary motor cortex receive projections from the thalamic POm nucleus but not from the VPM (Cicirata et al., 1986, Aldes, 1988, Hoffer and Alloway, 2001, Chakrabarti and Alloway, 2006). This knowledge becomes even more intuitive when one considers that the barrel cortex projections to the vM1 originate from the cells that are vertically aligned to layer IV septae (Alloway et al., 2004, Chakrabarti and Alloway, 2006). In other words, the whisker–related information converging to the vM1 is derived from the paralemniscal pathway. From studies in mice, similar observations have been drawn. Tracer studies have shown reciprocal connections between vM1 and the superficial layers (layers II-III and layer V) of both vibrissa S1 and S2 (Porter and White, 1983). Coupled physiological and anatomical studies in mice have revealed that superficial layers (layers II-III and Va) of vM1 receive strong inputs from S1, believed to be involved in sensorimotor integration and motor learning, while deeper layer cells (layers Vb and VI) receive only weak inputs from S1 (Mao et al., 2011). This, in spite of the fact, that there is considerable overlap between the long projection axons from S1 and the dendrites of vM1 deeper layer cells (Mao et al., 2011). However, this is understandable, considering that extensive overlap of axons and dendrites does not always extend to strong functional connections (Dantzker and Callaway, 2000, Callaway, 2002, White, 2002, Shepherd and Svoboda, 2005, Petreanu et al., 2009).

In light of these studies, the most likely explanation for not seeing a significant difference between the dendritic lengths of control and deprived group of layer Vb thick-tufted cells from the vibrissa motor cortex is their probable lack of strong inputs from the barrel cortex cells. It appears that the heavy projections from barrel cortex cells evade the layer Vb cells altogether and when present have rather weak input strength. This was generally the case apart from a few outlying cells that receive strong S1 input (Mao et al., 2011), which however, inadvertently, might not have been present in my sampled data set.

Another peculiar observation from the studied data set was that although statistically significant differences were missing, the trimmed group of motor cortex cells for most of the comparisons had slightly higher dendritic lengths than the control group of cells. This could very well be a random sampling bias and can only be confirmed by increasing the number of samples in the study. An alternative possibility is also feasible. In the experimental paradigm adopted for whisker trimming, the mystacial hairs of the animals were trimmed as close to the skin as possible every day. However, this method does not destroy the hair follicles, the muscles involved in their control or the afferent and efferent innervations. So it is conceivable that owing to the lack of input from the whiskers, the animals were trying to compensate with increased movements of the

whisker related muscles. If this were true, it could possibly explain the slightly longer dendrites. On the other hand, this could certainly be crosschecked by adopting sensory deafferentation of the whisker system as the deprivation paradigm and then looking at the vM1 cells.

4.6 Methodological caveats

A serious methodological limitation of the study presented in this thesis and in any *in vitro* study as such, is the extent of preserved structure in the cyto-architecture. Invariably, a fraction of the neuronal processes, especially, the distal apical arborisations, get cut during the brain-slicing procedure and are likely to underestimate the apical tuft lengths. This could potentially lead to an unintended bias if one of the groups gets more affected than the other. This was also mentioned in the spine count study by Larkman discussed above, where distal apical tuft spine counts, admittedly, could have been lower than what had been reported. However, I have tried to keep this source of bias to a minimum by keeping all the factors constant while preparing brain slices from both the groups of animals and hence, it can be assumed than any loss of dendritic architecture has been kept identical in both the groups. Another possible source of error in this study could arise from the cell filling itself. Although, biocytin staining is a very reliably established process, one cannot rule out the lack of staining in very fine dendritic segments due to various conceivable reasons. This could then also lead to a conservative estimate of dendritic lengths. However, this is very rare, and if present, would only affect a very negligible fraction of cells. The values of dendritic lengths reported in this study, are however in good agreement with the values reported previously (Groh et al., 2010). Also, to rule out experimenter bias in this study, random subsets of cells from both groups were reconstructed double blind by two independent experienced investigators and were compared to the values I obtained myself. Needless to say, the values obtained from these two independent sources were in good agreement, differing from each other by less than 1%.

4.7 Conclusions and outlook

The results presented in this thesis show the existence of experience-dependent dendritic remodelling in adult neocortical cells. Although, evidences exist, both in support and against dendritic remodelling in the face of either presence or lack of sensory inputs in established neurocircuitry of an adult neocortex, this study was unique in that, it tested the possibility of adult structural plasticity in dendrites of a genetically identified class of layer V cells with identified input and output projections. This was important for the fact that one could relate the observed changes

to the functional changes known to exist resulting from experimental manipulations of the projection systems to and from these cells. Layer V thick-tufted neurons form an important output projection source to several sub-cortical targets and those in the barrel cortex receive input from the main afferent systems in the whisker-to-barrel system, carrying vital information about the external world to the relevant sensorium of the animal. However, as adult cortical plasticity is believed to be layer and cell-type specific, one has to be cautious before extending the observations from the thick-tufted layer V pyramidal neurons to other cortical cells. A case in point is the other type of cells investigated in this thesis, namely, the vibrissae motor cortex layer V thick-tufted GLT neurons. Given the reciprocal connections between the primary somatosensory barrel cortex and the vibrissae motor cortex as well as the incoming thalamocortical projections to the latter, it was surprising to not see any changes in these cells after whisker-deprivation. However, as discussed before, this could have been due to the deprivation protocol employed in the study that perhaps did not affect these cells. It needs to be seen whether these cells show dendritic structural plasticity in the face of other deprivation protocols. Having investigated the experience-dependent plastic changes in the thick-tufted layer V pyramidal neurons in barrel and motor cortices, it might be a logical step to study them in the visual cortex after sensory deprivation (e.g. monocular deprivation). Subsequently, it would be very interesting to study the thin-tufted neurons of layer V pyramidal neurons, which, apart from forming the other predominant cell type in layer V, lack an elaborate dendritic arborisation in the superficial cortical layers. Whether the loci of plastic changes, if any, in thin-tufted neurons are more concentrated in the basal parts of the dendritic arborisation, in contrast to the thick-tufted neurons, would help us understand the different plasticity mechanisms employed by the various cell types better. The observations can then probably be causally linked to the information pathways to and from these cells and would also help us investigate the different levels of sensory processing in the adult nervous system. The ultimate goal forward would then be to extend these studies in a layer by layer manner, until we have a comprehensive overview of the various extents of plasticity and their mechanisms employed by the cells constituting the so called cortical column.

5 References

Agmon A, Connors BW (1991) Thalamocortical responses of mouse somatosensory (barrel) cortex in vitro. Neuroscience 41:365-379.

Ahissar E, Zacksenhouse M (2001) Temporal and spatial coding in the rat vibrissal system. Progress in brain research 130:75-87.

Aldes LD (1988) Thalamic connectivity of rat somatic motor cortex. Brain research bulletin 20:333-348.

Alitto HJ, Usrey WM (2003) Corticothalamic feedback and sensory processing. Curr Opin Neurobiol 13:440-445.

Allen NJ, Barres BA (2005) Signaling between glia and neurons: focus on synaptic plasticity. Curr Opin Neurobiol 15:542-548.

Alloway KD (2008) Information processing streams in rodent barrel cortex: the differential functions of barrel and septal circuits. Cereb Cortex 18:979-989.

Alloway KD, Zhang M, Chakrabarti S (2004) Septal columns in rodent barrel cortex: functional circuits for modulating whisking behavior. The Journal of comparative neurology 480:299-309.

Andersen P, Lomo T (1967) Control of hippocampal output by afferent volley frequency. Progress in brain research 27:400-412.

Arabzadeh E, Zorzin E, Diamond ME (2005) Neuronal encoding of texture in the whisker sensory pathway. PLoS biology 3:e17.

Aronoff R, Matyas F, Mateo C, Ciron C, Schneider B, Petersen CC (2010) Long-range connectivity of mouse primary somatosensory barrel cortex. The European journal of neuroscience 31:2221-2233.

Artola A, Singer W (1987) Long-term potentiation and NMDA receptors in rat visual cortex. Nature 330:649-652.

Belford GR, Killackey HP (1979) The development of vibrissae representation in subcortical trigeminal centers of the neonatal rat. The Journal of comparative neurology 188:63-74.

Bermejo R, Friedman W, Zeigler HP (2005) Topography of whisking II: interaction of whisker and pad. Somatosensory & motor research 22:213-220.

Brecht M (2007) Barrel cortex and whisker-mediated behaviors. Current Opinion in Neurobiology 17:408-416.

Brecht M, Grinevich V, Jin TE, Margrie T, Osten P (2006) Cellular mechanisms of motor control in the vibrissal system. Pflugers Archiv : European journal of physiology 453:269-281.

Brecht M, Krauss A, Muhammad S, Sinai-Esfahani L, Bellanca S, Margrie TW (2004a) Organization of rat vibrissa motor cortex and adjacent areas according to cytoarchitectonics, microstimulation, and intracellular stimulation of identified cells. The Journal of comparative neurology 479:360-373.

Brecht M, Sakmann B (2002) Dynamic representation of whisker deflection by synaptic potentials in spiny stellate and pyramidal cells in the barrels and septa of layer 4 rat somatosensory cortex. The Journal of physiology 543:49-70.

Brecht M, Schneider M, Sakmann B, Margrie TW (2004b) Whisker movements evoked by stimulation of single pyramidal cells in rat motor cortex. Nature 427:704-710.

Buonomano DV, Merzenich MM (1998) Cortical plasticity: from synapses to maps. Annual review of neuroscience 21:149-186.

Bureau I, von Saint Paul F, Svoboda K (2006) Interdigitated paralemniscal and lemniscal pathways in the mouse barrel cortex. PLoS biology 4:e382.

Callaway EM (2002) Cell type specificity of local cortical connections. Journal of neurocytology 31:231-237.

Carvell GE, Simons DJ (1990) Biometric analyses of vibrissal tactile discrimination in the rat. The Journal of neuroscience : the official journal of the Society for Neuroscience 10:2638-2648.

Celikel T, Sakmann B (2007) Sensory integration across space and in time for decision making in the somatosensory system of rodents. Proceedings of the National Academy of Sciences of the United States of America 104:1395-1400.

Chakrabarti S, Alloway KD (2006) Differential origin of projections from SI barrel cortex to the whisker representations in SII and MI. The Journal of comparative neurology 498:624-636.

Chakrabarti S, Zhang M, Alloway KD (2008) MI neuronal responses to peripheral whisker stimulation: relationship to neuronal activity in si barrels and septa. Journal of neurophysiology 100:50-63.

Chang FL, Greenough WT (1982) Lateralized effects of monocular training on dendritic branching in adult split-brain rats. Brain research 232:283-292.

Cheetham CE, Hammond MS, McFarlane R, Finnerty GT (2008) Altered sensory experience induces targeted rewiring of local excitatory connections in mature neocortex. The Journal of neuroscience : the official journal of the Society for Neuroscience 28:9249-9260.

Chen CC, Tam D, Brumberg JC (2011) Sensory deprivation differentially impacts the dendritic development of pyramidal versus non-pyramidal neurons in layer 6 of mouse barrel cortex. Brain structure & function.

Cicirata F, Angaut P, Cioni M, Serapide MF, Papale A (1986) Functional organization of thalamic projections to the motor cortex. An anatomical and electrophysiological study in the rat. Neuroscience 19:81-99.

Cline HT (2001) Dendritic arbor development and synaptogenesis. Curr Opin Neurobiol 11:118-126.

Crair MC, Horton JC, Antonini A, Stryker MP (2001) Emergence of ocular dominance columns in cat visual cortex by 2 weeks of age. The Journal of comparative neurology 430:235-249.

Crowley JC, Katz LC (1999) Development of ocular dominance columns in the absence of retinal input. Nature neuroscience 2:1125-1130.

Crowley JC, Katz LC (2000) Early development of ocular dominance columns. Science 290:1321-1324.

Cruikshank SJ, Urabe H, Nurmikko AV, Connors BW (2010) Pathway-specific feedforward circuits between thalamus and neocortex revealed by selective optical stimulation of axons. Neuron 65:230-245.

Cudeiro J, Sillito AM (2006) Looking back: corticothalamic feedback and early visual processing. Trends in neurosciences 29:298-306.

Dantzker JL, Callaway EM (2000) Laminar sources of synaptic input to cortical inhibitory interneurons and pyramidal neurons. Nature neuroscience 3:701-707.

Daw N (2009) Visual Development: Springer.

de Kock CP, Bruno RM, Spors H, Sakmann B (2007) Layer- and cell-type-specific suprathreshold stimulus representation in rat primary somatosensory cortex. The Journal of physiology 581:139-154.

De Paola V, Holtmaat A, Knott G, Song S, Wilbrecht L, Caroni P, Svoboda K (2006) Cell type-specific structural plasticity of axonal branches and boutons in the adult neocortex. Neuron 49:861-875.

Denk W, Strickler JH, Webb WW (1990) Two-photon laser scanning fluorescence microscopy. Science 248:73-76.

Deschenes M, Urbain, N (2009) Vibrissal afferents from trigeminus to cortices. Scholarpedia 4.

Diamond ME, Armstrong-James M, Ebner FF (1993) Experience-dependent plasticity in adult rat barrel cortex. Proceedings of the National Academy of Sciences of the United States of America 90:2082-2086.

Diamond ME, Huang W, Ebner FF (1994) Laminar comparison of somatosensory cortical plasticity. Science 265:1885-1888.

Diamond ME, von Heimendahl M, Knutsen PM, Kleinfeld D, Ahissar E (2008) 'Where' and 'what' in the whisker sensorimotor system. Nature reviews Neuroscience 9:601-612.

Ebara S, Kumamoto K, Matsuura T, Mazurkiewicz JE, Rice FL (2002) Similarities and differences in the innervation of mystacial vibrissal follicle-sinus complexes in the rat and cat: a confocal microscopic study. The Journal of comparative neurology 449:103-119.

Feldman DE, Brecht M (2005) Map plasticity in somatosensory cortex. Science 310:810-815.

Feldman ML, Peters A (1979) A technique for estimating total spine numbers on Golgi-impregnated dendrites. The Journal of comparative neurology 188:527-542.

Ferezou I, Haiss F, Gentet LJ, Aronoff R, Weber B, Petersen CC (2007) Spatiotemporal dynamics of cortical sensorimotor integration in behaving mice. Neuron 56:907-923.

Finnerty GT, Roberts LS, Connors BW (1999) Sensory experience modifies the short-term dynamics of neocortical synapses. Nature 400:367-371.

Fox K (2008) Barrel Cortex: Cambridge University Press.

Fox K, Wong RO (2005) A comparison of experience-dependent plasticity in the visual and somatosensory systems. Neuron 48:465-477.

Freeman WJ (1998) The neurobiology of multimodal sensory integration. Integrative Physiological and Behavioral Science Volume 33:124-129

Freeman WJ (2011) Understanding perception through neural "codes". IEEE transactions on bio-medical engineering 58:1884-1890.

Frostig RD (2006) Functional organization and plasticity in the adult rat barrel cortex: moving out-of-the-box. Curr Opin Neurobiol 16:445-450.

Fu M, Zuo Y (2011) Experience-dependent structural plasticity in the cortex. Trends in neurosciences 34:177-187.

Furuta T, Kaneko T, Deschenes M (2009) Septal neurons in barrel cortex derive their receptive field input from the lemniscal pathway. The Journal of neuroscience : the official journal of the Society for Neuroscience 29:4089-4095.

Furuta T, Urbain N, Kaneko T, Deschenes M (2010) Corticofugal control of vibrissa-sensitive neurons in the interpolaris nucleus of the trigeminal complex. The Journal of neuroscience : the official journal of the Society for Neuroscience 30:1832-1838.

Gong S, Doughty M, Harbaugh CR, Cummins A, Hatten ME, Heintz N, Gerfen CR (2007) Targeting Cre recombinase to specific neuron populations with bacterial artificial chromosome constructs. The Journal of neuroscience : the official journal of the Society for Neuroscience 27:9817-9823.

Gong S, Kus L, Heintz N (2010) Rapid bacterial artificial chromosome modification for large-scale mouse transgenesis. Nature protocols 5:1678-1696.

Gong S, Yang XW, Li C, Heintz N (2002) Highly efficient modification of bacterial artificial chromosomes (BACs) using novel shuttle vectors containing the R6Kgamma origin of replication. Genome research 12:1992-1998.

Gong S, Zheng C, Doughty ML, Losos K, Didkovsky N, Schambra UB, Nowak NJ, Joyner A, Leblanc G, Hatten ME, Heintz N (2003) A gene expression atlas of the central nervous system based on bacterial artificial chromosomes. Nature 425:917-925.

Greenough WT, Chang FL (1988) Dendritic pattern formation involves both oriented regression and oriented growth in the barrels of mouse somatosensory cortex. Brain research 471:148-152.

Greenough WT, Juraska JM, Volkmar FR (1979) Maze training effects on dendritic branching in occipital cortex of adult rats. Behavioral and neural biology 26:287-297.

Greenough WT, Larson JR, Withers GS (1985) Effects of unilateral and bilateral training in a reaching task on dendritic branching of neurons in the rat motor-sensory forelimb cortex. Behavioral and neural biology 44:301-314.

Greenough WT, Volkmar FR (1973) Pattern of dendritic branching in occipital cortex of rats reared in complex environments. Experimental neurology 40:491-504.

Groh A, de Kock CP, Wimmer VC, Sakmann B, Kuner T (2008) Driver or coincidence detector: modal switch of a corticothalamic giant synapse controlled by spontaneous activity and short-term depression. The Journal of neuroscience : the official journal of the Society for Neuroscience 28:9652-9663.

Groh A, Meyer HS, Schmidt EF, Heintz N, Sakmann B, Krieger P (2010) Cell-type specific properties of pyramidal neurons in neocortex underlying a layout that is modifiable depending on the cortical area. Cereb Cortex 20:826-836.

Grutzendler J, Kasthuri N, Gan WB (2002) Long-term dendritic spine stability in the adult cortex. Nature 420:812-816.

Guic-Robles E, Valdivieso C, Guajardo G (1989) Rats can learn a roughness discrimination using only their vibrissal system. Behavioural brain research 31:285-289.

Guido W, Weyand T (1995) Burst responses in thalamic relay cells of the awake behaving cat. Journal of neurophysiology 74:1782-1786.

Hallman LE, Schofield BR, Lin CS (1988) Dendritic morphology and axon collaterals of corticotectal, corticopontine, and callosal neurons in layer V of primary visual cortex of the hooded rat. The Journal of comparative neurology 272:149-160.

Harris RM, Woolsey TA (1981) Dendritic plasticity in mouse barrel cortex following postnatal vibrissa follicle damage. The Journal of comparative neurology 196:357-376.

Hattox AM, Priest CA, Keller A (2002) Functional circuitry involved in the regulation of whisker movements. The Journal of comparative neurology 442:266-276.

Heintz N (2004) Gene expression nervous system atlas (GENSAT). Nature neuroscience 7:483.

Helmchen F, Svoboda K, Denk W, Tank DW (1999) In vivo dendritic calcium dynamics in deep-layer cortical pyramidal neurons. Nature neuroscience 2:989-996.

Hensch TK (2004) Critical period regulation. Annual review of neuroscience 27:549-579.

Hickmott PW, Ethell IM (2006) Dendritic plasticity in the adult neocortex. The Neuroscientist : a review journal bringing neurobiology, neurology and psychiatry 12:16-28.

Hickmott PW, Steen PA (2005) Large-scale changes in dendritic structure during reorganization of adult somatosensory cortex. Nature neuroscience 8:140-142.

Hofer SB, Mrsic-Flogel TD, Bonhoeffer T, Hubener M (2009) Experience leaves a lasting structural trace in cortical circuits. Nature 457:313-317.

Hoffer ZS, Alloway KD (2001) Organization of corticostriatal projections from the vibrissal representations in the primary motor and somatosensory cortical areas of rodents. The Journal of comparative neurology 439:87-103.

Hoffer ZS, Hoover JE, Alloway KD (2003) Sensorimotor corticocortical projections from rat barrel cortex have an anisotropic organization that facilitates integration of inputs from whiskers in the same row. The Journal of comparative neurology 466:525-544.

Holtmaat A, Bonhoeffer T, Chow DK, Chuckowree J, De Paola V, Hofer SB, Hubener M, Keck T, Knott G, Lee WC, Mostany R, Mrsic-Flogel TD, Nedivi E, Portera-Cailliau C, Svoboda K, Trachtenberg JT, Wilbrecht L (2009) Long-term, high-resolution imaging in the mouse neocortex through a chronic cranial window. Nature protocols 4:1128-1144.

Holtmaat A, Wilbrecht L, Knott GW, Welker E, Svoboda K (2006) Experience-dependent and cell-type-specific spine growth in the neocortex. Nature 441:979-983.

Holtmaat AJ, Trachtenberg JT, Wilbrecht L, Shepherd GM, Zhang X, Knott GW, Svoboda K (2005) Transient and persistent dendritic spines in the neocortex in vivo. Neuron 45:279-291.

Hooks BM, Hires SA, Zhang YX, Huber D, Petreanu L, Svoboda K, Shepherd GM (2011) Laminar analysis of excitatory local circuits in vibrissal motor and sensory cortical areas. PLoS biology 9:e1000572.

Horikawa K, Armstrong WE (1988) A versatile means of intracellular labeling: injection of biocytin and its detection with avidin conjugates. Journal of neuroscience methods 25:1-11.

Hubel DH, Wiesel TN (1959) Receptive fields of single neurones in the cat's striate cortex. The Journal of physiology 148:574-591.

Hubel DH, Wiesel TN (1962) Receptive fields, binocular interaction and functional architecture in the cat's visual cortex. The Journal of physiology 160:106-154.

Hubel DH, Wiesel TN (1968) Receptive fields and functional architecture of monkey striate cortex. The Journal of physiology 195:215-243.

Hubel DH, Wiesel TN (1970) The period of susceptibility to the physiological effects of unilateral eye closure in kittens. The Journal of physiology 206:419-436.

Hubel DH, Wiesel TN (1977) Ferrier lecture. Functional architecture of macaque monkey visual cortex. Proceedings of the Royal Society of London Series B, Containing papers of a Biological character Royal Society 198:1-59.

Hubel DH, Wiesel TN, LeVay S (1977) Plasticity of ocular dominance columns in monkey striate cortex. Philosophical transactions of the Royal Society of London Series B, Biological sciences 278:377-409.

Hubener M, Schwarz C, Bolz J (1990) Morphological types of projection neurons in layer 5 of cat visual cortex. The Journal of comparative neurology 301:655-674.

Jacobs B, Schall M, Scheibel AB (1993) A quantitative dendritic analysis of Wernicke's area in humans. II. Gender, hemispheric, and environmental factors. The Journal of comparative neurology 327:97-111.

Jin TE, Witzemann V, Brecht M (2004) Fiber types of the intrinsic whisker muscle and whisking behavior. The Journal of neuroscience : the official journal of the Society for Neuroscience 24:3386-3393.

Kaas JH (1997) Topographic maps are fundamental to sensory processing. Brain research bulletin 44:107-112.

Katz LC, Constantine-Paton M (1988) Relationships between segregated afferents and postsynaptic neurones in the optic tectum of three-eyed frogs. The Journal of neuroscience : the official journal of the Society for Neuroscience 8:3160-3180.

Keck T, Mrsic-Flogel TD, Vaz Afonso M, Eysel UT, Bonhoeffer T, Hubener M (2008) Massive restructuring of neuronal circuits during functional reorganization of adult visual cortex. Nature neuroscience 11:1162-1167.

Killackey HP, Belford G, Ryugo R, Ryugo DK (1976) Anomalous organization of thalamocortical projections consequent to vibrissae removal in the newborn rat and mouse. Brain research 104:309-315.

Kleinfeld D, Ahissar E, Diamond ME (2006) Active sensation: insights from the rodent vibrissa sensorimotor system. Curr Opin Neurobiol 16:435-444.

Kleinfeld D, Sachdev RN, Merchant LM, Jarvis MR, Ebner FF (2002) Adaptive filtering of vibrissa input in motor cortex of rat. Neuron 34:1021-1034.

Knutsen PM, Pietr M, Ahissar E (2006) Haptic object localization in the vibrissal system: behavior and performance. The Journal of neuroscience : the official journal of the Society for Neuroscience 26:8451-8464.

Kolb B, Whishaw IQ (1998) Brain plasticity and behavior. Annual review of psychology 49:43-64.

Komendantov AO, Ascoli GA (2009) Dendritic excitability and neuronal morphology as determinants of synaptic efficacy. Journal of neurophysiology 101:1847-1866.

Koralek KA, Jensen KF, Killackey HP (1988) Evidence for two complementary patterns of thalamic input to the rat somatosensory cortex. Brain research 463:346-351.

Kossel A, Lowel S, Bolz J (1995) Relationships between dendritic fields and functional architecture in striate cortex of normal and visually deprived cats. The Journal of neuroscience : the official journal of the Society for Neuroscience 15:3913-3926.

Kossut M (1992) Plasticity of the barrel cortex neurons. Progress in neurobiology 39:389-422.

Kossut M, Hand PJ, Greenberg J, Hand CL (1988) Single vibrissal cortical column in SI cortex of rat and its alterations in neonatal and adult vibrissa-deafferented animals: a quantitative 2DG study. Journal of neurophysiology 60:829-852.

Kullmann DM (2012) The Mother of All Battles 20 years on: is LTP expressed pre- or postsynaptically? The Journal of physiology 590:2213-2216.

Land PW, Simons DJ (1985) Metabolic and structural correlates of the vibrissae representation in the thalamus of the adult rat. Neuroscience letters 60:319-324.

Larkman A, Mason A (1990) Correlations between morphology and electrophysiology of pyramidal neurons in slices of rat visual cortex. I. Establishment of cell classes. The Journal of neuroscience : the official journal of the Society for Neuroscience 10:1407-1414.

Larkman AU (1991) Dendritic morphology of pyramidal neurones of the visual cortex of the rat: III. Spine distributions. The Journal of comparative neurology 306:332-343.

Larkum ME, Kaiser KM, Sakmann B (1999a) Calcium electrogenesis in distal apical dendrites of layer 5 pyramidal cells at a critical frequency of back-propagating action potentials. Proceedings of the National Academy of Sciences of the United States of America 96:14600-14604.

Larkum ME, Zhu JJ, Sakmann B (1999b) A new cellular mechanism for coupling inputs arriving at different cortical layers. Nature 398:338-341.

Larkum ME, Zhu JJ, Sakmann B (2001) Dendritic mechanisms underlying the coupling of the dendritic with the axonal action potential initiation zone of adult rat layer 5 pyramidal neurons. The Journal of physiology 533:447-466.

Larsen DD, Wickersham IR, Callaway EM (2007) Retrograde tracing with recombinant rabies virus reveals correlations between projection targets and dendritic architecture in layer 5 of mouse barrel cortex. Frontiers in neural circuits 1:5.

Lavallee P, Urbain N, Dufresne C, Bokor H, Acsady L, Deschenes M (2005) Feedforward inhibitory control of sensory information in higher-order thalamic nuclei. The Journal of neuroscience : the official journal of the Society for Neuroscience 25:7489-7498.

Lee LJ, Erzurumlu RS (2005) Altered parcellation of neocortical somatosensory maps in N-methyl-D-aspartate receptor-deficient mice. The Journal of comparative neurology 485:57-63.

Lee WC, Huang H, Feng G, Sanes JR, Brown EN, So PT, Nedivi E (2006) Dynamic remodeling of dendritic arbors in GABAergic interneurons of adult visual cortex. PLoS biology 4:e29.

Lu SM, Lin RC (1993) Thalamic afferents of the rat barrel cortex: a light- and electron-microscopic study using Phaseolus vulgaris leucoagglutinin as an anterograde tracer. Somatosensory & motor research 10:1-16.

Lubke J, Feldmeyer D (2007) Excitatory signal flow and connectivity in a cortical column: focus on barrel cortex. Brain structure & function 212:3-17.

Mainen ZF, Sejnowski TJ (1996) Influence of dendritic structure on firing pattern in model neocortical neurons. Nature 382:363-366.

Malenka RC (2003) The long-term potential of LTP. Nature reviews Neuroscience 4:923-926.

Malenka RC, Bear MF (2004) LTP and LTD: an embarrassment of riches. Neuron 44:5-21.

Malenka RC, Nicoll RA (1999) Long-term potentiation--a decade of progress? Science 285:1870-1874.

Maletic-Savatic M, Malinow R, Svoboda K (1999) Rapid dendritic morphogenesis in CA1 hippocampal dendrites induced by synaptic activity. Science 283:1923-1927.

Mao T, Kusefoglu D, Hooks BM, Huber D, Petreanu L, Svoboda K (2011) Long-range neuronal circuits underlying the interaction between sensory and motor cortex. Neuron 72:111-123.

Markram H, Lubke J, Frotscher M, Roth A, Sakmann B (1997) Physiology and anatomy of synaptic connections between thick tufted pyramidal neurones in the developing rat neocortex. The Journal of physiology 500 (Pt 2):409-440.

McCarley RW, Benoit O, Barrionuevo G (1983) Lateral geniculate nucleus unitary discharge in sleep and waking: state- and rate-specific aspects. Journal of neurophysiology 50:798-818.

McCormick DA, Feeser HR (1990) Functional implications of burst firing and single spike activity in lateral geniculate relay neurons. Neuroscience 39:103-113.

Mehta SB, Whitmer D, Figueroa R, Williams BA, Kleinfeld D (2007) Active spatial perception in the vibrissa scanning sensorimotor system. PLoS biology 5:e15.

Meyer HS, Wimmer VC, Oberlaender M, de Kock CP, Sakmann B, Helmstaedter M (2010) Number and laminar distribution of neurons in a thalamocortical projection column of rat vibrissal cortex. Cereb Cortex 20:2277-2286.

Mitchinson B, Grant RA, Arkley K, Rankov V, Perkon I, Prescott TJ (2011) Active vibrissal sensing in rodents and marsupials. Philosophical transactions of the Royal Society of London Series B, Biological sciences 366:3037-3048.

Mizrahi A, Katz LC (2003) Dendritic stability in the adult olfactory bulb. Nature neuroscience 6:1201-1207.

Morishima M, Kawaguchi Y (2006) Recurrent connection patterns of corticostriatal pyramidal cells in frontal cortex. The Journal of neuroscience : the official journal of the Society for Neuroscience 26:4394-4405.

Mountcastle VB (1957) Modality and topographic properties of single neurons of cat's somatic sensory cortex. Journal of neurophysiology 20:408-434.

Mountcastle VB (1988) The Gordon Wilson lecture. Representations and the construction of reality. Transactions of the American Clinical and Climatological Association 99:70-90.

Mountcastle VB (1998) Perceptual Neuroscience: The Cerebral Cortex. Cambridge, MA: Harvard University Press.

Mountcastle VB (2003) Introduction. Computation in cortical columns. Cereb Cortex 13:2-4.

Mountcastle VB, Davies PW, Berman AL (1957) Response properties of neurons of cat's somatic sensory cortex to peripheral stimuli. Journal of neurophysiology 20:374-407.

Neafsey EJ, Bold EL, Haas G, Hurley-Gius KM, Quirk G, Sievert CF, Terreberry RR (1986) The organization of the rat motor cortex: a microstimulation mapping study. Brain research 396:77-96.

O'Connor DH, Huber D, Svoboda K (2009) Reverse engineering the mouse brain. Nature 461:923-929.

Oberlaender M, Ramirez A, Bruno RM (2012) Sensory experience restructures thalamocortical axons during adulthood. Neuron 74:648-655.

Parker D (2010) Neuronal network analyses: premises, promises and uncertainties. Philosophical transactions of the Royal Society of London Series B, Biological sciences 365:2315-2328.

Petersen CC (2007) The functional organization of the barrel cortex. Neuron 56:339-355.

Petersen CC, Sakmann B (2000) The excitatory neuronal network of rat layer 4 barrel cortex. The Journal of neuroscience : the official journal of the Society for Neuroscience 20:7579-7586.

Petreanu L, Mao T, Sternson SM, Svoboda K (2009) The subcellular organization of neocortical excitatory connections. Nature 457:1142-1145.

Pierret T, Lavallee P, Deschenes M (2000) Parallel streams for the relay of vibrissal information through thalamic barreloids. The Journal of neuroscience : the official journal of the Society for Neuroscience 20:7455-7462.

Poirazi P, Mel BW (2001) Impact of active dendrites and structural plasticity on the memory capacity of neural tissue. Neuron 29:779-796.

Porter LL, White EL (1983) Afferent and efferent pathways of the vibrissal region of primary motor cortex in the mouse. The Journal of comparative neurology 214:279-289.

Rakic P (1976) Prenatal genesis of connections subserving ocular dominance in the rhesus monkey. Nature 261:467-471.

Ramcharan EJ, Gnadt JW, Sherman SM (2000) Burst and tonic firing in thalamic cells of unanesthetized, behaving monkeys. Visual neuroscience 17:55-62.

Rhodes PA, Llinas RR (2001) Apical tuft input efficacy in layer 5 pyramidal cells from rat visual cortex. The Journal of physiology 536:167-187.

Rutledge LT, Wright C, Duncan J (1974) Morphological changes in pyramidal cells of mammalian neocortex associated with increased use. Experimental neurology 44:209-228.

Sakata S, Harris KD (2009) Laminar structure of spontaneous and sensory-evoked population activity in auditory cortex. Neuron 64:404-418.

Schaefer AT, Larkum ME, Sakmann B, Roth A (2003) Coincidence detection in pyramidal neurons is tuned by their dendritic branching pattern. Journal of neurophysiology 89:3143-3154.

Scheibel A, Conrad T, Perdue S, Tomiyasu U, Wechsler A (1990) A quantitative study of dendrite complexity in selected areas of the human cerebral cortex. Brain and cognition 12:85-101.

Schiller J, Helmchen F, Sakmann B (1995) Spatial profile of dendritic calcium transients evoked by action potentials in rat neocortical pyramidal neurones. The Journal of physiology 487 (Pt 3):583-600.

Schiller J, Schiller Y, Stuart G, Sakmann B (1997) Calcium action potentials restricted to distal apical dendrites of rat neocortical pyramidal neurons. The Journal of physiology 505 (Pt 3):605-616.

Shepherd GM, Svoboda K (2005) Laminar and columnar organization of ascending excitatory projections to layer 2/3 pyramidal neurons in rat barrel cortex. The Journal of neuroscience : the official journal of the Society for Neuroscience 25:5670-5679.

Simons DJ, Land PW (1987) Early experience of tactile stimulation influences organization of somatic sensory cortex. Nature 326:694-697.

Simons DJ, Woolsey TA (1984) Morphology of Golgi-Cox-impregnated barrel neurons in rat SmI cortex. The Journal of comparative neurology 230:119-132.

Steriade M, McCormick DA, Sejnowski TJ (1993) Thalamocortical oscillations in the sleeping and aroused brain. Science 262:679-685.

Stuart GJ, Sakmann B (1994) Active propagation of somatic action potentials into neocortical pyramidal cell dendrites. Nature 367:69-72.

Sur M, Rubenstein JL (2005) Patterning and plasticity of the cerebral cortex. Science 310:805-810.

Tailby C, Wright LL, Metha AB, Calford MB (2005) Activity-dependent maintenance and growth of dendrites in adult cortex. Proceedings of the National Academy of Sciences of the United States of America 102:4631-4636.

Thivierge JP, Marcus GF (2007) The topographic brain: from neural connectivity to cognition. Trends in neurosciences 30:251-259.

Trachtenberg JT, Chen BE, Knott GW, Feng G, Sanes JR, Welker E, Svoboda K (2002) Long-term in vivo imaging of experience-dependent synaptic plasticity in adult cortex. Nature 420:788-794.

Tunturi AR (1950) Physiological determination of the arrangement of the afferent connections to the middle ectosylvian auditory area in the dog. The American journal of physiology 162:489-502.

Uylings HB, Kuypers K, Diamond MC, Veltman WA (1978) Effects of differential environments on plasticity of dendrites of cortical pyramidal neurons in adult rats. Experimental neurology 62:658-677.

Van der Loos H, Woolsey TA (1973) Somatosensory cortex: structural alterations following early injury to sense organs. Science 179:395-398.

van Ooyen A, Duijnhouwer J, Remme MW, van Pelt J (2002) The effect of dendritic topology on firing patterns in model neurons. Network 13:311-325.

Veinante P, Deschenes M (1999) Single- and multi-whisker channels in the ascending projections from the principal trigeminal nucleus in the rat. The Journal of neuroscience : the official journal of the Society for Neuroscience 19:5085-5095.

Voigts J, Sakmann B, Celikel T (2008) Unsupervised whisker tracking in unrestrained behaving animals. Journal of neurophysiology 100:504-515.

Volkmar FR, Greenough WT (1972) Rearing complexity affects branching of dendrites in the visual cortex of the rat. Science 176:1445-1447.

Weisz N, Wienbruch C, Hoffmeister S, Elbert T (2004) Tonotopic organization of the human auditory cortex probed with frequency-modulated tones. Hearing research 191:49-58.

Welker E, Hoogland PV, Van der Loos H (1988) Organization of feedback and feedforward projections of the barrel cortex: a PHA-L study in the mouse. Experimental brain research Experimentelle Hirnforschung Experimentation cerebrale 73:411-435.

Weller WL, Johnson JI (1975) Barrels in cerebral cortex altered by receptor disruption in newborn, but not in five-day-old mice (Cricetidoe and Muridae). Brain research 83:504-508.

White EL (2002) Specificity of cortical synaptic connectivity: emphasis on perspectives gained from quantitative electron microscopy. Journal of neurocytology 31:195-202.

Wiesel TN (1982) Postnatal development of the visual cortex and the influence of environment. Nature 299:583-591.

Wiesel TN, Hubel DH (1963) Single-Cell Responses in Striate Cortex of Kittens Deprived of Vision in One Eye. Journal of neurophysiology 26:1003-1017.

Wilbrecht L, Holtmaat A, Wright N, Fox K, Svoboda K (2010) Structural plasticity underlies experience-dependent functional plasticity of cortical circuits. The Journal of neuroscience : the official journal of the Society for Neuroscience 30:4927-4932.

Wimmer VC, Broser PJ, Kuner T, Bruno RM (2010) Experience-induced plasticity of thalamocortical axons in both juveniles and adults. The Journal of comparative neurology 518:4629-4648.

Woolsey TA, Van der Loos H (1970) The structural organization of layer IV in the somatosensory region (SI) of mouse cerebral cortex. The description of a cortical field composed of discrete cytoarchitectonic units. Brain research 17:205-242.

Wu CS, Ballester Rosado CJ, Lu HC (2011) What can we get from 'barrels': the rodent barrel cortex as a model for studying the establishment of neural circuits. The European journal of neuroscience 34:1663-1676.

Xu HT, Pan F, Yang G, Gan WB (2007) Choice of cranial window type for in vivo imaging affects dendritic spine turnover in the cortex. Nature neuroscience 10:549-551.

Xu T, Yu X, Perlik AJ, Tobin WF, Zweig JA, Tennant K, Jones T, Zuo Y (2009) Rapid formation and selective stabilization of synapses for enduring motor memories. Nature 462:915-919.

Yang G, Pan F, Gan WB (2009) Stably maintained dendritic spines are associated with lifelong memories. Nature 462:920-924.

Yu C, Derdikman D, Haidarliu S, Ahissar E (2006) Parallel thalamic pathways for whisking and touch signals in the rat. PLoS biology 4:e124.

Zuo Y, Yang G, Kwon E, Gan WB (2005) Long-term sensory deprivation prevents dendritic spine loss in primary somatosensory cortex. Nature 436:261-265.

6 Acknowledgements

I want to take this opportunity to express my thanks to the people without whom this thesis would not have been a reality. I would like to start by thanking Prof. Dr. Bert Sakmann for giving me the opportunity to work in his laboratory at the Max Planck Institute of Neurobiology, and Prof. Dr. Tobias Bonhoeffer, also from the Max Planck Institute of Neurobiology, for being my doctoral mentor and a part of my thesis committee. This thesis probably would not have come to the present point without the enormous personal support of P.D. Dr. Felix Felmy from the L.M.U. Munich and Dr. Jürgen Haag from the Max Planck Institute of Neurobiology. I would also like to thank the members of the Sakmann group, Dr. Thorben Kurz and Dr. med. Hanno Meyer, for their support at various points in this project.

My doctoral endeavours were largely financed by Boehringer Ingelheim Fonds (B.I.F.). I cannot emphasize enough, the personal role played by its awesome team in supporting me through a tough time. I personally owe my gratitude to all its members. B.I.F. also gave me the chance to meet and get to know grantees from all over the world, some of whom I got to know personally and found to be, above all, nice human beings.

I want to thank my parents at the outset, for being my *raison d'être.* To them as well, I dedicate this thesis. I also owe my appreciation, thanks and gratitude to all the wonderful people I have met at the Max Planck Institute over the last five years, some of whom have become very good friends. A journey that began what seems like yesterday, managed to bring me close to these people with whom I have enjoyed quality times, mostly with, but also without countless *'Helle'*. You all have made the painful journey of a PhD seem ever so easier with all your support, love and indulgence. And without some of your encouragement through my particularly hard times, this thesis would probably not have seen the light of day. To Marcus 'ze red-neck' Knopp, Onur 'Turkish' Gökce and Anja Friedrich, my heartfelt thanks.

Lastly, all these years in Berlin, Munich and beyond have also been the most formative in my life. I have come across numerous (and at times countless) people in my personal life. Some of these experiences, I have been grateful to have had and have cherished; the others rather to the contrary. However, I appreciate having had these experiences as they have shaped me, and my *tabula rasa* as John Locke would put it. I would like to dedicate this thesis to these people, who have been part of my experiences, in every whichever way, and to life, for giving me these experiences, many of which I am sure, are yet to come. If you are reading this, you know who you are. To all the music groups I have discovered over the years, without you this journey would have been rougher! To 'Seppl' Ivens for being what he is and hopefully would always be, the best human being I have come across till now. And to *Baalin*, about which I could write a whole novel, which remains and would continue to be, the biggest love of my life! So here's to '*vida pura',* '*dickes B',* and all that they entail! *Pura Vida*! Pour tout le monde!